



**TÉCNICO**  
LISBOA

# **Proca field perturbations in higher-dimensional AdS and Schwarzschild-AdS spacetimes**

**David Duarte César Lopes**

Thesis to obtain the Master of Science Degree in

**Engineering Physics**

Supervisor: Prof. José Pizarro de Sande e Lemos

## **Examination Committee**

Chairperson: Prof. Ana Maria Vergueiro Monteiro Cidade Mourão

Supervisor: Prof. José Pizarro de Sande e Lemos

Member of the Committee: Prof. Antonino Flachi

**December 2023**



To my mother and my grandfather Vá.



## **Acknowledgments**

I thank Tiago Vasques Fernandes for very useful discussions and for his infinite patience and dedication put in this work. Although it is not possible to mention him in the front cover, he indeed acted as my co-supervisor. I also thank my supervisor, José Sande Lemos, for proposing this problem to me, and whose knowledge and availability were determinant throughout the thesis.

On a more personal note, I thank my mother, Sara, with whom my life began and with whom my life will end. I also thank the rest of my family and friends for their support.



## Resumo

Perturbações de campos em espaços-tempo com buracos negros são consideradas em vários contextos, desde a investigação da dinâmica de buracos negros astrofísicos até ao estudo de teorias de gravidade quântica. Um espaço-tempo perturbado vibra com frequências características, conhecidas como modos quasi-normais. Em espaços-tempo assintoticamente anti-de Sitter (AdS), estes são estudados no contexto da correspondência AdS/teoria de campo conformal (CFT), onde as frequências dos modos quasi-normais determinam a escala de tempo da termalização da CFT.

Nós estudamos perturbações de campos de Proca em espaços-tempo AdS e Schwarzschild-AdS com  $d$ -dimensões. Obtemos as equações de Proca decompondo o campo segundo o seu comportamento tensorial na esfera. Demonstramos que as equações formam dois setores completamente separados: o setor tipo-vetorial, que engloba  $d - 3$  graus de liberdade desacoplados do campo, governados por uma única equação do tipo-onda; o setor tipo-escalar, que descreve os restantes dois graus de liberdade do campo, governados por duas equações do tipo-onda acopladas. Nós mostramos que as últimas desacoplam em AdS com  $d$  dimensões, e calculamos as soluções exatas de modos normais para perturbações de Proca neste espaço-tempo, impondo condições de fronteira de Dirichlet no infinito. Adicionalmente, recuperamos os resultados para perturbações de Maxwell quando a massa do campo de Proca tende para zero. A estabilidade linear em Schwarzschild-AdS perante perturbações de Proca tipo-vetorial e monopolo é provada. Também calculamos numericamente os modos quasi-normais de perturbações de Proca em Schwarzschild-AdS com 4, 5, 6, 7 dimensões, e desenvolvemos um estudo analítico do espetro para buracos negros pequenos.

**Palavras-chave:** Buracos negros, modos quasi-normais, campos de Proca, espaço-tempo AdS, espaço-tempo Schwarzschild-AdS, dimensões superiores.



## Abstract

Field perturbations in black hole spacetimes have been considered in a variety of contexts, from probing the dynamics of astrophysical black holes to studying quantum gravity theories. A perturbed spacetime vibrates with characteristic frequencies, known as quasinormal modes. In asymptotically anti-de Sitter (AdS) spacetimes, these are studied in the context of the AdS/conformal field theory (CFT) correspondence, where the quasinormal mode frequencies determine the thermalization timescale of the CFT.

We study Proca field perturbations in  $d$ -dimensional AdS and Schwarzschild-AdS spacetimes. We obtain the Proca equations by decomposing the field according to its tensorial behaviour on the sphere. We demonstrate that the equations form two completely separated sectors: the vector-type sector, which accounts for  $d - 3$  decoupled degrees of freedom of the field, governed by a single wave-like equation; the scalar-type sector, which describes the remaining two degrees of freedom of the field, ruled by two coupled wave-like equations. We show that the latter decouple in higher-dimensional AdS, and we compute the exact normal mode solutions of Proca field perturbations in this spacetime, imposing Dirichlet boundary conditions at infinity. Additionally, the Maxwell field results are recovered by taking the massless limit of the Proca field. In Schwarzschild-AdS, linear stability is proved against vector-type and monopole Proca field perturbations. We also compute numerically the Proca field quasinormal modes in 4, 5, 6, 7-dimensional Schwarzschild-AdS, and perform an analytical study of the spectrum for small black holes.

**Keywords:** Black holes, quasinormal modes, Proca fields, AdS spacetime, Schwarzschild-AdS spacetime, higher dimensions.



# Contents

Acknowledgments . . . . .	v
Resumo . . . . .	vii
Abstract . . . . .	ix
List of Tables . . . . .	xiii
List of Figures . . . . .	xv
Preface . . . . .	xvii
<b>1 Introduction</b>	<b>1</b>
1.1 Black holes and quasinormal modes . . . . .	1
1.2 Black hole perturbation theory . . . . .	2
1.3 Field perturbations in asymptotically AdS spacetimes . . . . .	2
1.4 Proca field perturbations in gravitational backgrounds . . . . .	4
1.5 Thesis outline . . . . .	5
<b>2 Proca field perturbations</b>	<b>7</b>
2.1 Proca field in curved spacetime . . . . .	7
2.2 Proca field perturbations in spaces with warped product topology . . . . .	9
2.2.1 Proca field equations in spaces with warped product topology . . . . .	9
2.2.2 Decomposition of the Proca field and harmonic expansion . . . . .	9
2.2.3 Separation of Proca field equations . . . . .	11
2.2.4 Proca field perturbations in a spherically symmetric $(2 + n)$ -background . . . . .	13
2.3 Maxwell field perturbations . . . . .	14
<b>3 Normal modes of Proca field perturbations in <math>d</math>-dimensional AdS</b>	<b>18</b>
3.1 Initial considerations and boundary conditions . . . . .	18
3.2 Proca field perturbations in AdS . . . . .	19
3.2.1 Proca field equations . . . . .	19
3.2.2 Normal mode solutions . . . . .	20
3.3 Maxwell field perturbations in AdS . . . . .	21
3.3.1 Maxwell field equations . . . . .	21
3.3.2 Normal mode solutions . . . . .	22

<b>4</b>	<b>Quasinormal modes of Proca field perturbations in <math>d</math>-dimensional Schwarzschild-AdS</b>	<b>23</b>
4.1	Proca field equations in Schwarzschild-AdS spacetime . . . . .	23
4.2	Analytical study of the quasinormal mode spectrum . . . . .	25
4.2.1	Boundary conditions . . . . .	25
4.2.2	Main properties of the spectrum and asymptotic solutions near infinity . . . . .	25
4.2.3	Schwarzschild-AdS stability against Maxwell and Proca field perturbations . . . . .	28
4.3	Numerical methods to compute quasinormal modes . . . . .	30
4.3.1	Horowitz-Hubeny method . . . . .	30
4.3.2	Numerical integration of the equations of motion . . . . .	36
4.4	Numerical results . . . . .	38
4.4.1	Effect of the mass of the field on the quasinormal mode spectrum . . . . .	39
4.4.2	Quasinormal mode spectrum as a function of the black hole radius . . . . .	45
4.4.3	Higher overtones . . . . .	49
4.4.4	Dependence on $l$ and the eikonal limit . . . . .	52
4.5	The long-wavelength approximation for small Schwarzschild-AdS black holes . . . . .	56
4.5.1	Vector-type Proca and Maxwell field perturbations . . . . .	57
4.5.2	Monopole Proca field perturbations . . . . .	65
4.5.3	Scalar-type Maxwell field perturbations . . . . .	67
4.5.4	Higher multipoles of scalar-type Proca field perturbations . . . . .	69
<b>5</b>	<b>Conclusion</b>	<b>71</b>
5.1	Achievements . . . . .	71
5.2	Future Work . . . . .	73
<b>A</b>	<b>Spherical harmonics on the <math>n</math>-sphere</b>	<b>81</b>
A.1	Initial considerations . . . . .	81
A.2	Scalar spherical harmonics . . . . .	81
A.3	Vector spherical harmonics . . . . .	82
A.4	Properties under rotation and parity transformations . . . . .	83
<b>B</b>	<b>Hypergeometric differential equation</b>	<b>85</b>
B.1	Main properties . . . . .	85
B.2	Normal modes in pure AdS . . . . .	86
B.2.1	Proca field and vector-type Maxwell field perturbations . . . . .	86
B.2.2	Scalar-type Maxwell field perturbations . . . . .	88
<b>C</b>	<b>Chandrasekhar's approach to isospectrality</b>	<b>91</b>

# List of Tables

4.1	Fundamental mode of $l = 1$ vector-type Maxwell and Proca perturbations in 4, 5, 6, 7-dimensional Schwarzschild-AdS spacetime with $r_h = 100$ , $r_h = 1$ and $r_h = 0.05$ , for different values of the mass of the field. . . . .	40
4.2	Fundamental mode of $l = 0$ Proca perturbations in 4, 5, 6, 7-dimensional Schwarzschild-AdS spacetime with $r_h = 100$ , $r_h = 1$ and $r_h = 0.05$ , for different values of the mass of the field. . . . .	41
4.3	Fundamental mode frequencies of $l = 1$ scalar-type electromagnetic perturbations in 4, 5, 6, 7-dimensional Schwarzschild-AdS for different black hole sizes. . . . .	42
4.4	Fundamental mode of the $l = 1$ electromagnetic polarization of scalar-type Proca perturbations in 4, 5, 6, 7-dimensional Schwarzschild-AdS spacetime with $r_h = 100$ , $r_h = 1$ and $r_h = 0.05$ , for different values of the mass of the field. . . . .	43
4.5	Fundamental mode of the $l = 1$ non-electromagnetic polarization of scalar-type Proca perturbations in 4, 5, 6, 7-dimensional Schwarzschild-AdS spacetime with $r_h = 100$ , $r_h = 1$ and $r_h = 0.05$ , for different values of the mass of the field. . . . .	43
4.6	Fundamental quasinormal mode frequencies of $l = 2$ Proca field perturbations in 5, 6, 7-dimensional Schwarzschild-AdS, for a Proca field with mass $\mu = 0.2$ and different black hole sizes, in the large black hole regime. . . . .	46
4.7	Fundamental quasinormal mode frequencies of $l = 2$ Proca perturbations in 5, 6, 7-dimensional Schwarzschild-AdS, for a Proca field with mass $\mu = 0.2$ and different black hole sizes, in the intermediate and small black hole regimes. The values for $r_h = 0$ are for pure AdS, computed with Eq. (3.15). . . . .	48
4.8	Lowest modes of $l = 0, 1$ and $\mu = 0.5$ Proca field perturbations in 5, 6, 7-dimensional Schwarzschild-AdS with $r_h = 1$ . For the empty cells, none of the methods implemented converged. . . . .	49
4.9	Fundamental, first and second overtones of $l = 1$ vector-type and scalar-type Maxwell field perturbations in 5, 6, 7-dimensional Schwarzschild-AdS spacetime with $r_h = 100$ . In 6-dimensional Schwarzschild-AdS, the convergence of Horowitz-Hubeny method allowed to find the $k = 3, 4$ modes as well. . . . .	51
4.10	Fundamental quasinormal mode frequencies of $\mu = 0.5$ Proca perturbations in the eikonal limit for 5, 6, 7-dimensional Schwarzschild-AdS black holes with $r_h = 100$ . . . . .	54

4.11 Values of $\beta$ for the fundamental mode of $\mu = 0.5$ Proca field perturbations in 5, 6, 7-dimensional Schwarzschild-AdS black holes with $r_h = 100$ , computed from fitting the real ( $\beta_R$ ) and imaginary ( $\beta_I$ ) parts of the numerical results to Eq. (4.57). The analytical results of [63] for scalar field perturbations are also displayed. . . . .	54
4.12 Fundamental mode of $\mu = 0.5$ vector-type Proca perturbations in 5, 6, 7-dimensional Schwarzschild-AdS spacetime with $r_h = 1$ , for different values of the angular momentum number $l$ . . . . .	55
4.13 Imaginary part of vector-type quasinormal frequencies for some of the allowed values of $d, l, \mu$ , for black holes with sizes $r_h = 0.1$ and $r_h = 0.01$ . The analytical results were computed from Eq. (4.90). . . . .	62
4.14 Imaginary part of vector-type quasinormal frequencies for some of the allowed values of $d, l, \mu$ , for black holes with sizes $r_h = 0.1$ and $r_h = 0.01$ . The analytical results were computed from Eq. (4.91). . . . .	63
4.15 Imaginary part of vector-type quasinormal frequencies for some of the allowed values of $d, l, \mu$ , for black holes with sizes $r_h = 0.1$ and $r_h = 0.01$ . The analytical results were computed from Eq. (4.93). . . . .	64
4.16 Imaginary part of monopole quasinormal frequencies for some of the allowed values of $d, \mu$ , for black holes with sizes $r_h = 0.1$ , $r_h = 0.01$ and $r_h = 0.001$ . The analytical results were computed from Eq. (4.99). . . . .	66
4.17 Imaginary part of scalar-type electromagnetic quasinormal frequencies for some of the allowed values of $d, l$ , for black holes with sizes $r_h = 0.1$ and $r_h = 0.01$ . The analytical results were computed from Eq. (4.109). . . . .	68

# List of Figures

4.1	Effective potentials of $l = 1$ scalar-type electromagnetic perturbations for the 4, 5, 6, 7, 8-dimensional Schwarzschild-AdS black holes with $r_h = 2$ . . . . .	27
4.2	Convergence curves for the fundamental mode of $l = 1$ vector-type $\mu = 0.2$ Proca field perturbations, for 6-dimensional Schwarzschild black holes with sizes $r_h = 1$ (Left) and $r_h = 0.6$ (Right). For $r_h \lesssim 1$ , a small decrease in the black hole size significantly worsens the convergence of the solution: for $r_h = 1$ one achieves a precision up to the fifth significant figure at $N \gtrsim 100$ , whereas for $r_h = 0.6$ such precision is only reached for $N \gtrsim 200$ . $\omega_{\text{fit}}$ is extracted from the fit of $\omega(N) = \omega_{\text{fit}} + c_2 e^{-c_3 N} \sin(c_4 N + c_5)$ to the convergence curves.	33
4.3	Convergence curves for the fundamental mode $k = 0$ (Left) and for the second overtone $k = 2$ (Right) of $l = 1$ vector-type $\mu = 0.2$ Proca field perturbations in 6-dimensional Schwarzschild-AdS, with $r_h = 100$ . For the $k = 0$ mode the method converges better (frequency oscillates around its sixth significant figure for $N \simeq 75$ ) than for the $k = 2$ mode (frequency oscillates around its sixth significant figure for $N \simeq 120$ ). The $\omega_{\text{fit}}$ values are also displayed. . . . .	34
4.4	Convergence curves for the fundamental mode of vector-type $\mu = 0.2$ Proca perturbations in 4-dimensional Schwarzschild-AdS (Left) and 5-dimensional Schwarzschild-AdS (Right), for a black hole with size $r_h = 100$ . While in 6-dimensional Schwarzschild-AdS the convergence curves have a sinusoidal shape, in $d = 4, 5, 7$ -dimensional Schwarzschild-AdS the curves exponentially decay without oscillating, making the determination of $\omega_{\text{fit}}$ less accurate. . . . .	34
4.5	Singular points of Eq. (4.26) in the complex plane for a $r_h = 1$ Schwarzschild-AdS black hole in: 6 (Left), 7 (Right) and 8 (Middle) dimensions. For the Horowitz-Hubeny method to work, all the zeroes of $f$ should lie outside the blue circle. For $d > 7$ and $r_h \gtrsim \mathcal{O}(0.1)$ , this no longer happens. . . . .	35
4.6	Contour plot of the absolute value of the solution evaluated at $r^{(f)}$ , in the phase space of complex frequencies. The blue regions encompass the quasinormal modes. Note that the fundamental mode is constrained to a very small region of frequencies, whereas this region is larger for the first overtone. Moreover, for the second overtone, a broad region of low absolute value modes is formed, impeding the determination of the frequency, at least for such value of $r^{(f)}$ . . . . .	38

4.7	Effect of the field's mass ( $\mu \in [0.1, 2.0]$ ) on the fundamental quasinormal spectrum of vector-type and scalar-type $l = 1$ Proca perturbations in 4, 5, 6, 7-dimensional Schwarzschild-AdS, with $r_h = 1$ . We also plotted the results for a Maxwell perturbation, which should be compared with the Proca small mass limit. . . . .	44
4.8	Comparison between the spectra for scalar field perturbations and for non-electromagnetically polarized Proca field perturbations in 7-dimensional Schwarzschild-AdS, with $r_h = 1, l = 1$ . In the small-mass limit these are nearly isospectral, in agreement with Eq. (2.62). . . .	45
4.9	Fundamental quasinormal frequencies of $l = 2$ vector-type Proca perturbations in 5, 6, 7-dimensional Schwarzschild-AdS spacetimes for a Proca field with mass $\mu = 0.2$ as a function of the black hole radius, in the large black hole regime. For large black holes, the frequencies scale linearly with the radius of the horizon. Fit results: for $d = 5$ , $\Re\epsilon(\omega) = 2.01926r_h + 0.219492$ ; for $d = 6$ , $\Re\epsilon(\omega) = 3.00834r_h + 0.205195$ ; and for $d = 7$ , $\Re\epsilon(\omega) = 3.84754r_h + 0.214392$ . . . . .	46
4.10	"Special" purely imaginary modes scaling with the inverse of the black hole radius, found for scalar-type Maxwell perturbations in 5, 6, 7-dimensional Schwarzschild-AdS. Fit results: for $d = 5$ , $-\Im\omega = 1.50823r_h^{-1} - 9.47993 \times 10^{-5}$ ; for $d = 6$ , $-\Im\omega = 1.33694r_h^{-1} - 2.14671 \times 10^{-4}$ ; and for $d = 7$ , $-\Im\omega = 1.25203r_h^{-1} - 5.33241 \times 10^{-5}$ . . . . .	47
4.11	Real part of the quasinormal mode frequencies for $l = 2, \mu = 0.2$ , Proca perturbations in 5-dimensional Schwarzschild-AdS spacetime in the small black hole regime. In the limit $r_h \rightarrow 0$ , the frequencies approach those of pure AdS, given by Eq. (3.15). . . . .	48
4.12	Effect of the field's mass ( $\mu \in [0.1, 2.0]$ ) on $k = 0, 1$ and $l = 0, 1$ Proca field modes, in 7-dimensional Schwarzschild-AdS, with $r_h = 1$ . The mass of the field seems to have a similar effect on $k = 0, 1$ overtones. . . . .	50
4.13	Numerical gaps for vector-type (left) and scalar-type (right) electromagnetic perturbations in 6-dimensional Schwarzschild-AdS. The higher the overtone, the closest the gap is to the one predicted in [21]. . . . .	52
4.14	Radial profile of the effective potential for $l = 1, l = 60$ and $l = 100$ vector-type Proca field perturbations, with $\mu = 0.5$ , in 7-dimensional Schwarzschild-AdS spacetime with $r_h = 1$ : for sufficiently large $l$ , the potential develops a well, accommodating long-lived modes. . .	53
4.15	Imaginary part of fundamental quasinormal modes of $\mu = 0.5$ Proca perturbations in the eikonal limit for 5, 6, 7-dimensional Schwarzschild-AdS black hole with $r_h = 100$ . These were fitted to Eq. (4.57), showing an agreement with [63, 64]. . . . .	54
4.16	Imaginary part of fundamental modes for $\mu = 0.5$ vector-type Proca perturbations in the eikonal limit, $l \gg 1$ , in 5, 6, 7-dimensional Schwarzschild-AdS, with $r_h = 1$ . For sufficiently large $l$ , the mode damping becomes exponentially small with $l$ . . . . .	55

## Preface

I declare that this document is an original work of my own authorship and that it fulfills all the requirements of the Code of Conduct and Good Practices of the Universidade de Lisboa.

The research presented was developed at Centro de Astrofísica e Gravitação (CENTRA), in the physics department of Instituto Superior Técnico. The work was done in collaboration with my supervisor, Prof. José Sande Lemos, and with the PhD researcher Tiago Vasques Fernandes. Chapters 2 and 3 are being submitted to publication, and Chapter 4 is being prepared for submission. The works published or to be published in this thesis are 2 in total, namely:

- D. Lopes, T. V. Fernandes, and J. P. S. Lemos, “Normal modes of Proca field perturbations in  $\text{AdS}_d$  spacetime”, *Physical Review D*, in submission (2023). (Chapters 2 and 3)
- D. Lopes, T. V. Fernandes, and J. P. S. Lemos, “Quasinormal modes of Proca field perturbations in higher-dimensional Schwarzschild-AdS spacetimes”, *Physical Review D*, to be submitted (2024). (Chapter 4)



# Chapter 1

## Introduction

### 1.1 Black holes and quasinormal modes

General relativity remains the most successful theory of gravitation since its publication, in 1915, by Albert Einstein. The concept of force in Newtonian theory was substituted by the concept of spacetime curvature in general relativity, which is nothing more than a manifestation of mass existence, mathematically encoded in the Einstein field equations. Among the most remarkable solutions to these equations are black hole solutions, containing regions of spacetime from which, classically, nothing, not even light, can escape from [1–3]. Black holes were thought to be purely theoretical objects for many years, and only in the latter half of the twentieth century they began to be increasingly accepted as fundamental bodies of our universe, culminating with the first-time detected gravitational waves, in 2015, by the LIGO collaboration [4], and with the two famous black hole images published by the EHT collaboration: the first one in 2019, in the center of the M87 galaxy, and the second one in 2022, in the center of our galaxy [5]. Different phenomena may contribute to the formation of black holes, with stellar collapse being a recognized factor in their creation. Furthermore, collisions between compact object binaries, such as two black holes or neutron stars, are believed to also play a role on their formation. The process of collision between two black holes may be divided into three different stages. The first stage is called the inspiral, characterized by a slow shrinking of the binary orbit, with energy being carried away through weak gravitational waves. The second stage is called the merger, happening when the black holes get sufficiently close to each other and become dynamically unstable, culminating in the formation of a single larger black hole. In the process, strong gravitational radiation is emitted, making this stage highly non-linear and impossible to study with any perturbative analytical approach. The final stage is called the ringdown, characterized by the settling of the final black hole into a more stable state. In this stage, the gravitational radiation emitted is weak enough to be treated linearly, and the final black hole “rings” with characteristic frequencies, called quasinormal modes.

Quasinormal modes are particularly important because they only depend on the properties of the black hole, such as its mass and charge, and are independent of the initial configuration that excited them [6, 7]. The term “quasi” alludes to the dissipative nature of the black hole, which emits energy

away to infinity through gravitational waves. Quasinormal modes have complex associated frequencies, whose real part represents the actual frequency of oscillation, whereas the imaginary part represents the decay timescale of the modes. While in resonant conservative systems a state can be described by a superposition of independent normal modes at all times, quasinormal modes do not provide such a complete expansion, which just reflects the fact that the system is not stationary. In astrophysical settings, the study of black hole quasinormal modes is key to understand the signals obtained by the existing gravitational antennas, such as LIGO and VIRGO, and by the new generation of gravitational antennas, such as the space-based interferometer LISA, expected to launch in 2037. In this context, the search is essentially focused on the lowest overtone modes, i.e., the modes with lowest frequencies, as these are the ones which dominate the gravitational-wave signals, providing insights, namely, on no-hair theorems [8] and scattering and absorption processes in black holes [9]. Additionally, investigation of black hole quasinormal modes provides information on the linear stability of the perturbed spacetime: if all the quasinormal modes are damped, the spacetime is linearly stable against such perturbations. In astrophysical contexts, determining the stability of a perturbed spacetime is of great interest, as unstable solutions cannot exist in nature and usually hint for state transitions.

## 1.2 Black hole perturbation theory

The study of linear field perturbations in gravitational backgrounds dates back to the seminal works of Regge and Wheeler [10], and Zerilli [11], which studied gravitational perturbations in four-dimensional Schwarzschild spacetime and showed that these can be reduced to two Schrödinger-like equations, by decomposing the perturbations according to their transformation properties under parity. The associated quasinormal modes are obtained by solving these Schrödinger-like equations with the appropriate boundary conditions. This is the general formalism to obtain quasinormal modes in spherically symmetric spacetimes, and it is known as the Regge-Wheeler-Zerilli formalism. The problem of linear perturbations in higher-dimensional spacetimes was only addressed in the beginning of the twenty-first century, after the works of Ishibashi and Kodama [12–14] (see also [15]). Their formalism generalizes the Regge-Wheeler-Zerilli formalism by expanding perturbations in higher-dimensional scalar, vector and tensor spherical harmonics, which independently form complete bases on the  $(d - 2)$ -sphere. According to their tensorial behaviour on the sphere, perturbations are separated in scalar-type, vector-type and tensor-type perturbations, which decouple at the linear level. With such a decomposition, the field equations can be once again written as Schrödinger-like equations, whose potential now also depends on the spacetime dimension.

## 1.3 Field perturbations in asymptotically AdS spacetimes

Anti-de Sitter (AdS) spacetime is the maximally symmetric vacuum solution to the Einstein field equations with negative cosmological constant [1, 2, 16]. Despite its simplicity, it exhibits unusual causal properties, related to the existence of a timelike conformal boundary at spatial infinity. This makes AdS

non-globally hyperbolic, meaning that, for fields to describe well-defined dynamics in AdS, besides providing initial data on a spacelike hypersurface, one needs to prescribe suitable boundary conditions at spatial infinity [17]. When one imposes Dirichlet (reflective) boundary conditions at infinity, with fields bouncing off from spatial infinity back to the AdS bulk, the system is conservative, as there is no energy lost at spatial infinity. In this case, the field modes are normal modes, with real associated frequencies. Scalar field normal modes in  $d$ -dimensional AdS were obtained firstly in [18], by imposing such conditions. [19] determined all of the possible boundary conditions that ensure well-defined dynamics for scalar, electromagnetic and gravitational perturbations in  $d$ -dimensional AdS: for  $d \geq 7$ , electromagnetic and gravitational perturbations define unique stable dynamics in AdS, as the Dirichlet boundary condition is a requirement to ensure square integrability of the solution; on the other hand, for scalar-type electromagnetic and gravitational perturbations in  $d = 4, 5, 6$ , and vector-type electromagnetic and gravitational perturbations in  $d = 4$ , a whole one-parameter family of boundary conditions (including Dirichlet and Neumann conditions) is allowed. This can be physically interpreted by analyzing the behaviour of the effective potential appearing in the Schrödinger-like equation: if the potential is repulsive enough near infinity, it completely reflects back the fields without them reaching the boundary. Exact solutions for the normal modes of scalar, electromagnetic and gravitational perturbations in higher-dimensional AdS were obtained in [19–21].

Asymptotically AdS spacetimes are, in simple terms, spacetimes that approach AdS geometry as one gets sufficiently close to spatial infinity, although in the bulk they may exhibit very different features from AdS, such as the presence of black holes. Quasinormal modes in asymptotically AdS spacetimes gained large interest due to the AdS/CFT correspondence [22], which establishes a duality between quantum gravity theories in  $d$ -dimensional AdS and conformal field theories (CFT) living on its  $(d - 1)$ -dimensional boundary. According to it, a large black hole in AdS is dual to the thermal state of the CFT. Quasinormal modes have then a direct interpretation within this framework: they describe how the perturbed thermal state of the CFT returns to equilibrium. Moreover, they allow to study non-perturbative effects of strongly coupled field theories, such as quark-gluon plasmas, which cannot be studied with the usual perturbative approaches of quantum field theory [23]. Also, as aforementioned, quasinormal modes allow to infer on the linear stability of a spacetime, which in the AdS/CFT correspondence is of great interest, as the transition from a stable solution to an unstable one is related to the thermodynamic phase transition on the CFT side [24]. For such geometries, exact quasinormal mode solutions cannot in general be found and one needs to rely on numerical methods to compute the quasinormal mode spectrum. These have been extensively studied, see e.g. [25–39]. In this work we will be interested in perturbations in Schwarzschild-AdS spacetimes, which are asymptotically AdS spacetimes containing a Schwarzschild black hole in the bulk. These were first considered by [28] for scalar field perturbations in  $d = 4$  and by [30] in  $d = 4, 5, 7$ . Scalar, electromagnetic and Weyl perturbations in  $d = 3$  were studied in [31]. Electromagnetic and gravitational perturbations in 4-dimensional Schwarzschild-AdS were studied in [32–34]. Since then, different kinds of perturbations were studied in a variety of asymptotically AdS spacetimes, in order to better understand the role of quasinormal modes in the AdS/CFT correspondence, cf. [36, 37] for great reviews on the subject. We will focus on Proca field perturbations, which we

now review.

## 1.4 Proca field perturbations in gravitational backgrounds

A massive spin-1 (Proca) field propagating in  $d$ -dimensional spacetime has  $d - 1$  degrees of freedom and can be viewed as the generalization of a massless spin-1 (Maxwell or electromagnetic) field, with the latter having one less degree of freedom, due to the gauge invariance of Maxwell field equations. One of the first works regarding Proca field perturbations in black hole spacetimes was done in [40], which obtained the Proca field equations in 4-dimensional Schwarzschild spacetime and observed that these could not in general be decoupled. [41] showed that the Proca field equations reduced to a single second-order differential equation for a purely monopole (spherically symmetric) Proca field. Yet, for higher multipoles, the equations could not be decoupled. This work was continued in [42], which studied numerically the quasinormal modes of spherically symmetric Proca field perturbations in 4-dimensional Schwarzschild and Schwarzschild-AdS spacetimes, having also found the exact normal mode solutions of a purely monopole Proca field propagating in AdS. [43] studied general Proca field perturbations in 4-dimensional Schwarzschild and Schwarzschild-de Sitter spacetimes, with a particular focus on their late-time behaviour, for which only the asymptotic form of the solutions was required. The quasinormal mode analysis of general Proca field perturbations in 4-dimensional Schwarzschild spacetime was done in [44]. More recently, [45] showed that, for higher multipoles, the Proca field equations in 4-dimensional AdS spacetime could be reduced to three decoupled second-order differential equations, and determined their exact normal mode solutions imposing Dirichlet boundary conditions at spatial infinity. Generalization to higher dimensions was firstly considered in [46], which obtained the Proca field equations in  $(2 + n)$ -dimensional spherically symmetric black hole spacetimes using the Ishibashi-Kodama formalism (see also [47]). Perturbations were separated in two distinct sectors: the vector-type sector, characterized by a single second-order differential equation describing  $d - 3$  decoupled degrees of freedom of the Proca field; the scalar-type sector, characterized by a coupled system of two second-order differential equations, describing the remaining 2 degrees of freedom. The study of [46] was centered in Hawking radiation and the coupled system was solved numerically. Yet, a possible strategy to analytically decouple the scalar-type sector remained elusive. In 2018, [48] has demonstrated the separability of the Proca field equations in  $d$ -dimensional Kerr-NUT-(A)dS geometries by using the latter called FKKS ansatz. [48] also performed a quasinormal mode analysis of Proca field perturbations in Kerr spacetime by using the separated equations, being able to describe two of the three polarizations of the field, whose results agreed with the ones previously obtained by solving directly the coupled system [49] (see also [50]). [51] performed a quasinormal mode analysis of Proca field perturbations in 4-dimensional Schwarzschild-AdS spacetime using the FKKS ansatz and taking the NUT parameter and angular momentum to zero. In particular, [51] showed that the FKKS ansatz decouples the scalar-type modes successfully, although it cannot describe the vector-type mode. Still, little is known about Proca field perturbations in higher-dimensional spacetimes. One of the objectives of this thesis is to bridge this gap.

## 1.5 Thesis outline

We study Proca field perturbations in higher-dimensional AdS and Schwarzschild-AdS spacetimes.

In Chapter 2, we review the Ishibashi-Kodama formalism [12–14] to study linear field perturbations in higher-dimensional static gravitational spacetimes, and apply it to Proca field perturbations in  $(d = 2 + n)$ -dimensional spherically symmetric black hole spacetimes. This was done in [46], although our equations are written in terms of “rescaled” variables as in [44, 45, 51], for which they become explicitly Schrödinger-like equations.

In Chapter 3, we apply the study of Chapter 2 to higher-dimensional AdS spacetimes, obtaining the exact normal mode solutions of Proca field perturbations, imposing Dirichlet boundary conditions at infinity.

In Chapter 4, we study Proca field quasinormal modes in higher-dimensional Schwarzschild-AdS spacetimes. Schwarzschild-AdS spacetime is proven to be linearly stable against vector-type and monopole Proca field perturbations, in any dimension. A numerical quasinormal mode analysis is performed for Proca field perturbations in 4, 5, 6, 7-dimensional Schwarzschild-AdS. Additionally, an analytical analysis of the quasinormal mode spectrum is performed for small black holes.

Appendix A reviews scalar and vector spherical harmonics in  $n$  dimensions, which are crucial to expand the Proca field in higher-dimensional spherically symmetric backgrounds.

Appendix B reviews the hypergeometric differential equation and the fundamental properties of the hypergeometric function.

Appendix C reviews Chandrasekhar’s approach to establish isospectrality between modes of different types of perturbations.



## Chapter 2

# Proca field perturbations

### 2.1 Proca field in curved spacetime

The action of a massive vector field (Proca field) minimally coupled to a generic  $d$ -dimensional curved spacetime with cosmological constant can be written as

$$S = \int d^d x \sqrt{-g} \left( \frac{R - 2\Lambda}{16\pi} - \frac{1}{2} \mu^2 A_\mu A^\mu - \frac{1}{4} F_{\mu\nu} F^{\mu\nu} \right) , \quad (2.1)$$

where  $g$  is the determinant of the metric,  $g_{\mu\nu}$ ,  $R$  is the Ricci scalar, defined as the trace of the Ricci tensor,  $R_{\mu\nu}$ ,  $\Lambda$  is the cosmological constant,  $A_\mu$  is the Proca field with mass  $\mu$  and  $F_{\mu\nu}$  is the Proca field strength, defined by

$$F_{\mu\nu} = \nabla_\mu A_\nu - \nabla_\nu A_\mu , \quad (2.2)$$

obeying the internal equations

$$\nabla_{[\mu} F_{\alpha\beta]} = 0 . \quad (2.3)$$

The equations of motion for the fields are obtained by applying the variational principle to the action Eq. (2.1). A variation with respect to  $g_{\mu\nu}$  yields the Einstein field equations for  $g_{\mu\nu}$

$$R_{\mu\nu} - \frac{1}{2} g_{\mu\nu} R + \Lambda g_{\mu\nu} = 8\pi T_{\mu\nu} , \quad (2.4)$$

where  $T_{\mu\nu}$  is the Proca stress-energy tensor, defined by

$$T_{\mu\nu} = \mu^2 A_\mu A_\nu + g^{\alpha\beta} F_{\mu\alpha} F_{\nu\beta} - g_{\mu\nu} \left( \frac{\mu^2}{2} A_\alpha A^\alpha + \frac{1}{4} F_{\alpha\beta} F^{\alpha\beta} \right) . \quad (2.5)$$

In addition, the Bianchi identities for  $g_{\mu\nu}$ ,

$$\nabla^\nu \left( R_{\mu\nu} - \frac{1}{2} g_{\mu\nu} R + \Lambda g_{\mu\nu} \right) = 0 , \quad (2.6)$$

imply the conservation law for  $T_{\mu\nu}$ ,

$$\nabla^\nu T_{\mu\nu} = 0 \quad . \quad (2.7)$$

Either by varying the action with respect to  $A_\mu$  or by using the conservation law for  $T_{\mu\nu}$ , one obtains the Proca field equations for  $A_\mu$

$$\nabla_\nu F^{\mu\nu} + \mu^2 A^\mu = 0 \quad . \quad (2.8)$$

Taking the divergence in Eq. (2.8), i.e.  $\nabla_\mu \nabla_\nu F^{\mu\nu} + \mu^2 \nabla_\mu A^\mu = 0$ , and due to the antisymmetry of  $F_{\mu\nu}$ , the Bianchi identity for  $A_\mu$  becomes

$$\nabla^\mu A_\mu = 0 \quad . \quad (2.9)$$

It is important to point out that, when  $\mu \neq 0$ , Eq. (2.9) is a direct consequence of the field equations Eq. (2.8), so that  $A_\mu$  describes  $d - 1$  degrees of freedom, as one component of the field can always be obtained from the others by integrating Eq. (2.9). On the other hand, for  $\mu = 0$ ,  $A_\mu$  corresponds to the Maxwell field and the equations Eq. (2.8) become invariant under the gauge transformation

$$A^\mu \rightarrow A^\mu + \partial^\mu \chi \quad , \quad (2.10)$$

where  $\chi$  is a scalar field. The Bianchi identity Eq. (2.9) is no longer a consequence of the field equations: instead it becomes the usual Lorenz gauge for the Maxwell field. Even after imposing this gauge, a residual gauge freedom remains as Eq. (2.9) is invariant under Eq. (2.10) if  $\chi$  obeys the Klein-Gordon field equation, i.e.  $\nabla_\mu \nabla^\mu \chi = 0$ . Hence, the Maxwell field describes  $d - 2$  degrees of freedom. In  $d = 4$ , the previous discussion implies that, while the Proca field describes three degrees of freedom, corresponding to two transversal polarizations and one longitudinal polarization, the residual gauge freedom of the Maxwell field eliminates the longitudinal polarization, so that in total the Maxwell field describes two degrees of freedom, corresponding to the usual two transversal polarizations.

The full physical picture of a Proca field propagating in curved spacetime can only be obtained by solving Eqs. (2.4) and (2.8) simultaneously for both  $g_{\mu\nu}$  and  $A_\mu$ . Since this cannot be done analytically, we perform a perturbative approach, taking only into account linear perturbations around the trivial solution  $A_\mu = 0$ . Since  $T_{\mu\nu}$  in Eq. (2.5) is of second order in  $A_\mu$ , perturbations in the Proca field do not induce a curvature perturbation on  $g_{\mu\nu}$  at first order. Thus, at first order, the Einstein field equations Eq. (2.4) completely decouple from the Proca field equations Eq. (2.8), reducing to the Einstein field equations in vacuum with cosmological constant: the metric  $g_{\mu\nu}$  corresponds to the background metric, as if no perturbations in  $A_\mu$  were made. One is left with the Proca field equations Eq. (2.8), which are to be solved for  $A_\mu$  in the fixed background. In the next section, we show how the Proca field can be decomposed in spacetimes with warped product topology, writing Eq. (2.8) in this rather generic background, following closely [12, 14, 19, 46, 47].

## 2.2 Proca field perturbations in spaces with warped product topology

### 2.2.1 Proca field equations in spaces with warped product topology

We consider a  $(d = m + n)$ -dimensional spacetime, with  $d \geq 4$  and  $n \geq 2$ , whose manifold structure can be factorized as the warped product  $\mathcal{M}^d = \mathcal{N}^m \times \mathcal{K}^n$ . For one to distinguish between tensors living on the different manifolds  $\mathcal{M}^d$ ,  $\mathcal{N}^m$  and  $\mathcal{K}^n$ , we use greek indices  $\mu, \nu, \dots$  for tensors on  $\mathcal{M}^d$ , latin indices in the range  $a, b, \dots, h$  for tensors on  $\mathcal{N}^m$  and latin indices in the range  $i, j, \dots$  for tensors on  $\mathcal{K}^n$ . The line element of  $(\mathcal{M}^d, g)$  is written in coordinates  $x^\mu = (y^a, z^i)$  as

$$g_{\mu\nu} dx^\mu dx^\nu = h_{ab}(y) dy^a dy^b + r^2(y) \gamma_{ij}(z) dz^i dz^j \quad , \quad (2.11)$$

where  $h_{ab}(y)$  and  $\gamma_{ij}(z)$  are the metrics on  $\mathcal{N}^m$  and  $\mathcal{K}^n$ , respectively, and  $r(y)$  is the scalar field that warps the product. We also assume that  $(\mathcal{N}^m, h)$  is a Lorentzian manifold, and  $(\mathcal{K}^n, \gamma)$  is a Riemannian manifold with constant curvature, satisfying

$$\hat{R}_{ij} = K(n-1)\gamma_{ij} \quad , \quad (2.12)$$

with  $K = 0$  (foliated by planes),  $K = 1$  (foliated by spheres) or  $K = -1$  (foliated by hyperboloids). The non-vanishing Christoffel symbols  $\Gamma_{\nu\rho}^\mu$  associated to  $(\mathcal{M}^d, g)$  can be written in coordinates  $x^\mu$  as

$$\Gamma_{bc}^a = \tilde{\Gamma}_{bc}^a \quad , \quad \Gamma_{ij}^a = -r(\partial^a r) \gamma_{ij} \quad , \quad \Gamma_{aj}^i = \frac{\partial_a r}{r} \delta_j^i \quad , \quad \Gamma_{jk}^i = \hat{\Gamma}_{jk}^i \quad , \quad (2.13)$$

where  $\tilde{\Gamma}_{bc}^a$  and  $\hat{\Gamma}_{jk}^i$  are the Christoffel symbols associated to  $(\mathcal{N}^m, h)$  and  $(\mathcal{K}^n, \gamma)$ , respectively. The projections of Eq. (2.8) on  $\mathcal{N}^m$  and  $\mathcal{K}^n$  are written as

$$\tilde{\nabla}_b F^{ab} + n \frac{\partial_b r}{r} F^{ab} + \hat{\nabla}_j F^{aj} + \mu^2 A^a = 0 \quad , \quad (2.14)$$

$$\tilde{\nabla}_b F^{ib} + n \frac{\partial_b r}{r} F^{ib} + \hat{\nabla}_j F^{ij} + \mu^2 A^i = 0 \quad , \quad (2.15)$$

where  $\tilde{\nabla}_b$  and  $\hat{\nabla}_i$  denote the covariant derivatives associated to  $(\mathcal{N}^m, h)$  and  $(\mathcal{K}^n, \gamma)$ , respectively. These equations are supplemented with the Bianchi identity Eq. (2.9)

$$\tilde{\nabla}_a A^a + n \frac{\partial_a r}{r} A^a + \hat{\nabla}_i A^i = 0 \quad . \quad (2.16)$$

### 2.2.2 Decomposition of the Proca field and harmonic expansion

To further simplify the field equations, one exploits the symmetric structure of the  $\mathcal{K}^n$  space, studying how the field behaves under a transformation in the  $z^i$  coordinates. Essentially, the strategy is to project the field into components that are orthogonal to  $\mathcal{K}^n$  and components that are tangent to  $\mathcal{K}^n$ . Then, according to their tensorial behaviour on  $\mathcal{K}^n$ , these are expanded in the appropriate harmonics. The  $A_\mu$

field can be written as

$$A_\mu dx^\mu = A_a^{(o)} dy^a + A_i^{(t)} dz^i \quad , \quad (2.17)$$

where  $A_a^{(o)}$  denotes the projection of  $A_\mu$  orthogonal to  $\mathcal{K}^n$  and  $A_i^{(t)}$  denotes the projection of  $A_\mu$  tangent to  $\mathcal{K}^n$ . The latter can be further decomposed using the Helmholtz-Hodge decomposition [12], which allows one to write uniquely  $A_i^{(t)}$ , a covector field living on the cotangent space of a Riemannian manifold (in this case  $\mathcal{K}^n$ ), as the sum of a longitudinal covector field,  $\hat{\nabla}_i A^{(S)}$ , and a transverse covector field,  $A_i^{(V)}$ :

$$A_i^{(t)} = A_i^{(V)} + \hat{\nabla}_i A^{(S)} \quad , \quad \hat{\nabla}^i A^{(V)}_i = 0 \quad . \quad (2.18)$$

$A_a^{(o)}$  and  $A^{(S)}$  behave as scalars on the cotangent space of  $\mathcal{K}^n$  and are called the scalar-type components of  $A_\mu$ , while  $A_i^{(V)}$ , a covector on the cotangent space of  $\mathcal{K}^n$ , is called the vector-type component of  $A_\mu$  (we will call both  $A^{(V)i}$  and  $A_i^{(V)}$  vector-type components, as they can always be related through  $A_i^{(V)} = \gamma_{ij} A^{(V)j}$ ). When the Proca field is written in terms of these variables, equations Eqs. (2.14)-(2.16) are decomposed in two completely decoupled sectors: the scalar-type sector, containing equations that only relate scalar-type variables; the vector-type sector, described by a single equation for the vector-type variable. We will come back to this in Section 2.2.3. The scalar-type components of  $A_\mu$  can be expanded in scalar harmonics  $\mathbb{S}_{\vec{k}_s}$ , which form a complete basis on  $\mathcal{K}^n$ , satisfying

$$\left( \hat{\square} + k_s^2 \right) \mathbb{S}_{\vec{k}_s} = 0 \quad , \quad \int d\gamma_n \mathbb{S}_{\vec{k}_s} \mathbb{S}_{\vec{k}'_s} = \delta_{\vec{k}_s \vec{k}'_s} \quad , \quad (2.19)$$

where  $\hat{\square} = \gamma^{ij} \hat{\nabla}_i \hat{\nabla}_j$  and  $-k_s^2$  is the eigenvalue of  $\hat{\square}$  on  $\mathcal{K}^n$ . If  $\mathcal{K}^n = \mathcal{S}^n$ , one has the result (see Appendix A)

$$k_s^2 = l(l + n - 1) \quad , \quad l = 0, 1, 2, \dots \quad , \quad (2.20)$$

whereas if  $K = -1, 0$ ,  $k_s$  takes continuous values bounded by a lower limit [15]. We choose a basis such that to each harmonic is associated an index  $\vec{k}_s$ , which encodes not only the eigenvalue of the  $\mathcal{K}^n$  manifold, but also the eigenvalues of the lower-dimensional embedded spaces (see Appendix A). Similarly, the vector-type component of  $A_\mu$  can be expanded in vector harmonics  $\mathbb{V}_{\vec{k}_v i}$ , which also form a complete basis on  $\mathcal{K}^n$ , satisfying

$$\left( \hat{\square} + k_v^2 \right) \mathbb{V}_{\vec{k}_v i} = 0 \quad , \quad \int d\gamma_n \gamma^{ij} \mathbb{V}_{\vec{k}_v i} \mathbb{V}_{\vec{k}'_v j} = \delta_{\vec{k}_v \vec{k}'_v} \quad , \quad \hat{\nabla}_i \mathbb{V}_{\vec{k}_v}^i = 0 \quad . \quad (2.21)$$

If  $\mathcal{K}^n = \mathcal{S}^n$ , one has the result (see Appendix A)

$$k_v^2 = l(l + n - 1) - 1 \quad , \quad l = 1, 2, 3, \dots \quad , \quad (2.22)$$

whereas if  $K = -1, 0$ ,  $k_v$  takes continuous values [12]. We expand the scalar-type components of the field,  $\{A_a^{(o)}, A^{(S)}\}$ , as

$$A_a^{(o)}(y, z) = \sum_{\vec{k}_s} A_{\vec{k}_s a}^{(o)}(y) \mathbb{S}_{\vec{k}_s}(z) \quad , \quad (2.23)$$

$$A^{(S)}(y, z) = \sum_{\vec{k}_s} C_{\vec{k}_s}^-(y) \mathbb{S}_{\vec{k}_s}^-(z) \quad , \quad (2.24)$$

while for the vector-type component,  $A_i^{(V)}$ , one has

$$A_i^{(V)}(y, z) = \sum_{\vec{k}_v} \phi_{\vec{k}_v}^-(y) \mathbb{V}_{\vec{k}_v i}^-(z) \quad . \quad (2.25)$$

Here,  $C_{\vec{k}_s}^-(y)$  and  $\phi_{\vec{k}_s}^-(y)$  are scalar fields on  $\mathcal{N}^m$ , while  $A_{\vec{k}_s a}^-(y)$  is a covector field on the cotangent space of  $\mathcal{N}^m$ . Note that the  $m + 1$  scalar-type components cover  $m$  degrees of freedom, as Eq. (2.9) needs to be satisfied, whereas the vector-type component covers  $n - 1$  degrees of freedom (note the transverse condition of  $\mathbb{V}_{\vec{k}_v i}^-$  in Eq. (2.21)). These variables cover in total  $n + m - 1 = d - 1$  degrees of freedom, as expected for a Proca field.

### 2.2.3 Separation of Proca field equations

The Helmholtz-Hodge decomposition allows one to separate the Proca field equations in two completely decoupled sectors: the scalar-type sector and the vector-type sector. To see this, note firstly that one can use the Helmholtz-Hodge decomposition on  $F^{aj}$  in Eq. (2.14), so that the divergenceless vector of the decomposition (corresponding to the vector-type variable) completely vanishes and Eq. (2.14) relates only scalar-type terms. The same argument can be used to write Eq. (2.16) in terms of scalar-type components only. Note that Eq. (2.15) can be decomposed in a similar fashion. Indeed, Eq. (2.15) has the structure of  $\eta^i = 0$ , where  $\eta^i$  can be found by expanding  $F^{bi}$  in terms of  $\{A^{(o)b}, A^{(S)}, A^{(V)i}\}$ . Thus, one can decompose Eq. (2.15) as  $\hat{\nabla}^i \eta_{(S)} + \eta_{(V)}^i = 0$  and, taking the divergence on  $\mathcal{K}^n$ , i.e.,  $\hat{\nabla}_i \eta^i = 0$ , yields

$$\hat{\square} \eta_{(S)} = 0 \quad , \quad (2.26)$$

which relates scalar-type components only. On the other hand, taking the Laplacian on  $\mathcal{K}^n$ , i.e.,  $\hat{\square} \eta^i = 0$ , yields

$$\hat{\square} \eta_{(V)}^i - \hat{R}^{ij} \eta_{(V)j} = 0 \quad , \quad (2.27)$$

where we used  $\hat{\square} \hat{\nabla}^i \eta_{(S)} = \hat{\nabla}^i \hat{\square} \eta_{(S)} + \hat{R}^{ij} \hat{\nabla}_j \eta_{(S)}$  and substituted Eq. (2.26), as well as  $\hat{\nabla}^i \eta_{(S)} = -\eta_{(V)}^i$ . Since Eq. (2.12) holds by assumption, Eq. (2.27) is for the vector-type component only. To see explicitly this decomposition, we now substitute the expanded Proca field in the equations of motion. Substitution in Eq. (2.14) yields

$$\sum_{\vec{k}_s} \left[ \tilde{\nabla}_b \left( \tilde{\nabla}^a A_{\vec{k}_s}^b - \tilde{\nabla}^b A_{\vec{k}_s}^a \right) + n \frac{\tilde{\nabla}_b r}{r} \left( \tilde{\nabla}^a A_{\vec{k}_s}^b - \tilde{\nabla}^b A_{\vec{k}_s}^a \right) + \left( \frac{k_s^2}{r^2} + \mu^2 \right) A_{\vec{k}_s}^a - \frac{k_s^2}{r^2} \partial^a C_{\vec{k}_s}^- \right] \mathbb{S}_{\vec{k}_s}^- = 0 \quad , \quad (2.28)$$

where we used the transverse condition  $\hat{\nabla}_i \mathbb{V}_{\vec{k}_v}^i = 0$ . Furthermore, Eq. (2.16) is written as

$$\sum_{\vec{k}_s} \left[ \tilde{\nabla}_b A_{\vec{k}_s}^b + n \frac{\partial_b r}{r} A_{\vec{k}_s}^b - \frac{k_s^2}{r^2} C_{\vec{k}_s}^- \right] \mathbb{S}_{\vec{k}_s}^- = 0 \quad . \quad (2.29)$$

These are clearly equations belonging to the scalar-type sector. On the other hand, Eq. (2.15) contains both scalar-type and vector-type variables:

$$\begin{aligned} & \sum_{\vec{k}_v} \left[ \tilde{\square} \phi_{\vec{k}_v} + \frac{(n-2)}{r} (\partial^b r) (\partial_b \phi_{\vec{k}_v}) - \left( \frac{k_v^2 + \hat{R}/n}{r^2} + \mu^2 \right) \phi_{\vec{k}_v} \right] \mathbb{V}_{\vec{k}_v}^i + \\ & + \sum_{\vec{k}_s} \left[ \tilde{\square} C_{\vec{k}_s} + (n-2) \frac{\partial_b r}{r} \partial^b C_{\vec{k}_s} - \mu^2 C_{\vec{k}_s} - \hat{\nabla}_b A_{\vec{k}_s}^b - (n-2) \frac{\partial_b r}{r} A_{\vec{k}_s}^b \right] \hat{\nabla}^i \mathbb{S}_{\vec{k}_s} = 0 \quad , \end{aligned} \quad (2.30)$$

where we used

$$\hat{\nabla}_j \hat{\nabla}_i \mathbb{V}_{\vec{k}_v}^j = \hat{\nabla}_i \hat{\nabla}_j \mathbb{V}_{\vec{k}_v}^j + \hat{R}_{mi} \mathbb{V}_{\vec{k}_v}^m \quad , \quad (2.31)$$

with  $\hat{R}_{mi}$  given by Eq. (2.12). Taking the divergence  $\hat{\nabla}_i$  of Eq. (2.30) yields

$$\sum_{\vec{k}_s} \left[ \tilde{\square} C_{\vec{k}_s} + (n-2) \frac{\partial_b r}{r} \partial^b C_{\vec{k}_s} - \mu^2 C_{\vec{k}_s} - \hat{\nabla}_b A_{\vec{k}_s}^b - (n-2) \frac{\partial_b r}{r} A_{\vec{k}_s}^b \right] \left( -k_s^2 \mathbb{S}_{\vec{k}_s} \right) = 0 \quad , \quad (2.32)$$

which is an equation relating scalar-type components only, whereas taking the Laplacian  $\hat{\square}$  yields

$$\begin{aligned} & \sum_{\vec{k}_v} \left[ \tilde{\square} \phi_{\vec{k}_v} + \frac{(n-2)}{r} (\partial^b r) (\partial_b \phi_{\vec{k}_v}) - \left( \frac{k_v^2 + \hat{R}/n}{r^2} + \mu^2 \right) \phi_{\vec{k}_v} \right] \left( -k_v^2 \mathbb{V}_{\vec{k}_v}^i \right) + \\ & + \sum_{\vec{k}_s} \left[ \tilde{\square} C_{\vec{k}_s} + (n-2) \frac{\partial_b r}{r} \partial^b C_{\vec{k}_s} - \mu^2 C_{\vec{k}_s} - \hat{\nabla}_b A_{\vec{k}_s}^b - (n-2) \frac{\partial_b r}{r} A_{\vec{k}_s}^b \right] \left( \hat{R}^{ij} \hat{\nabla}_j \mathbb{S}_{\vec{k}_s} - \hat{\nabla}^i \hat{\square} \mathbb{S}_{\vec{k}_s} \right) = 0 \quad , \end{aligned} \quad (2.33)$$

where we again used the commutator Eq. (2.31). The term proportional to  $\hat{\nabla}^i \hat{\square} \mathbb{S}_{\vec{k}_s}$  vanishes from Eq. (2.32), and substituting Eq. (2.30) in Eq. (2.33) gives

$$\sum_{\vec{k}_v} \left[ \tilde{\square} \phi_{\vec{k}_v} + \frac{(n-2)}{r} (\partial^b r) (\partial_b \phi_{\vec{k}_v}) - \left( \frac{k_v^2 + \hat{R}/n}{r^2} + \mu^2 \right) \phi_{\vec{k}_v} \right] \left( -k_v^2 - K(n-1) \right) \mathbb{V}_{\vec{k}_v}^i = 0 \quad , \quad (2.34)$$

which is an equation for the vector-type component only. We then have shown explicitly that the Proca field equations give rise to two completely decoupled sectors: the scalar-type sector, described by Eqs. (2.28), (2.29) and (2.32); and the vector-type sector, described by Eq. (2.34).

Due to the orthogonality conditions of the harmonics, the resulting equations of motion need to be satisfied for all  $\vec{k}_s, \vec{k}_v$  in the sums. In what follows, we will drop the sums as well as the indexes  $\vec{k}_s, \vec{k}_v$  in the fields, with the constant reminder that we are solving for the infinitely many modes of the system. The scalar-type equations can be further simplified by substituting Eq. (2.29) in Eq. (2.28), giving an expression for  $A^a$  only:

$$\tilde{\square} A^a - \hat{R}_b^a A^b + n \frac{\partial_b r}{r} \tilde{\nabla}_b A^a - \left( \frac{k_s^2}{r^2} + \mu^2 \right) A^a + n \tilde{\nabla}^a \left( \frac{\partial_b r}{r} \right) A^b + \frac{2 \partial^a r}{r} \left( \hat{\nabla}_b A^b + n \frac{\partial_b r}{r} A^b \right) = 0 \quad , \quad (2.35)$$

whereas  $C$  is determined from Eq. (2.32)

$$\tilde{\square} C + (n-2) \frac{\partial_b r}{r} \partial_b C - \left( \mu^2 + \frac{k_s^2}{r^2} \right) C + 2 \frac{\partial_b r}{r} A_b = 0 \quad . \quad (2.36)$$

These are supplemented by the Bianchi identity

$$\tilde{\nabla}_b A^b + n \frac{\partial_b r}{r} A^b - \frac{k_s^2}{r^2} C = 0 \quad . \quad (2.37)$$

For completeness, we also write the vector-type equation of motion Eq. (2.34) in the more compact form

$$\tilde{\square} \phi + \frac{(n-2)}{r} (\partial^b r) (\partial_b \phi) - \left[ \frac{k_v^2 + \hat{R}/n}{r^2} + \mu^2 \right] \phi = 0 \quad . \quad (2.38)$$

## 2.2.4 Proca field perturbations in a spherically symmetric $(2+n)$ -background

The analysis done so far, leading to Eqs. (2.35)-(2.38), holds for all spacetimes with the warped product topology assumed in Section 2.2.1. In this section, we study how these equations simplify when we restrict ourselves to the case  $m = 2$ , with  $y^a = (t, r)$  and line element on  $\mathcal{N}^2$  given by

$$h_{ab} dy^a dy^b = -f(r) dt^2 + \frac{1}{f(r)} dr^2 \quad , \quad (2.39)$$

where  $f(r)$  is a scalar field on  $\mathcal{N}^2$  depending only on  $r$ . Furthermore, we assume  $r(y) = r$  and  $\mathcal{K}^n = \mathcal{S}^n$ , so that Eqs. (2.20) and (2.22) hold. Equation (2.11) then becomes

$$g_{\mu\nu} dx^\mu dx^\nu = -f(r) dt^2 + \frac{1}{f(r)} dr^2 + r^2 d\Omega_n^2 \quad , \quad (2.40)$$

where  $d\Omega_n^2$  is the line element of the  $n$ -sphere. The background geometry Eq. (2.40) still includes a large variety of interesting cases, such as the  $(2+n)$ -dimensional spherically symmetric black hole spacetimes. The non-vanishing Christoffel symbols and Ricci tensor components of  $h_{ab}$  are

$$\tilde{\Gamma}_{tt}^r = \frac{f f'}{2} \quad , \quad \tilde{\Gamma}_{rt}^t = \frac{f'}{2f} \quad , \quad \tilde{\Gamma}_{rr}^r = -\frac{f'}{2f} \quad , \quad \tilde{R}_t^t = \tilde{R}_r^r = -\frac{f''}{2} \quad . \quad (2.41)$$

### Higher multipoles

Using the results of Sections 2.2.2 and 2.2.3, the vector-type component of the Proca field covers  $d - 3$  degrees of freedom in the spherically symmetric background. The vector-type equation of motion Eq. (2.38) becomes

$$\hat{\mathcal{D}}_l u_V = 0 \quad , \quad (2.42)$$

where we defined  $\phi(r, t) = u_V(r, t) r^{1-\frac{n}{2}}$  and the operator  $\hat{\mathcal{D}}_l$  as

$$\hat{\mathcal{D}}_l = -\partial_t^2 + \partial_{r_*}^2 - f \left( \frac{(l+1)(l+n-2)}{r^2} + \frac{(n-2)(n-4)}{4r^2} f + \frac{(n-2)}{2r} f' + \mu^2 \right) \quad . \quad (2.43)$$

The remaining two degrees of freedom of the Proca field, described by its scalar-type components, obey the equations of motion Eqs. (2.35)-(2.37). In the background Eq. (2.40), these are written as

$$\hat{\mathcal{D}}_l u_1 + \frac{(n-2)f}{r^2} \left( 1 - f + \frac{r f'}{2} \right) u_1 + f' (\partial_t u_2 - \partial_{r_*} u_1) = 0 \quad , \quad (2.44)$$

$$\hat{\mathcal{D}}_l u_2 + f \left( \frac{n-2}{r^2} - \frac{2(n-1)}{r^2} f + \frac{(n-1)}{r} f' \right) u_2 - \frac{f}{r} \left( f' - \frac{2f}{r} \right) u_3 = 0 \quad , \quad (2.45)$$

$$\hat{\mathcal{D}}_l u_3 + f \frac{(n-2)}{r^2} u_3 + \frac{2fl(l+n-1)}{r^2} u_2 = 0 \quad , \quad (2.46)$$

$$\partial_t u_1 - \partial_{r_*} u_2 = \frac{f}{r} \left( \frac{n}{2} u_2 - u_3 \right) \quad , \quad (2.47)$$

where  $u_1(t, r)$ ,  $u_2(t, r)$  and  $u_3(t, r)$  are defined by  $A_t(t, r) = u_1(t, r)r^{-n/2}$ ,  $A_r(t, r) = u_2(t, r)f^{-1}r^{-n/2}$  and  $C(t, r) = \frac{u_3(t, r)}{l(l+n-1)}r^{1-\frac{n}{2}}$ . Without loss of generality, we can choose  $u_1$  to be completely determined from  $u_2, u_3$ , so that the scalar-type physical degrees of freedom are completely described by the coupled system Eqs. (2.45) and (2.46). This system may be written

$$\hat{\mathcal{D}}_l \mathbf{u} = \mathbf{K} \mathbf{u} \quad , \quad (2.48)$$

where  $\mathbf{K}$  is a  $2 \times 2$  matrix that couples the modes and  $\mathbf{u} = (u_2 \quad u_3)^T$ . If  $\mathbf{K}$  is diagonalizable, one can write  $\mathbf{K} = \mathbf{P}^{-1} \mathbf{M} \mathbf{P}$ , with  $\mathbf{M}$  diagonal and having entries given by the eigenvalues of  $\mathbf{K}$ , and  $\mathbf{P}$  with columns given by the corresponding eigenvectors. Making  $\mathbf{q} = \mathbf{P} \mathbf{u}$ , one sees that if  $\partial_{r_*} \mathbf{P}^{-1} = 0$ , the system can be trivially decoupled.

### Monopole mode

Modes with  $l = 0$  are spherically symmetric, having only one physical degree of freedom, independently of the dimension of the spacetime. Furthermore, this is a scalar-type degree of freedom, as vector spherical harmonics are only defined for  $l \geq 1$ . Setting  $u_3 = 0$  ( $\hat{\nabla}^i \mathbb{S} = 0$ ) in Eq. (2.45), one finds the equation of motion ruling monopole Proca perturbations in the spherically symmetric background to be

$$\left( -\partial_t^2 + \partial_{r_*}^2 - f \left( \frac{n(n+2)}{4r^2} f - \frac{n}{2r} f' + \mu^2 \right) \right) u_2 = 0 \quad . \quad (2.49)$$

## 2.3 Maxwell field perturbations

A Maxwell (electromagnetic) field perturbation can be viewed as the limit of a Proca field perturbation when  $\mu = 0$ . However, in this case, the field equations are gauge-invariant and the field loses one physical degree of freedom, which becomes a pure-gauge one. Thus, one cannot simply set  $\mu = 0$  in the results above, as the equations of motion found only hold for  $\mu \neq 0$ . Equation (2.9) no longer follows directly from the field equations, becoming simply a gauge choice. In order to distinguish between the physical degrees of freedom and the pure-gauge ones, it is useful to work with gauge-invariant variables rather than with  $A_\mu$ . Under the gauge transformation Eq. (2.10), the fields transform as (using the notation of Eqs. (2.17) and (2.18))

$$A_a^{(o)} \rightarrow A_a^{(o)} + \partial_a \chi \quad , \quad A_i^{(t)} = A_i^{(V)} + \hat{\nabla}_i A^{(S)} \rightarrow A_i^{(V)} + \hat{\nabla}_i \left( A^{(S)} + \chi \right) \quad . \quad (2.50)$$

One sees that the gauge freedom in  $A_\mu$  is only scalar, with the vector-type component of the Maxwell field being gauge-invariant. This means that, even in the  $\mu = 0$  limit, the vector-type component of  $A_\mu$  covers the same  $n - 1$  degrees of freedom as in the massive case. These are described by Eq. (2.38) after setting  $\mu = 0$ . The scalar-type sector is then expected to describe only  $m - 1$  degrees of freedom in the massless case, in order for the Maxwell field to have  $d - 2$  degrees of freedom. To see this, we start from Eqs. (2.14) and (2.15). Setting  $\mu = 0$  one has

$$\tilde{\nabla}_b \left( \tilde{\nabla}^a A^b - \tilde{\nabla}^b A^a \right) + n \frac{\partial_b r}{r} \left( \tilde{\nabla}^a A^b - \tilde{\nabla}^b A^a \right) + \frac{k_s^2}{r^2} (A^a - \partial^a C) = 0 \quad , \quad (2.51)$$

$$\tilde{\nabla}_b (A^b - \partial^b C) + (n - 2) \frac{\partial_b r}{r} (A^b - \partial^b C) = 0 \quad . \quad (2.52)$$

This motivates the definition of the field

$$B^a = A^a - \partial^a C \quad , \quad (2.53)$$

which is gauge-invariant. Indeed, one can expand  $\chi(y, z) = \sum_{\vec{k}_s} \chi_{\vec{k}_s}(y) \mathbb{S}_{\vec{k}_s}(z)$ , so that, under the gauge transformation,  $A_a \rightarrow A_a + \partial_a \chi$  and  $C \rightarrow C + \chi$ . In terms of  $B^a$ , the equations of motion become

$$\tilde{\nabla}_b \left( \tilde{\nabla}^a B^b - \tilde{\nabla}^b B^a \right) + n \frac{\partial_b r}{r} \left( \tilde{\nabla}^a B^b - \tilde{\nabla}^b B^a \right) + \frac{k_s^2}{r^2} B^a = 0 \quad , \quad (2.54)$$

$$\tilde{\nabla}_b (r^{n-2} B^b) = 0 \quad . \quad (2.55)$$

Note that this transformation completely removes a pure-gauge degree of freedom from the system, as  $\{A^a, C\} \rightarrow \{B^a\}$ . This only happens in the massless case, where  $B^a$  factorizes. So, as expected, the Maxwell scalar-type sector only describes  $m - 1$  (physical) degrees of freedom.

In the spherically symmetric background described in Section 2.2.4, Eqs. (2.54) and (2.55) give the equation of motion for the physical mode

$$\hat{\mathcal{D}}_i^{s=1} u_{(\text{EM})} = 0 \quad , \quad (2.56)$$

where we defined  $B_r(t, r) = u_{(\text{EM})}(t, r) f^{-1} r^{1-\frac{n}{2}}$  and the operator

$$\hat{\mathcal{D}}_i^{s=1} = -\partial_t^2 + \partial_{r_*}^2 - f \left( \frac{l(l+n-1)}{r^2} + \frac{n(n-2)}{4r^2} f - \frac{n-2}{2r} f' \right) \quad . \quad (2.57)$$

On the other hand,  $B_t(t, r) = u_t(t, r) r^{1-\frac{n}{2}}$  is completely determined from  $u_{(\text{EM})}$  by the relation

$$\partial_t u_t(t, r) = \frac{\partial_{r_*} (u_{(\text{EM})} r^{\frac{n}{2}-1})}{r^{\frac{n}{2}-1}} \quad . \quad (2.58)$$

In this case, the scalar-type sector of the Maxwell field covers one degree of freedom, as expected.

The physical degree of freedom,  $u_{(\text{EM})}$ , can be also related to the pure-gauge degree of freedom,  $C$ , which turns out to be very important in the interpretation of the results, specially the numerical ones.

We take Eq. (2.36) and write it in terms of the gauge-invariant variables,  $B_a$ , as

$$\tilde{\square}C + n\frac{\partial^b r}{r}\partial_b C - \left(\mu^2 + \frac{k_s^2}{r^2}\right)C + 2\frac{\partial^b r}{r}B_b = 0 \quad . \quad (2.59)$$

In the spherically symmetric background, Eq. (2.59) reads

$$\hat{\mathcal{D}}_l^{s=0}(ru_3) - \mu^2 fru_3 = 2l(l+n-1)f^2 r^{\frac{n}{2}-1}B_r \quad , \quad (2.60)$$

where we defined the operator

$$\hat{\mathcal{D}}_l^{s=0} = \partial_{r_*}^2 - \partial_t^2 - f \left( \frac{l(l+n-1)}{r^2} + \frac{n(n-2)}{4r^2}f + \frac{n}{2r}f' \right) \quad , \quad (2.61)$$

which rules linear scalar field perturbations on a spherically symmetric background, i.e.  $\hat{\mathcal{D}}_l^{s=0}\chi = 0$  for a perturbed scalar field  $\chi$  [30]. In the massless limit, the RHS of Eq. (2.60) vanishes after applying  $\hat{\mathcal{D}}_l^{s=1}$ , with Eq. (2.60) becoming

$$\hat{\mathcal{D}}_l^{s=1} \left( f^{-1} \hat{\mathcal{D}}_l^{s=0}(ru_3) \right) = 0 \quad . \quad (2.62)$$

Thus, in the massless limit, one can completely factorize the equation of motion for  $u_3$  in two wave equations: the “inner” one, for  $ru_3$ , satisfying the scalar field equation; the “outer one”, for  $u_{(\text{EM})}$ , satisfying the scalar-type Maxwell field equation. If  $\hat{\mathcal{D}}_l^{s=0}(ru_3) = 0$ ,  $u_{(\text{EM})} = u_t = 0$  and, from the definition of  $B_a$ ,  $A_a = \partial_a C$  are pure-gauge. Thus, the degree of freedom described by the “inner” wave equation only has physical significance when  $\mu \neq 0$ . In the small-mass limit, it is however reasonable to expect its modes to approach the modes of scalar field perturbations. On the other hand,  $u_{(\text{EM})}$  is gauge-invariant and the degree of freedom described by the “outer” wave-equation remains physical in the massless limit. In the small-mass limit, its modes are expected to approach those of scalar-type Maxwell perturbations. This allows us to identify the polarizations in the (in principle) coupled scalar-type sector: one just takes the small-mass limit of the Proca perturbation and compares its modes with those of scalar field and Maxwell field (scalar-type) perturbations.

Lastly, note that the results obtained in this section are for  $l \geq 1$ . It is known that the monopole mode of a Maxwell perturbation does not have dynamical degrees of freedom [44, 46, 53]. Indeed, in this case, the field equations are simply given by

$$\tilde{\nabla}^b \left( r^n \tilde{F}_{ab} \right) = 0 \quad , \quad (2.63)$$

where  $\tilde{F}_{ab}$  is the gauge-invariant tensor living only on  $\mathcal{N}^2$  (omitting the  $\vec{k}_s$  indices),

$$\tilde{F}_{ab} = \tilde{\nabla}_a A_b - \tilde{\nabla}_b A_a \quad , \quad (2.64)$$

which completely determines the single degree of freedom of the system. In the background Eq. (2.40), Eq. (2.63) reads

$$\partial_t \tilde{F}_{tr} = 0 \quad , \quad \partial_r \left( r^n \tilde{F}_{tr} \right) = 0 \quad , \quad (2.65)$$

and so

$$\tilde{F}_{tr}(t, r) = \frac{Q}{r^n} \quad , \quad (2.66)$$

where  $Q$  is a constant, which can be interpreted as the total charge of the system. Thus, the unique degree of freedom of the system, described by  $\tilde{F}_{tr}$ , is non-dynamical, with  $A_\mu$  being just the sum of a pure-gauge term and a static Coulomb-like field. Observe that this is precisely the result one expects from performing the multipole expansion of the electric potential outside a charge distribution.

## Chapter 3

# Normal modes of Proca field perturbations in $d$ -dimensional AdS

### 3.1 Initial considerations and boundary conditions

In this chapter, we apply the formalism developed in Chapter 2 to a  $d$ -dimensional AdS background. We further assume that the perturbations have time-dependence of the form  $u(t, r) = u(r)e^{-i\omega t}$ , where  $\omega$  are interpreted as the mode frequencies. By doing so, the perturbation equations become eigenvalue equations for  $\omega$  with associated eigenfunctions  $u$

$$\partial_{r_*}^2 u + (\omega^2 - V(r)) u = 0 \quad . \quad (3.1)$$

In the literature, Eq. (3.1) is usually called a Schrödinger-like equation, and  $V$  is interpreted as an effective potential that rules the dynamics of the perturbations. As stated in Chapter 1, the choice of boundary conditions in asymptotically AdS spacetimes is a subtle question, as not all boundary conditions ensure well-defined dynamics for the fields [19]. [19] showed that Maxwell field perturbations in  $d \geq 7$  AdS require the Dirichlet boundary condition at spatial infinity, i.e.  $u(r = \infty) = 0$ , to ensure square-integrability of the solution, in the sense of  $\int_0^\infty u^* u f^{-1} dr$ . On the other hand, for  $d = 4, 5, 6$ -dimensional AdS, a whole one-parameter family of boundary conditions is allowed, including the usual Dirichlet and Neumann boundary conditions. For Proca field perturbations, the Dirichlet boundary condition seems to be required for all spacetime dimensions, with an interesting exception occurring in 4-dimensional AdS<sup>1</sup>. In the latter case, while for  $\mu^2 L^2 \geq 3/4$  one must take the Dirichlet boundary condition, for  $0 < \mu^2 L^2 < 3/4$  a whole one-parameter family of boundary conditions is again allowed. This is particularly intriguing, as the potential remains diverging at infinity for masses in this range.

In this work, we always impose Dirichlet boundary conditions on the fields at spatial infinity, as these seem to be the most physically intuitive (at least in the classical sense). In this case, the conservation of energy in the spacetime is easily understood: the AdS boundary acts like a perfect mirror and there

---

<sup>1</sup>Thanks to Tiago Fernandes for pointing this out.

is no energy flux across it. In particular, the modes are normal modes, being purely oscillating, with real associated frequencies. Other boundary conditions were studied in e.g. [54].

In AdS, one has, in global coordinates,

$$f(r) = 1 + \frac{r^2}{L^2} \quad , \quad (3.2)$$

where  $L^2 = -\frac{(d-1)(d-2)}{2\Lambda}$ . The tortoise coordinate,  $r_*$ , is obtained from

$$r_*(r) = \int \frac{dr}{f(r)} = L \arctan\left(\frac{r}{L}\right) - \frac{\pi L}{2} + r_*(\infty) \quad , \quad (3.3)$$

where  $r_*(\infty)$  is the (finite) value of the tortoise coordinate at spatial infinity. Without loss of generality, one can set  $r_*(\infty) = \frac{\pi L}{2}$  so that  $r_*(r) = L \arctan(r/L)$  and the region of interest gets mapped from  $r \in (0, +\infty)$  to  $r_* \in (0, \frac{\pi L}{2})$ .

## 3.2 Proca field perturbations in AdS

### 3.2.1 Proca field equations

The vector-type sector is described solely by Eq. (2.42), which in AdS is written

$$\partial_{r_*}^2 u_V + (\omega_V^2 - V^{(V)})u_V = 0 \quad , \quad (3.4)$$

where  $V^{(V)}$  is the effective potential ruling the dynamics of the vector-type modes, given by

$$V^{(V)} = f \left( \frac{n(n-2)}{4L^2} + \frac{(2l+n)(2l+n-2)}{4r^2} + \mu^2 \right) \quad . \quad (3.5)$$

On the other hand, the scalar-type sector is described by the system of two coupled differential equations, Eqs. (2.45) and (2.46), which may be written as

$$\partial_{r_*}^2 \mathbf{u} + (\omega_S^2 \mathbf{I} - \mathbf{V}^{(S)})\mathbf{u} = 0 \quad , \quad (3.6)$$

with  $\mathbf{u} = (u_2 \quad u_3)^T$  and  $\mathbf{V}^{(S)}$  the potential matrix mixing the two scalar-type modes, given by

$$\mathbf{V}^{(S)} = f \left( \begin{array}{cc} \frac{4l(l+n-1)+n(n+2)}{4r^2} + \frac{n(n-2)}{4L^2} + \mu^2 & -\frac{2}{r^2} \\ -\frac{2l(l+n-1)}{r^2} & \frac{4l(l+n-1)+(n-4)(n-2)}{4r^2} + \frac{n(n-2)}{4L^2} + \mu^2 \end{array} \right) \quad . \quad (3.7)$$

Equation (3.6) may be diagonalized by performing, for example,

$$u_2 = u_{(-)} + u_{(+)} \quad , \quad u_3 = (l+n-1)u_{(-)} - lu_{(+)} \quad , \quad (3.8)$$

which yields, in terms of  $u_{(-)}, u_{(+)}$ ,

$$\begin{aligned}\hat{\mathcal{D}}_{l+1}u_{(+)} &= 0 \quad , \\ \hat{\mathcal{D}}_{l-1}u_{(-)} &= 0 \quad .\end{aligned}\tag{3.9}$$

Thus, in AdS, one can condense the Proca field equations as

$$\partial_{r_*}^2 u_S + (\omega_S^2 - V_{j_S})u_S = 0 \quad ,\tag{3.10}$$

with  $S = \{(+), (-), V\}$  and

$$V_{j_S} = f \left( \frac{n(n-2)}{4L^2} + \frac{(2j_S+n)(2j_S+n-2)}{4r^2} + \mu^2 \right) \quad ,\tag{3.11}$$

with  $j_{(+)} = l + 1$ ,  $j_{(-)} = l - 1$ ,  $j_V = l$ . Note that the modes are splitted in accordance with the angular momentum addition rules for a spin-1 field, i.e.,  $|l - 1| \leq j \leq l + 1$ , resembling a spin-orbit interaction between the spin projection of the field,  $s = 0, \pm 1$  (corresponding, respectively, to vector-type and scalar-type perturbations), and the angular momentum number of each multipole,  $l$ . Each mode is then identified with its total angular momentum number,  $j = l + s$ .

For  $n \neq 2, j_S \neq 0$ , the potential Eq. (3.11) diverges both at the origin and at infinity, essentially behaving as a “box” that traps the field inside of it. Near the origin, the potential can be interpreted as an infinite potential barrier, completely reflecting the field as it gets closer to  $r = 0$  (observe that, if a black hole was present, the barrier would have a finite height making the field leak energy into the black hole). Additionally, near spatial infinity, both the mass of the field and the trapping character of AdS intertwine to reflect the field back to the origin. Observe that the latter behaviour holds independently of what is present in the bulk of AdS. An interesting exception arises when  $n = 2$  and  $j_S = 0$ : although the potential at spatial infinity also shows the behaviour mentioned, the  $1/r^2$  term vanishes, making the potential approach a constant near the origin. This, however, will not have deep consequences in the physical results for the solutions, as we show in Appendix B.

Finally, note that the analysis done above is for modes with  $l \geq 1$ . For the monopole mode, one can start directly from Eq. (2.49) or substitute  $u_3 = 0$  in Eq. (3.8) to obtain

$$\hat{\mathcal{D}}_1 u_{(+)} = 0 \quad .\tag{3.12}$$

Thus, the monopole mode only has scalar-type (+) polarization, which again agrees with the addition rules of angular momentum, as for the monopole mode only  $j = 1$  is allowed.

### 3.2.2 Normal mode solutions

We now proceed to solve Eq. (3.10) analytically, writing it as

$$\partial_{r_*}^2 u_S + \left( \omega_S^2 - \frac{k_{1j_S}}{\sin^2\left(\frac{r_*}{L}\right)} - \frac{k_2}{\cos^2\left(\frac{r_*}{L}\right)} \right) u_S = 0 \quad ,\tag{3.13}$$

with  $k_{1j_S} = \frac{4j_S(j_S+n-1)+(n-2)n}{4L^2}$  and  $k_2 = \frac{(n-2)n+4\mu^2L^2}{4L^2}$ . Equation (3.13) is a second-order differential equation with three regular singular points, at  $r_* = 0$ ,  $r_* = \pm\pi L/2$ . It follows that it can be transformed, by an appropriate change of variables, into the standard hypergeometric differential equation (see Appendix B). Its solutions satisfying the regularity boundary condition at  $r = 0$  and the Dirichlet boundary condition at  $r = \infty$  can be written as

$$u_S(r) = \mathcal{A}_S \left(\frac{r}{L}\right)^{\frac{2j_S+d-2}{2}} \left(1 + \frac{r^2}{L^2}\right)^{k - \frac{\omega_S L}{2}} F_1 \left[ -k + \omega_S L, -k, j_S + \frac{d-1}{2}; \frac{r^2/L^2}{1+r^2/L^2} \right] , \quad (3.14)$$

with

$$\omega_S L = 2k + j_S + \frac{d-1}{2} + \frac{1}{2} \sqrt{(d-3)^2 + 4\mu^2 L^2} , \quad k = 0, 1, 2, \dots . \quad (3.15)$$

Setting  $d = 4$ , the result agrees with [45]. As discussed in Section 3.2.1, the monopole mode only contains scalar-type (+) polarization, so that its normal modes may be obtained by setting  $j_{(+)} = 1$  in Eqs. (3.14) and (3.15). In particular, observe that the lowest frequency mode of the complete Proca spectrum corresponds to a  $l = 1$  perturbation (with scalar-type (−) polarization), not to the  $l = 0$  perturbation. An interesting feature of the spin-orbit splitting of the spectrum is that, for the same multipole  $l \geq 1$ , the  $k + 1$ -overtone with polarization (−) is isospectral to the  $k$ -overtone with polarization (+).

### 3.3 Maxwell field perturbations in AdS

#### 3.3.1 Maxwell field equations

Although the equations of motion are simpler for Maxwell field perturbations, the associated effective potentials show some interesting features that do not appear in the massive case. Take, for example, the vector-type component of the Maxwell field, ruled by Eq. (3.5) with  $\mu = 0$ . While at the origin the potential essentially remains unaltered, at infinity its behaviour now depends on the dimension of the spacetime: for  $n \neq 2$  it still diverges, whereas for  $n = 2$  it now approaches a constant. The difference between massless and massive cases is even more notorious in the scalar-type sector. While the Maxwell vector-type potential is simply the Proca vector-type potential after setting  $\mu = 0$ , the scalar-type sector is described by Eq. (2.56), which reads in AdS

$$\partial_{r_*}^2 u_{(\text{EM})} + \left( \omega_{(\text{EM})}^2 - V_{(\text{EM})}^{(\text{S})} \right) u_{(\text{EM})} = 0 , \quad (3.16)$$

with

$$V_{(\text{EM})}^{(\text{S})} = f \left( \frac{(n-2)(n-4)}{4L^2} + \frac{(2l+n)(2l+n-2)}{4r^2} \right) . \quad (3.17)$$

While for  $n = 2, 4$  the potential approaches a constant at spatial infinity, for  $n = 3$  it is not bounded from below, dipping to  $-\infty$ . These novel features of the potentials are intricately related with the aforementioned allowed boundary conditions one may choose at spatial infinity to define stable dynamics in AdS.

### 3.3.2 Normal mode solutions

Similarly to what was done for Proca field perturbations, we now determine the normal modes of Maxwell field perturbations that satisfy the regularity condition at  $r = 0$  and the Dirichlet condition at  $r = \infty$ . For the vector-type component, the normal modes are found by simply setting  $\mu = 0, S = V$  in Eqs. (3.14) and (3.15). On the other hand, for scalar-type perturbations, one needs to solve Eq. (3.16), which can be also written as

$$\partial_{r_*}^2 u_{(\text{EM})} + \left( \omega^2 - \frac{k_1}{\sin^2\left(\frac{r_*}{L}\right)} - \frac{k_2}{\cos^2\left(\frac{r_*}{L}\right)} \right) u_{(\text{EM})} = 0 \quad , \quad (3.18)$$

with  $k_1 = \frac{4l(l+n-1)+(n-2)n}{4L^2}$  and  $k_2 = \frac{(n-2)(n-4)}{4L^2}$ . This is done in Appendix B, yielding Eq. (3.14) with  $S = (\text{EM}), j_{(\text{EM})} = l$  and

$$\begin{aligned} \omega_{(\text{EM})}L &= 2k + l + 2 \quad , \quad d = 4 \quad , \quad k = 0, 1, 2, \dots \quad , \\ \omega_{(\text{EM})}L &\in \mathbb{R}^+ \quad , \quad d = 5 \quad , \\ \omega_{(\text{EM})}L &= 2k + l + d - 3 \quad , \quad d > 5 \quad , \quad k = 0, 1, 2, \dots \quad . \end{aligned} \quad (3.19)$$

So, while for  $d \neq 5$  the normal mode frequency spectrum is discrete, for  $d = 5$  the Dirichlet condition does not impose any restriction on the frequencies, yielding a continuous normal mode spectrum. These results agree with [20]. In particular, we believe a deeper analysis needs to be performed to better understand this peculiar behaviour in 5-dimensional AdS.

## Chapter 4

# Quasinormal modes of Proca field perturbations in $d$ -dimensional Schwarzschild-AdS

### 4.1 Proca field equations in Schwarzschild-AdS spacetime

The results from Chapter 3 are for pure  $d$ -dimensional AdS spacetime. This is an interesting case, as it captures the dynamics of a Proca field in a simple but non-trivial spacetime. Moreover, it provides a background geometry where the scalar-type modes of the Proca field completely decouple. Indeed, one is left with modes splitted by their total angular momentum number,  $j = l + s$ , with  $s = 0$  for vector-type modes and  $s = \pm 1$  for scalar-type modes, in analogy with a spin-orbit interaction between the field's proper spin and the angular momentum of each multipole. A question that naturally arises is if the study can be extended to physically richer spacetimes, such as black hole spacetimes. In this case, the black hole dissipates energy from the system and the latter can no longer be described as a superposition of independent normal modes. Instead, the modes are now quasinormal, with complex associated frequencies, whose imaginary part encodes the decay of the modes into the black hole. In this chapter, we study the quasinormal modes of Proca field perturbations in  $d$ -dimensional Schwarzschild-AdS spacetime, mainly with  $d = 4, 5, 6, 7$ , although generalization to higher-dimensions is straightforward. Schwarzschild-AdS spacetime is a non-rotating and uncharged asymptotically AdS spacetime. Thus, it shares the same features as AdS near the boundary, while having a Schwarzschild black hole in its bulk. In global coordinates, the line element of Schwarzschild-AdS is written as Eq. (2.40), with

$$f(r) = 1 + \frac{r^2}{L^2} - \left(\frac{r_0}{r}\right)^{d-3} = 1 + \frac{r^2}{L^2} - \left(1 + \frac{r_h^2}{L^2}\right) \left(\frac{r_h}{r}\right)^{d-3}, \quad (4.1)$$

where  $r_0$  is related to the mass of the black hole,  $M$ , by  $M = ((d-2)A_{d-2}r_0^{d-3})/16\pi$ , with  $A_{d-2}$  being the area of a  $(d-2)$ -sphere,  $A_{d-2} = 2\pi^{(d-1)/2}/\Gamma[(d-1)/2]$ . Schwarzschild-AdS spacetime has a

single event horizon, which is the unique real and positive zero of  $f(r)$ ,  $r_h$ . The equations of motion of Proca field perturbations in Schwarzschild-AdS are still given by Eqs. (2.42), (2.45) and (2.46), as the only restriction imposed on the spacetime was to be of the form Eq. (2.40). Substituting Eq. (4.1) in these equations and making the Fourier transformation to the frequency domain, the effective potential ruling the dynamics of the vector-type component of the Proca field in  $d$ -dimensional Schwarzschild-AdS spacetime is

$$V^{(V)} = f \left( \frac{(d-4)(d-2) + 4\mu^2 L^2}{4L^2} + \frac{(2l+d-4)(2l+d-2)}{4r^2} + \frac{d(d-4)}{4r_h^2} \left(1 + \frac{r_h^2}{L^2}\right) \left(\frac{r_h}{r}\right)^{d-1} \right), \quad (4.2)$$

while the scalar-type components are governed by

$$\mathbf{V}^{(S)} = \begin{pmatrix} V_{22}^{(S)} & V_{23}^{(S)} \\ V_{32}^{(S)} & V_{33}^{(S)} \end{pmatrix}, \quad (4.3)$$

with

$$\begin{aligned} V_{22}^{(S)} &= f \left( \frac{(d-4)(d-2) + 4\mu^2 L^2}{4L^2} + \frac{4l(l+d-3) + d(d-2)}{4r^2} - \frac{3(d-2)^2}{4r_h^2} \left(1 + \frac{r_h^2}{L^2}\right) \left(\frac{r_h}{r}\right)^{d-1} \right), \\ V_{23}^{(S)} &= f \left( -\frac{2}{r^2} + \frac{d-1}{4r_h^2} \left(1 + \frac{r_h^2}{L^2}\right) \left(\frac{r_h}{r}\right)^{d-1} \right), \\ V_{32}^{(S)} &= -\frac{2l(l+d-3)f}{r^2}, \\ V_{33}^{(S)} &= f \left( \frac{(d-4)(d-2) + 4\mu^2 L^2}{4L^2} + \frac{4l(l+d-3) + (d-4)(d-6)}{4r^2} - \frac{d(d-4)}{4r_h^2} \left(1 + \frac{r_h^2}{L^2}\right) \left(\frac{r_h}{r}\right)^{d-1} \right), \end{aligned}$$

for modes with  $l > 0$ . The monopole mode,  $l = 0$ , follows

$$V^{(S,l=0)} = f \left( \frac{(d-4)(d-2) + 4\mu^2 L^2}{4L^2} + \frac{d(d-2)}{4r^2} - \frac{3(d-2)^2}{4r_h^2} \left(1 + \frac{r_h^2}{L^2}\right) \left(\frac{r_h}{r}\right)^{d-1} \right). \quad (4.4)$$

For Maxwell field perturbations, the vector-type potential is simply Eq. (4.2) with  $\mu = 0$ , while the scalar-type potential is given by Eq. (2.56)

$$V_{(EM)}^{(S)} = f \left( \frac{(d-4)(d-6)}{4L^2} + \frac{(2l+d-4)(2l+d-2)}{4r^2} - \frac{(3d-8)(d-4)}{4r_h^2} \left(1 + \frac{r_h^2}{L^2}\right) \left(\frac{r_h}{r}\right)^{d-1} \right). \quad (4.5)$$

As the perturbation equations all have the form

$$\partial_{r_*}^2 \mathbf{u} + (\omega^2 \mathbf{I} - \mathbf{V}(r)) \mathbf{u} = 0, \quad (4.6)$$

a complete analysis of the potentials is the key to study the analytical properties of the quasinormal modes. In the next section, we start by discussing the appropriate boundary conditions at the horizon and at spatial infinity. We then obtain the asymptotic form of the solutions near infinity, which will also be important from the numerical point of view, as we shall explain. Finally, we study whether Schwarzschild-AdS is stable under Proca and Maxwell field perturbations.

## 4.2 Analytical study of the quasinormal mode spectrum

### 4.2.1 Boundary conditions

Quasinormal modes of black hole spacetimes are the solutions to the eigenvalue problem Eq. (4.6) with appropriate boundary conditions specified at the black hole horizon and far from the black hole. Since usually the effective potential ruling the perturbations vanishes at the event horizon, the only classically allowed boundary condition at  $r = r_h$  is an ingoing plane wave, so that  $\mathbf{u}$  should behave as

$$\mathbf{u}(r_*) \sim e^{-i\omega r_*} \quad , \quad r_* \rightarrow -\infty \quad , \quad (4.7)$$

or, in terms of the radial coordinate,  $r$ ,

$$\mathbf{u}(r) \sim (r - r_h)^{-\frac{i\omega}{f'(r_h)}} \quad , \quad r \rightarrow r_h \quad , \quad (4.8)$$

where we used  $f(r) = f'(r_h)(r - r_h) + \mathcal{O}((r - r_h)^2)$ . The remaining boundary condition is imposed far from the black hole and depends on the background one is considering. For example, in asymptotically flat and de Sitter spacetimes, the potential also vanishes at  $r_* = +\infty$  (corresponding to spatial infinity in the flat case and to the cosmological horizon in the de Sitter case), and one imposes an outgoing plane wave there [32, 37]. In asymptotically AdS spacetimes, we impose a Dirichlet boundary condition at spatial infinity for the rescaled variables, so that  $\mathbf{u} = 0$  as  $r, r_* \rightarrow \infty$ , although in some cases such condition is not unique, as aforementioned in Chapter 3. Quasinormal modes obeying other boundary conditions were studied in [54]. In what follows, we discuss the behaviour of the effective potentials Eqs. (4.2)-(4.5), as well as the properties of the asymptotic solutions to Eq. (4.6) near spatial infinity.

### 4.2.2 Main properties of the spectrum and asymptotic solutions near infinity

#### Proca and electromagnetic vector-type perturbations

The vector-type variable describes  $d - 3$  degrees of freedom of the Proca field and is governed by Eq. (4.6) with effective potential Eq. (4.2). Since the vector-type sector is invariant under the gauge transformation even in the massless case, Eq. (4.2) describes both Maxwell and Proca field perturbations. Note that the potential is always positive and can be written

$$V^{(V)} = \frac{(d-4)(d-2) + 4\mu^2 L^2}{4L^4} r^2 + \frac{(d-4)(d-2) + 2l(l+d-3) + 2\mu^2 L^2}{2L^2} + \mathcal{O}\left(\frac{1}{r}\right) \quad , \quad (4.9)$$

diverging at infinity for all values of the parameters, except when  $d = 4, \mu = 0$ . In this case, the potential approaches  $\frac{l(l+1)}{L^2}$ , as found in [32]. For  $d \neq 4, \mu \neq 0$ , the equation for the vector-type component near infinity yields, at first order,

$$\frac{r^4}{L^4} \partial_r^2 u_V^{(\infty)} + \frac{2r^3}{L^4} \partial_r u_V^{(\infty)} - \frac{(d-4)(d-2) + 4\mu^2 L^2}{4L^2} r^2 u_V^{(\infty)} = 0 \quad , \quad (4.10)$$

which can be solved analytically, giving

$$u_V^{(\infty)} = c_1 r^{-\frac{1}{2} - \frac{1}{2}\sqrt{(d-3)^2 + 4\mu^2 L^2}} + c_2 r^{-\frac{1}{2} + \frac{1}{2}\sqrt{(d-3)^2 + 4\mu^2 L^2}} , \quad (4.11)$$

where  $c_1$  and  $c_2$  are constants of integration. The Dirichlet boundary condition then implies  $c_2 = 0$  and  $u_V^{(\infty)} \sim r^{-\frac{1}{2} - \frac{1}{2}\sqrt{(d-3)^2 + 4\mu^2 L^2}}$ , at first order. On the other hand, when  $d = 4$  and  $\mu = 0$ , one has

$$\frac{r^4}{L^4} \partial_r^2 u_V^{(\infty)} + \frac{2r^3}{L^4} \partial_r u_V^{(\infty)} + \left( \omega^2 - \frac{l(l+1)}{L^2} \right) u_V^{(\infty)} = 0 , \quad (4.12)$$

giving the solution

$$u_V^{(\infty)} = c_1 e^{i \frac{\sqrt{\omega^2 L^2 - l(l+1)} L}{r}} + c_2 e^{-i \frac{\sqrt{\omega^2 L^2 - l(l+1)} L}{r}} . \quad (4.13)$$

In this case, the Dirichlet condition implies  $c_1 = -c_2$ , so that, at first order,  $u_V^{(\infty)} \sim r^{-1}$ . One thus always has

$$u_V^{(\infty)} \sim r^{-\frac{1}{2} - \frac{1}{2}\sqrt{(d-3)^2 + 4\mu^2 L^2}} [1 + \mathcal{O}(r^{-1})] , \quad (4.14)$$

which agrees with Eq. (3.14).

## Electromagnetic scalar-type perturbations

In the massless limit, the scalar-type sector describes only one physical degree of freedom, due to the gauge freedom. The equations of motion governing the scalar-type sector decouple to give Eq. (4.6) with effective potential Eq. (4.5). One can show that, for  $d \neq 5$ , the only solution satisfying the Dirichlet boundary condition at infinity is

$$u_{(\text{EM})}^{(\infty)} \sim r^{-\frac{1}{2} - \frac{1}{2}|d-5|} [1 + \mathcal{O}(r^{-1})] . \quad (4.15)$$

For  $d = 5$  the behaviour of the solution near infinity is

$$u_{(\text{EM})}^{(\infty, d=5)} = r^{-\frac{1}{2}} (c_1 + c_2 \log(r)) [1 + \mathcal{O}(r^{-1})] , \quad (4.16)$$

which vanishes for every  $c_1, c_2$  when the limit is taken. Note that now, for  $d > 4$ , there is always a region near the horizon where the potential is negative, as depicted in Fig. (4.1). As we will show in Section 4.2.3, this will make the stability study of the perturbations more complicated. Fig. (4.1) also shows the features of the potentials at spatial infinity: while for  $d \geq 7$  the potential diverges, for  $d = 4$  and  $d = 6$  it approaches a finite value. Additionally, for  $d = 5$ , the potential is unbounded from below, going to negative infinity near the boundary. This agrees with what was found in [55]: for  $d = 4, 5, 6$ , the potential behaviour near infinity allows a looser constraint on the boundary condition. In particular, one can impose an outgoing wave condition at infinity and recover the definition of quasinormal modes in asymptotically flat and de Sitter spacetimes.

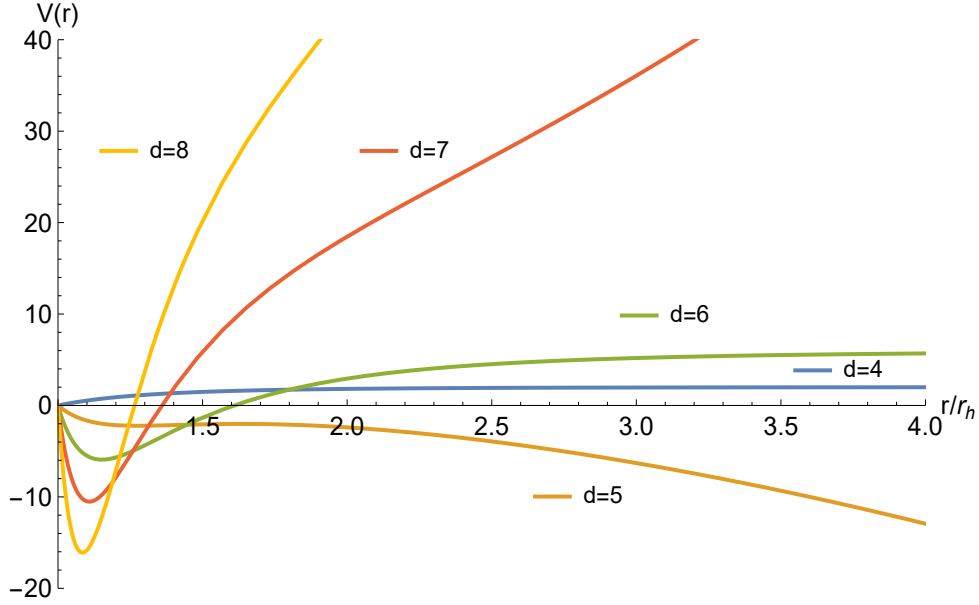


**Figure 4.1:** Effective potentials of  $l = 1$  scalar-type electromagnetic perturbations for the 4, 5, 6, 7, 8-dimensional Schwarzschild-AdS black holes with  $r_h = 2$ .

### Proca monopole mode

The Proca monopole mode is ruled by Eq. (4.6) with potential Eq. (4.4). While the scalar-type modes are coupled for higher multipoles, the monopole mode only has one degree of freedom, due to its spherical symmetry, being described by a single second-order differential equation. A similar analysis to what was done for the vector-type component also yields Eq. (4.14) for the asymptotic monopole solution subject to the Dirichlet condition.

### Higher multipoles of Proca scalar-type perturbations

For higher multipoles,  $l > 0$ , the scalar-type Proca sector is coupled. Equation (4.6) is now a system of two coupled second order differential equations, whose effective potential is the matrix Eq. (4.3) mixing the two scalar-type modes. To be able to distinguish between them, we define two polarizations: the non-electromagnetic polarization, which reduces to a pure-gauge degree of freedom in the electromagnetic limit and to the unique physical degree of freedom of the monopole mode; the electromagnetic polarization, which corresponds to the dynamical degree of freedom in the electromagnetic limit and has no physical monopole analogue. Note that Eq. (2.62) allows one to interpret the non-electromagnetic polarization as a scalar field polarization (we opted to call “non-electromagnetic polarization” instead of “scalar polarization” because the latter could create confusion with the already adopted “scalar-type” term). Indeed, in the small-mass limit, we expect the electromagnetic and non-electromagnetic polarizations to approach the (scalar-type) Maxwell field and scalar field modes, respectively. Also, observe that the nomenclature “scalar (field)-type” and “vector-type” adopted in [44, 51] to distinguish between the two polarizations only makes sense in four dimensional spacetimes, where the scalar-type and vector-type Maxwell modes are isospectral. In higher dimensional spacetimes, this no longer happens, making that nomenclature incorrect. Near infinity, the behaviour of Eq. (4.3) can be picked up by comparing

what was already done for pure AdS in Chapter 3. In this limit the modes decouple, yielding Eq. (3.10) with  $S = (+), (-)$ . The solutions near infinity after imposing the Dirichlet boundary condition can then be read off from Eq. (3.14), yielding Eq. (4.14) for both polarizations.

### 4.2.3 Schwarzschild-AdS stability against Maxwell and Proca field perturbations

The problem of stability of a spacetime against different kinds of perturbations is crucial to determine whether the system is physically viable or not. In particular, within the context of AdS/CFT, the transition from a stable solution to an unstable one in asymptotically AdS spacetimes is dual to the thermodynamic phase transition of the CFT [24]. Since perturbations in gravitational backgrounds can usually be described by Eq. (4.6), the problem of stability sums up to finding the quasinormal mode spectrum and to see if all the modes decay in time. Within our definitions, this means checking if all the mode frequencies have negative imaginary part. Although in general this is a hard task, in some situations the potential behaviour allows an analytical proof of stability, as we sketch below, following closely [32, 35]. Multiplying Eq. (4.6) by  $\mathbf{u}^\dagger$  and integrating in the region of interest one has

$$\left( \mathbf{u}^\dagger \frac{d\mathbf{u}}{dr_*} \right) \Big|_{r_*=-\infty}^{r_*=r_*^{(\infty)}} + \omega^2 \int_{-\infty}^{r_*^{(\infty)}} |\mathbf{u}|^2 dr_* = \int_{-\infty}^{r_*^{(\infty)}} \left( \left| \frac{d\mathbf{u}}{dr_*} \right|^2 + \mathbf{u}^\dagger \mathbf{V} \mathbf{u} \right) dr_* \quad , \quad (4.17)$$

where  $r_* = r_*^{(\infty)}$  is the finite value of the tortoise coordinate at Schwarzschild-AdS spatial infinity (in asymptotically flat and de Sitter spacetimes,  $r_* = \infty$  at spatial infinity and at the cosmological horizon, respectively). The boundary term in the LHS of Eq. (4.17) needs to be evaluated carefully: near infinity,  $f \sim r^2$  and Proca solutions behave as Eq. (4.14), yielding  $f \mathbf{u}^\dagger \frac{d\mathbf{u}}{dr} \sim r^{-\sqrt{(d-3)^2 + 4\mu^2 L^2}}$ , which vanishes when evaluated at  $r = +\infty$ ; similarly, Maxwell solutions in  $d \neq 5$  behave either as Eq. (4.14) or as Eq. (4.15) and so the term evaluated at spatial infinity also vanishes. On the other hand, for  $d = 5$ , scalar-type Maxwell solutions behave as Eq. (4.16), so that near infinity  $f \mathbf{u}^\dagger \frac{d\mathbf{u}}{dr} = -\frac{1}{2L^2} |c_1 + c_2 \log(r)|^2$ . Moreover, near the horizon, Eq. (4.7) gives  $\mathbf{u}^\dagger \frac{d\mathbf{u}}{dr_*} = -i\omega |\mathbf{u}(-\infty)|^2$  for all the solutions, with Eq. (4.17) yielding

$$i\omega A + \omega^2 B - C = \int_{-\infty}^{r_*^{(\infty)}} \left( \left| \frac{d\mathbf{u}}{dr_*} \right|^2 + \mathbf{u}^\dagger \mathbf{V} \mathbf{u} \right) dr_* \quad , \quad (4.18)$$

where  $A, B$  are real and non-negative,  $A = |\mathbf{u}(-\infty)|^2$  and  $B = \int_{-\infty}^{r_*^{(\infty)}} |\mathbf{u}|^2 dr_*$ , and  $C = \frac{1}{2L^2} \lim_{r \rightarrow \infty} |c_1 + c_2 \log(r)|^2$  for scalar-type Maxwell perturbations in 5-dimensional Schwarzschild-AdS,  $C = 0$  otherwise. Subtracting to Eq. (4.18) its hermitian adjoint, and further dividing by  $2i$  yields

$$\Re(\omega)A + 2\Re(\omega)\Im(\omega)B = \frac{1}{2i} \int_{-\infty}^{r_*^{(\infty)}} \mathbf{u}^\dagger (\mathbf{V} - \mathbf{V}^\dagger) \mathbf{u} dr_* \quad . \quad (4.19)$$

If  $\mathbf{V}$  is hermitian, the RHS of Eq. (4.19) vanishes and  $\Im(\omega) > 0$  implies  $\Re(\omega) = 0$ . This means that the unstable growing modes must be purely imaginary, a well established result since the seminal work of Vishveshwara [6]. This is a very important result when searching for instabilities numerically, as

instead of searching in a two-dimensional grid of complex  $\omega$ , one only needs to search for instabilities on the imaginary axis. One can also take the sum of Eq. (4.18) with its hermitian adjoint, yielding, with  $\Re(\omega) = 0$  and after dividing by 2,

$$-\Im(\omega) A - \Im(\omega)^2 B = \int_{-\infty}^{r_*^{(\infty)}} \left| \frac{d\mathbf{u}}{dr_*} \right|^2 dr_* + \frac{1}{2} \int_{-\infty}^{r_*^{(\infty)}} \mathbf{u}^\dagger (\mathbf{V} + \mathbf{V}^\dagger) \mathbf{u} dr_* + C \quad . \quad (4.20)$$

Thus, assuming  $\mathbf{V}$  is hermitian, if  $\mathbf{V}$  is positive definite (i.e.  $\mathbf{V}$  can be written  $\mathbf{V} = \mathbf{K}\mathbf{K}^\dagger$ ), the RHS of Eq. (4.20) is positive and  $\Im(\omega) < 0$ , proving stability. Although this provides a very practical method of proving stability, it is rather restrictive, as most of the effective potentials are not positive definite in the whole region of interest (take Fig. (4.1) as an example). In some cases, however, one can still address stability analytically by using the S-deformation technique, firstly introduced by Ishibashi and Kodama in [12–14]. Defining the operator

$$\mathbf{D} = \mathbf{I} \frac{d}{dr_*} + \mathbf{S}(r_*) \quad , \quad (4.21)$$

with  $\mathbf{S}$  hermitian, one can write Eq. (4.18) as

$$i\omega A + \omega^2 B - C = \int_{-\infty}^{r_*^{(\infty)}} \left( |\mathbf{D}\mathbf{u}|^2 + \mathbf{u}^\dagger \left( \mathbf{V} + \frac{d\mathbf{S}}{dr_*} - \mathbf{S}^2 \right) \mathbf{u} \right) dr_* - \left( \mathbf{u}^\dagger \mathbf{S} \mathbf{u} \right) \Big|_{r_*=-\infty}^{r_*=r_*^{(\infty)}} \quad . \quad (4.22)$$

Thus, if  $\mathbf{u}^\dagger \mathbf{S} \mathbf{u}$  is non-positive at spatial infinity, non-negative at  $r_* = -\infty$ , and if  $\mathbf{S}$  makes  $\tilde{\mathbf{V}} \equiv \mathbf{V} + \frac{d\mathbf{S}}{dr_*} - \mathbf{S}^2$  positive definite, then the results following from Eqs. (4.19) and (4.20) can be applied and one can establish stability. Of course, since there is not a systematic way of finding  $\mathbf{S}$ , the S-deformation procedure becomes specially helpful for simple potentials. For cumbersome potentials it is hard to guess the functional form of  $\mathbf{S}$ . In the latter cases, usually, a numerical study of stability needs to be performed.

Having set up the general procedure, we will now apply it to study analytically the stability of electromagnetic and Proca perturbations in Schwarzschild-AdS. As can be seen from Eq. (4.2), the potential ruling vector-type Proca and Maxwell field perturbations in Schwarzschild-AdS is the only one which is positive definite in the whole region of interest. It follows from Eqs. (4.19) and (4.20) that Schwarzschild-AdS is stable against these perturbations.

On the other hand, for scalar-type electromagnetic perturbations, the potential Eq. (4.5) dips to negative values close to the horizon when  $d > 5$ , whereas for  $d = 5$  it becomes unbounded from below (cf. last term of Eq. (2.57) and Fig. (4.1)). Setting

$$S = \frac{(d-4)f}{2r} \quad , \quad (4.23)$$

makes  $\tilde{V} = \frac{f(l(l+d-3))}{r^2} \geq 0$  and  $S = 0$  at the horizon. At spatial infinity  $S \sim r$  and, using Eq. (4.15), one has that, for  $d > 5$ ,  $S|u|^2 \sim r^{5-d}$ , which vanishes. Furthermore, for  $d = 5$ ,  $S|u|^2 = \frac{1}{2L^2} \lim_{r \rightarrow \infty} |c_1 + c_2 \log(r)|^2 = C$  at spatial infinity, so that the  $C$  terms cancel in Eq. (4.22). For  $d = 4$  there is no need to use the technique as the potential is already positive definite (also, note that for this case  $S = 0$ ). Thus,  $d$ -dimensional Schwarzschild-AdS is guaranteed to be stable against scalar-type Maxwell field perturbations as well.

Similarly, for the monopole mode of Proca perturbations, Eq. (4.4) becomes negative near the horizon. Making

$$S = \frac{(d-2)f}{2r} \quad , \quad (4.24)$$

the deformed potential is  $\tilde{V} = f\mu^2 \geq 0$ . At the horizon  $S = 0$  and at spatial infinity  $S|u|^2 \sim r^{-\sqrt{(d-3)^2+4\mu^2L^2}}$  vanishes, proving stability of Schwarzschild-AdS against the monopole mode of scalar-type Proca field perturbations.

For higher multipoles of scalar-type Proca perturbations, described by the coupled system Eq. (4.6) with potential Eq. (4.3), one cannot prove stability using this technique, as in this case the potential is non-hermitian, leading to terms in Eqs. (4.18) and (4.19) that do not allow such analysis. One could argue that there could be a S function transforming the non-hermitian potential into a hermitian one. However, this is not the case, as for the S-deformation to work one also needs to ensure that S itself is hermitian. From the relation between the old potential and the transformed one, if  $\tilde{V} \equiv \mathbf{V} + \frac{d\mathbf{S}}{dr_*} - \mathbf{S}^2$  is hermitian,  $\mathbf{V}$  needs to be hermitian. Thus, in this case, we can only test stability by computing numerically the quasinormal mode spectrum.

## 4.3 Numerical methods to compute quasinormal modes

Since for most background geometries, such as Schwarzschild-AdS, it is not possible to solve the eigenvalue problem Eq. (4.6) exactly, numerical methods to compute the quasinormal mode spectra of such spacetimes have been extensively studied. For a review of such techniques, we refer to [35–37, 39]. We compute the Proca and Maxwell field quasinormal mode spectrum in Schwarzschild-AdS using two different approaches: by applying the Horowitz-Hubeny method and by numerically integrating the equations of motion. In this section, we describe these two methods in detail.

### 4.3.1 Horowitz-Hubeny method

#### Description of the method

The Horowitz-Hubeny method is widely used to compute quasinormal modes in asymptotically AdS spacetimes, as the Dirichlet boundary condition at spatial infinity provides a power series equation for  $\omega$ , which can be solved numerically by truncating the series [30]. Considering the case of a single second-order differential equation, Eq. (4.6) can be written as

$$\partial_r^2 \psi + \frac{(f' - 2i\omega)}{f} \partial_r \psi - \frac{V}{f^2} \psi = 0 \quad , \quad (4.25)$$

where we factorized the behaviour of the solution near the horizon, i.e.,  $u(r) = e^{-i\omega r_*} \psi(r)$ . Equation (4.25) has  $d+1$  singular points: the  $d-1$  zeroes of  $f(r)$ ,  $r=0$  and  $r=\infty$ . Since both  $\lim_{r \rightarrow 0} f'(r)$  and  $\lim_{r \rightarrow 0} V(r)$  diverge,  $r=0$  is an irregular singular point. This does not constitute a problem, however, as the region of interest is only  $r_h < r < \infty$ . On the other hand, the zeroes of  $f$  are regular singular points, as they are non-degenerate. The  $r=\infty$  singularity is studied by writing  $x=1/r$ , which is always

finite in the range of interest. By doing so, one arrives at

$$s(x)(x-x_h)\partial_x^2\psi + t(x)\partial_x\psi + \frac{u(x)}{(x-x_h)}\psi = 0 \quad , \quad (4.26)$$

where

$$s(x) = \frac{x^4 f}{x-x_h} \quad , \quad t(x) = x^2 \partial_x(x^2 f) + 2i\omega x^2 \quad , \quad u(x) = -\frac{(x-x_h)V}{f} \quad . \quad (4.27)$$

Thus, taking the limit  $x \rightarrow 0$ , one sees that  $r = \infty$  is also a regular singular point (it is convenient to stick to the  $x$  coordinate, ranging from 0 to  $x_h = 1/r_h$ ). Fuchs' theorem guarantees that Eq. (4.26) admits a Frobenius solution near each of its regular singular points, namely, near  $x_h$ . The radius of convergence of the solution will be given by the minimum distance between  $x = x_h$  and the other singular points. One then has, near the horizon,  $x = x_h$ ,

$$\psi(x) = (x-x_h)^\alpha \sum_{m=0}^{\infty} a_m (x-x_h)^m \quad , \quad (4.28)$$

where  $a_m$  are coefficients that depend on the frequency (i.e.  $a_m = a_m(\omega)$ ), with  $a_0 \neq 0$ , and  $\alpha$  is a constant, determined from the indicial equation after imposing the boundary condition at the horizon. The polynomials  $s(x)$ ,  $t(x)$  and  $u(x)$  can also be expanded near the horizon, yielding

$$s(x) = \sum_{p=0}^{\infty} s_p (x-x_h)^p \quad , \quad t(x) = \sum_{p=0}^{\infty} t_p (x-x_h)^p \quad , \quad u(x) = \sum_{p=0}^{\infty} u_p (x-x_h)^p \quad , \quad (4.29)$$

where  $s_p$ ,  $t_p$  and  $u_p$  are coefficients independent of  $x$ . Substituting Eqs. (4.28) and (4.29) in Eq. (4.26) one gets

$$\sum_{m,p=0}^{\infty} [s_p(m+\alpha)(m+\alpha-1) + t_p(m+\alpha) + u_p] a_m (x-x_h)^{m+\alpha+p} = 0 \quad (4.30)$$

The term with  $m = p = 0$  is unique ( $m + \alpha + p$  can only give  $\alpha$  if  $m = p = 0$ ) and gives rise to the indicial equation for  $\alpha$

$$s_0\alpha(\alpha-1) + t_0\alpha + u_0 = 0 \quad . \quad (4.31)$$

Taking into account that  $s_0 = -x_h^2 f'(r_h)$ ,  $t_0 = 2x_h^2(i\omega - f'(r_h)/2)$  and  $u_0 = 0$ , the solutions to Eq. (4.31) are  $\alpha = 0$  or  $\alpha = 2i\omega/f'(r_h)$ , corresponding, respectively, to ingoing and outoing modes at the horizon. The boundary condition Eq. (4.8) sets  $\alpha = 0$ , so that only ingoing modes are allowed near the horizon. Setting this in Eq. (4.30), relabelling indexes and equating the terms for each power of  $(x-x_h)$ , one arrives at the recursion relation for the coefficients  $a_j$ ,

$$a_j = -\frac{1}{P_j} \sum_{m=0}^{j-1} [m(m-1)s_{j-m} + mt_{j-m} + u_{j-m}] a_m \quad , \quad (4.32)$$

where  $P_j = j(j-1)s_0 + jt_0$ . Without loss of generality, one can set  $a_0 = 1$  and solve recursively Eq. (4.32) up to a given order,  $N$ . The Dirichlet boundary condition at spatial infinity then yields

$$\psi(x=0) = \sum_{m=0}^{\infty} a_m(\omega) (-x_h)^m = 0 \quad , \quad (4.33)$$

which can be solved numerically for  $\omega$  by truncating the sum at a sufficiently large  $N$ . To see whether the  $N$  chosen is sufficiently large, one simply checks if the solution of the  $N$ -term sum is sufficiently close to the solution of the  $(N+1)$ -term sum, within the desired accuracy.

Similarly, for systems described by  $M$  coupled differential equations for  $M$  perturbation variables, Eq. (4.26) reads [51, 56]

$$s(x)(x-x_h)\partial_x^2\boldsymbol{\psi} + t(x)\partial_x\boldsymbol{\psi} + \frac{\mathbf{U}(x)}{(x-x_h)}\boldsymbol{\psi} = 0 \quad , \quad (4.34)$$

with  $\mathbf{U}(x) = -\frac{(x-x_h)\mathbf{V}}{f}$ . After expanding  $\boldsymbol{\psi}(x)$  near the horizon as

$$\boldsymbol{\psi}(x) = \sum_{m=0}^{\infty} \mathbf{a}_m(\omega)(x-x_h)^m \quad , \quad (4.35)$$

as well as  $s(x)$ ,  $t(x)$  and  $\mathbf{U}(x)$ , the coefficients  $\mathbf{a}_j$  obey

$$\mathbf{a}_j(\omega) = -\frac{1}{P_j} \sum_{m=0}^{j-1} [(m(m-1)s_{j-m} + mt_{j-m})\mathbf{I} + \mathbf{U}_{j-m}] \mathbf{a}_m(\omega) \quad , \quad (4.36)$$

and can be expanded as

$$\mathbf{a}_j(\omega) = \mathbf{B}_j(\omega)\mathbf{a}_0 \quad , \quad (4.37)$$

with matrices  $\mathbf{B}_j$  to be determined from Eq. (4.36),

$$\mathbf{B}_j(\omega) = -\frac{1}{P_j} \sum_{m=0}^{j-1} [(m(m-1)s_{j-m} + mt_{j-m})\mathbf{I} + \mathbf{U}_{j-m}] \mathbf{B}_m(\omega) \quad , \quad (4.38)$$

where we expanded  $\mathbf{a}_0$  in the suitable orthogonal basis

$$\mathbf{a}_0 = \sum_{i=1}^M a_i \mathbf{e}_i \quad , \quad (4.39)$$

with  $\mathbf{e}_1 = (1, 0, \dots, 0, 0)^T$ ,  $\mathbf{e}_2 = (0, 1, \dots, 0, 0)^T$ , etc.. The Dirichlet boundary condition at spatial infinity then yields

$$\psi(x=0) = \sum_{j=0}^{\infty} \mathbf{a}_j(\omega)(-x_h)^j = \left( \sum_{j=0}^{\infty} \mathbf{B}_j(\omega)(-x_h)^j \right) \mathbf{a}_0 = 0 \quad , \quad (4.40)$$

whose non-trivial solution fixes the values of  $\omega$  through

$$\det \left( \sum_{j=0}^{\infty} \mathbf{B}_j(\omega)(-x_h)^j \right) = 0 \quad . \quad (4.41)$$

As in the one-dimensional case, Eq. (4.41) can be solved numerically for  $\omega$  by truncating the sum at a sufficiently large  $N$ .

### Comments on the method's accuracy and reliability

At this point, we should make several remarks regarding this technique. The numerical results are always presented in units with  $L = 1$ . This can always be done, as the equations are all invariant under a rescaling in  $r$ . While this method performs well for large black holes,  $r_h \gg 1$ , it shows poor convergence properties for black holes with  $r_h \lesssim \mathcal{O}(1)$ . For small enough black holes (typically  $r_h \lesssim \mathcal{O}(0.1)$ ), it becomes impractical to compute the quasinormal mode spectrum with Horowitz-Hubeny method, not only due to the enormous computer time needed, but also due to the numerical error accumulation [30] (see, however, [33]). Such worsening of convergence is depicted in Fig. (4.2) for black holes with sizes  $r_h = 1$  and  $r_h = 0.6$ . One may also compare these with the left side of Fig. (4.3), computed for  $r_h = 100$ .

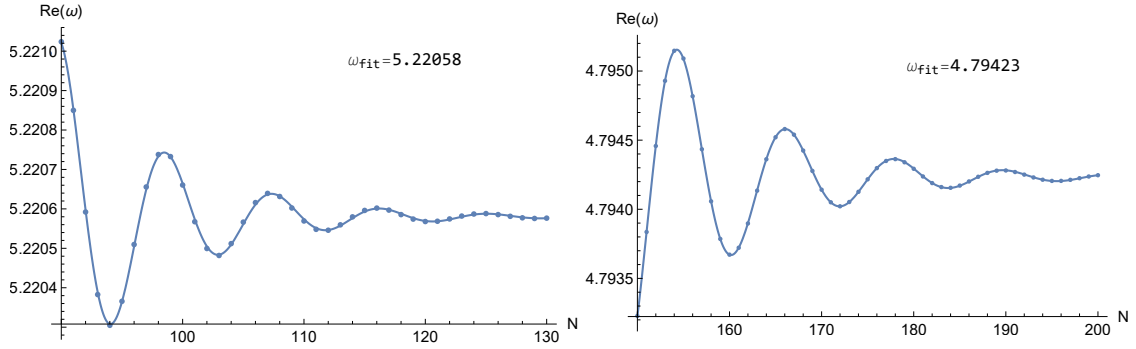


**Figure 4.2:** Convergence curves for the fundamental mode of  $l = 1$  vector-type  $\mu = 0.2$  Proca field perturbations, for 6-dimensional Schwarzschild black holes with sizes  $r_h = 1$  (Left) and  $r_h = 0.6$  (Right). For  $r_h \lesssim 1$ , a small decrease in the black hole size significantly worsens the convergence of the solution: for  $r_h = 1$  one achieves a precision up to the fifth significant figure at  $N \gtrsim 100$ , whereas for  $r_h = 0.6$  such precision is only reached for  $N \gtrsim 200$ .  $\omega_{\text{fit}}$  is extracted from the fit of  $\omega(N) = \omega_{\text{fit}} + c_2 e^{-c_3 N} \sin(c_4 N + c_5)$  to the convergence curves.

While the radius of the black hole affects the solutions' convergence properties the most, these also depend on the other parameters (whether perturbation-related or spacetime-related) of the system. We found that the dimension of the spacetime,  $d$ , and the overtone number,  $k$ , were the most impactful parameters on that regard. The dependence on  $d$  is easy to understand: after all, the shape of the potential is strongly related to  $d$ , specially for  $4 \leq d \leq 6$ . Concerning the overtone number, the minima of  $\psi(x = 0)$  becomes less pronounced for higher  $k$ , resulting in a poorer convergence (this will be illustrated in the next section). Figure (4.3) shows the solutions for  $\Re\epsilon(\omega)$  as a function of  $N$ , for perturbations differing only on the overtone number. For the fundamental mode, the solution reaches a precision up to the sixth significant figure with  $N \gtrsim 75$ , while for the second overtone this precision such precision is only reached for  $N \gtrsim 120$ . All of the results obtained for  $\Re\epsilon(\omega)$  can be equally reproduced for  $\Im\text{m}(\omega)$ .

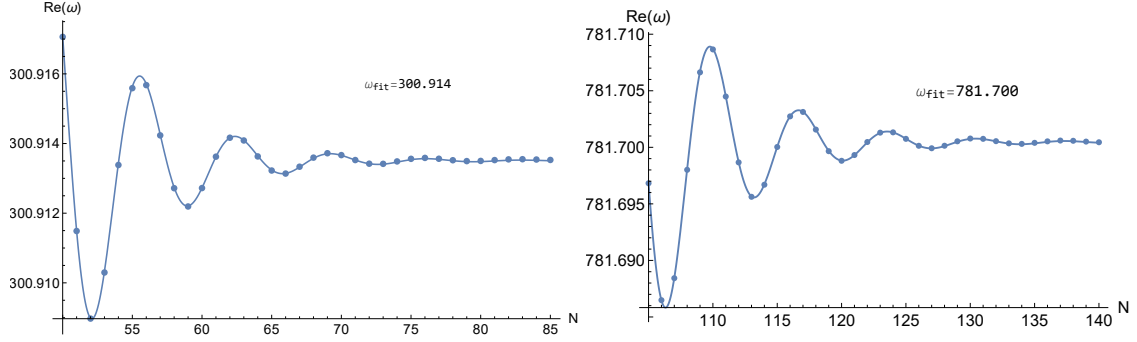


**Figure 4.3:** Convergence curves for the fundamental mode  $k = 0$  (Left) and for the second overtone  $k = 2$  (Right) of  $l = 1$  vector-type  $\mu = 0.2$  Proca field perturbations in 6-dimensional Schwarzschild-AdS, with  $r_h = 100$ . For the  $k = 0$  mode the method converges better (frequency oscillates around its sixth significant figure for  $N \simeq 75$ ) than for the  $k = 2$  mode (frequency oscillates around its sixth significant figure for  $N \simeq 120$ ). The  $\omega_{\text{fit}}$  values are also displayed.

To increase the accuracy of the results, instead of simply solving Eqs. (4.33) and (4.41) for a single large order  $N$ , we solved them for several orders and then fitted the convergence curve to  $\omega(N) = \omega_{\text{fit}} + c_2 e^{-c_3 N} \sin(c_4 N + c_5)$  (see also [30]). The desired solution was then determined by extracting  $\omega_{\text{fit}}$  from the fit. Observe that the reliability of the solutions depends on the convergence curve shape: while in 6-dimensional Schwarzschild-AdS these are indeed sinusoidally damped, we found that in 4, 5, 7-dimensional Schwarzschild-AdS these no longer oscillate, making it harder to determine an accurate value for the frequencies. This is illustrated in Fig. (4.4) for vector-type Proca field perturbations. It should be noted, however, that this behaviour was found to be independent of the perturbation-related parameters. Since scalar-type Proca field modes are coupled, it is reasonable to expect that these converge worse than the decoupled ones. Although such is true, the convergence of scalar-type and vector-type modes did not differ significantly for most parameters studied.

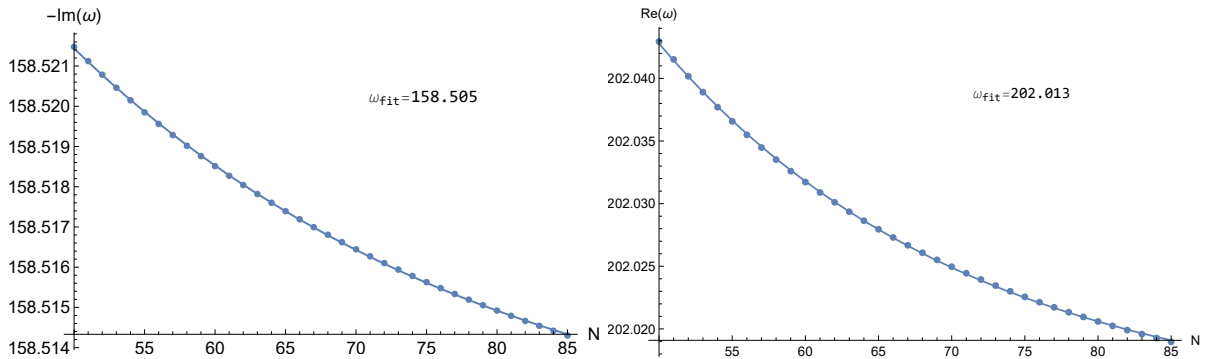


**Figure 4.4:** Convergence curves for the fundamental mode of vector-type  $\mu = 0.2$  Proca perturbations in 4-dimensional Schwarzschild-AdS (Left) and 5-dimensional Schwarzschild-AdS (Right), for a black hole with size  $r_h = 100$ . While in 6-dimensional Schwarzschild-AdS the convergence curves have a sinusoidal shape, in  $d = 4, 5, 7$ -dimensional Schwarzschild-AdS the curves exponentially decay without oscillating, making the determination of  $\omega_{\text{fit}}$  less accurate.

Lastly, we address a subtlety that arises from expanding the solution in a Frobenius series: the series remains valid only if the region of interest, from  $x = 0$  to  $x = x_h$ , is inside its radius of convergence, which, as we stated, is the distance between the point from which we initiate the expansion,  $x = x_h$ , and its closest singular point in the complex plane. Since the remaining singular points are given by the

zeroes of  $f$ , one needs to find these zeroes and check if they all lie outside the circle centered at  $x_h$  and with radius  $x_h$  in the complex plane. If not, and if it is not possible to perform a coordinate transformation that moves the singular points outside the circle, the Horowitz-Hubeny method fails [37, 57]. For large black holes, one can study this constraint analytically, as

$$f(\bar{x}) \simeq \frac{1}{\bar{x}^2 L^2} - \left(\frac{\bar{x}}{x_h}\right)^{d-3} = 0 \implies \bar{x}_{\bar{n}} = x_h e^{2\pi\bar{n}i/(d-1)} \quad , \quad \bar{n} = 0, 1, \dots, d-2 \quad . \quad (4.42)$$

Convergence of the series implies  $x_h < |\bar{x}_1 - \bar{x}_0|$ , which after using Eq. (4.42) yields

$$\frac{1}{2} < \sin\left(\frac{\pi}{d-1}\right) \implies d < 7 \quad . \quad (4.43)$$

Note that, for  $d = 7$ ,  $x_h$  lies precisely on the boundary of the convergence region. In this case, since Eq. (4.42) is only approximately satisfied, we need to check numerically if  $x_h$  is greater or smaller than the convergence radius. We found it was smaller, so that Horowitz-Hubeny method actually converges for  $d \leq 7$ , in the large black hole regime. For general-sized  $d$ -dimensional Schwarzschild-AdS black holes, such analytical solution for the zeroes of  $f$  cannot be found, and these need to be determined numerically. Although now the zeroes manifestly depend on the black hole radius, we once again found that, at least for the feasible radii to be studied with this method ( $r_h \gtrsim \mathcal{O}(0.1)$ ), the series only converges for  $d \leq 7$ . This is illustrated in Fig. (4.5) for  $r_h = 1$ .

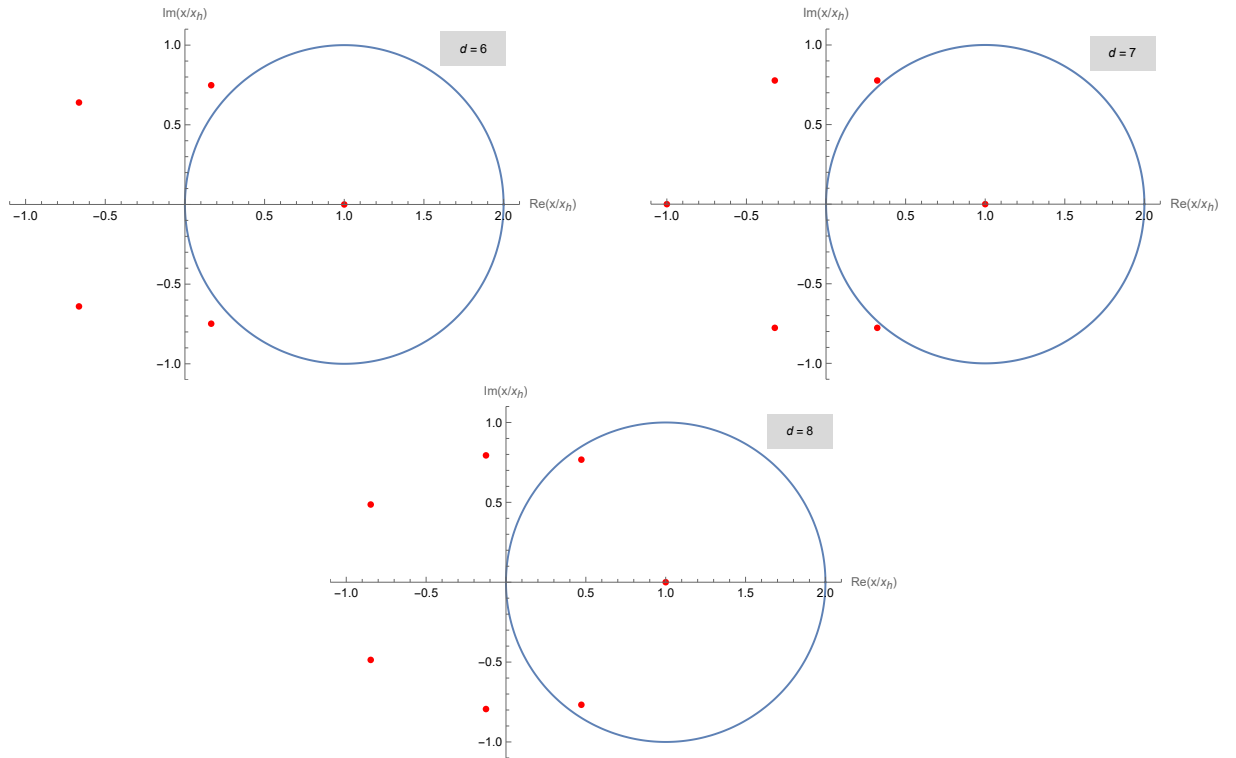


**Figure 4.5:** Singular points of Eq. (4.26) in the complex plane for a  $r_h = 1$  Schwarzschild-AdS black hole in: 6 (Left), 7 (Right) and 8 (Middle) dimensions. For the Horowitz-Hubeny method to work, all the zeroes of  $f$  should lie outside the blue circle. For  $d > 7$  and  $r_h \gtrsim \mathcal{O}(0.1)$ , this no longer happens.

## 4.3.2 Numerical integration of the equations of motion

### Description of the method

The poor convergence characteristics exhibited by the Horowitz-Hubeny method for small black holes and higher-dimensional spacetimes prompted us to exploit an alternative approach to compute the quasinormal mode spectrum. In [25], Chandrasekhar and Detweiler proposed the following method to compute quasinormal modes: start from a large value of  $r_*$ , say,  $r_*^{(f)}$ , where  $u_\infty(r_*^{(f)}) = u(r_*^{(\infty)})$ , with  $u(r_*^{(\infty)})$  determined from the asymptotic behaviour of the solution near  $r_*^{(\infty)}$ , and integrate numerically Eq. (4.6) down to an intermediate point,  $r_*^{(m)}$  ( $u_\infty$  denotes the inwardly numerically integrated solution). Similarly, start from a value of  $r_* = r_*^{(i)}$  close to the horizon, where  $u_h(r_*^{(i)}) = u(-\infty)$ , with  $u(-\infty)$  determined from the asymptotic behaviour of the solution near  $r_* = -\infty$ , and integrate numerically up to the same intermediate point ( $u_h$  denotes the outwardly numerically integrated solution). Since at this point the solutions need to be linearly dependent, one obtains the quasinormal frequencies by finding the roots of the Wronskian of the two solutions evaluated at  $r_*^{(m)}$ , i.e.  $(\partial_r u_\infty / \partial_r u_h)|_{r_*^{(m)}} = (u_\infty / u_h)|_{r_*^{(m)}}$ . In asymptotically flat and de Sitter spacetimes, the integration quickly becomes contaminated with the unwanted asymptotic behaviour of the solution. To see this, note that the leading-order solution near  $r_* = \pm\infty$  in these cases is

$$u(r_*) = c_1(\omega)e^{i\omega r_*} + c_2(\omega)e^{-i\omega r_*} \quad , \quad r_* \rightarrow \pm\infty \quad . \quad (4.44)$$

When one integrates the equation inwardly, starting at large  $r_*$ , the initial solution should be  $\sim e^{i\omega r_*}$ , which is exponentially large. However, this solution quickly becomes admixed with the exponentially suppressed solution  $\sim e^{-i\omega r_*}$ , so that the equation one is integrating no longer corresponds to that satisfying an outgoing boundary condition. The same happens with the outward integration.

In asymptotically AdS spacetimes, however, the solution converges at spatial infinity and the numerical instabilities mentioned do not appear. In this case, besides the strategy already mentioned, one can also do the simpler procedure: starting from the near-horizon point  $r_*^{(i)}$  and using the boundary condition Eq. (4.7), integrate Eq. (4.6) outwards to a large  $r_*^{(f)}$ . Since the asymptotic behaviour at spatial infinity is of the form

$$u(r) = c_1(\omega)u_1(r) + c_2(\omega)u_2(r) \quad , \quad (4.45)$$

with  $u_1$  and  $u_2$ , respectively, decaying and growing functions of  $r$ , the values of  $\omega$  that minimize the growing behaviour of the solution are easily found. For each  $\omega$ , one can fit the integrated solution near  $r_*^{(f)}$  to the expected behaviour Eq. (4.45) and extract the coefficient  $c_2$  from the fit. The quasinormal modes are found by solving numerically  $c_2(\omega) = 0$ . Due to the asymptotic behaviour of the solution, it is often sufficient to just minimize the solution at a sufficiently large point  $r^{(f)}$ , instead of performing the fit.

For a  $M \times M$  coupled system, the procedure is similar [39]: one needs to perform  $M$  integrations from the horizon, each of them for a different element of the suitable basis spanning the leading-order coefficients, e.g.,  $\{(1, 0, \dots, 0, 0), (0, 1, \dots, 0, 0), \dots, (0, 0, \dots, 1, 0), (0, 0, \dots, 0, 1)\}$ . One then computes the

matrix

$$\mathbf{S}(\omega, r) = \begin{pmatrix} u_1^{(1)} & \dots & u_1^{(M)} \\ \vdots & & \vdots \\ u_M^{(1)} & \dots & u_M^{(M)} \end{pmatrix}, \quad (4.46)$$

where  $u_i^{(j)}$  corresponds to the integrated solution of the  $i$ -th differential equation with respect to the  $j$ -th element of the basis. The quasinormal mode spectrum is then obtained by solving numerically

$$\det \left[ \mathbf{S} \left( \omega, r^{(f)} \right) \right] = 0, \quad (4.47)$$

for a sufficiently large  $r^{(f)}$ . To see whether  $r^{(f)}$  is sufficiently large, one computes the variation of the quasinormal mode frequency between the old  $r^{(f)}$  and the new one.

### Comments on the method's accuracy and reliability

This technique turns out to be very reliable to compute the quasinormal mode spectrum in asymptotically AdS spacetimes, specially the fundamental mode. For overtones with  $k \geq 1$ , the less pronounced minima makes it harder to find the correct solution for the mode frequency, as shown in Fig. (4.6). In general, we were able to find also the first and second overtones.

To start the integration from a point near the horizon,  $r^{(i)}$ , we expanded the solution as

$$u_h(r) = (r - r_h)^{-i\omega/f'(r_h)} \sum_{m=0}^N \alpha_m(\omega) (r - r_h)^m, \quad (4.48)$$

where the frequency dependent coefficients  $\alpha_m(\omega)$  are determined by substituting Eq. (4.48) in Eq. (4.6). We found that, for  $N \gtrsim 3$ , the order of the expansion did not influence the results, within the desired precision. Thus, we set the order at  $N = 5$ . Having found the coefficients  $\alpha_m$ , we integrated numerically Eq. (4.6) from  $r^{(i)} = r_h(1 + \epsilon)$ , with  $\epsilon \ll 1$ , using as initial conditions

$$\begin{aligned} u(r^{(i)}) &= u_h(r^{(i)}) \quad , \\ u'(r^{(i)}) &= u'_h(r^{(i)}) \quad , \end{aligned} \quad (4.49)$$

up to the point  $r^{(f)} = pr_h$ , where  $p \gg 1$ . While the choice of  $\epsilon$  does not influence the results within the desired precision, the choice of  $p$  does. This makes sense, since it is the choice of  $p$  that determines if the solution already reached its asymptotic infinity behaviour. Typically, the solutions started converging at  $p \sim 500$ . However, for small black holes or  $k \geq 1$  overtones, we had to increase this value until the solution started to converge. When even then the solution failed to converge, we matched the outward solution Eq. (4.48) with the inward solution

$$u_{\text{inf}}(r) = u_{\infty}(r) \sum_{m=0}^N \beta_m(\omega) r^{-m}, \quad (4.50)$$

at the intermediate point  $r = r^{(m)}$  whose variation was tested to check the reliability of the solutions. In

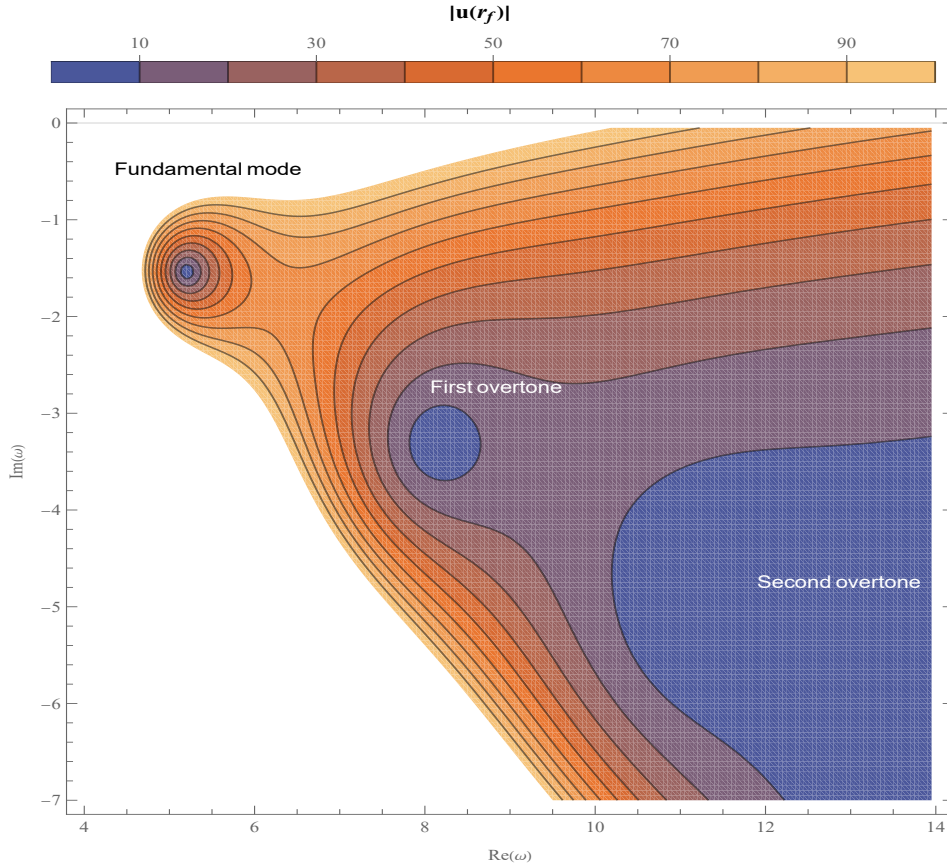


**Figure 4.6:** Contour plot of the absolute value of the solution evaluated at  $r^{(f)}$ , in the phase space of complex frequencies. The blue regions encompass the quasinormal modes. Note that the fundamental mode is constrained to a very small region of frequencies, whereas this region is larger for the first overtone. Moreover, for the second overtone, a broad region of low absolute value modes is formed, impeding the determination of the frequency, at least for such value of  $r^{(f)}$ .

Eq. (4.50),  $u_\infty(r)$  corresponds to the leading-order asymptotic behaviour of the solution, determined in Section 4.2.2. The quasinormal mode frequencies were then determined by minimizing the Wronskian

$$W(r, \omega) = u_h(r, \omega)u'_{\text{inf}}(r, \omega) - u'_h(r, \omega)u_{\text{inf}}(r, \omega) \quad , \quad (4.51)$$

evaluated at  $r = r^{(m)}$ .

## 4.4 Numerical results

Having outlined the numerical techniques, we now proceed to compute the quasinormal mode spectrum of Proca and Maxwell field perturbations in Schwarzschild-AdS. The distances are governed by two parameters: the radius of the black hole,  $r_h$ , and the radius of curvature of AdS,  $L$ . As aforementioned, the Schrödinger-like equations of motion are invariant under a rescaling on  $r, \mu, \omega$ , which corresponds to choosing the units of the physical quantities. In particular, one can perform the rescaling  $r \rightarrow rL$ ,  $\omega \rightarrow \omega/L$ ,  $\mu \rightarrow \mu/L$ , so that Eq. (4.6) is independent of  $L$ . Thus, without loss of generality, we fix  $L = 1$ . In asymptotically AdS spacetimes, the qualitative behaviour of the quasinormal spectrum highly

depends on the radius of the black hole [32, 34, 36, 58], so it is useful to do a separate study for three different types of black holes, according to their radii: large black holes, with  $r_h \gg 1$ , intermediate black holes, with  $r_h \simeq 1$ , and small black holes, with  $r_h \ll 1$ . In addition, the quasinormal mode spectrum may depend on the dimension of the spacetime,  $d$ , as well as on the perturbation-related parameters: the type of perturbation (scalar-type and vector-type), the mass of the field,  $\mu$ , the angular momentum number,  $l$ , and the overtone number,  $k$ . As stated before, our analysis focuses on  $d = 4, 5, 6, 7$ -dimensional Schwarzschild-AdS spacetimes. Generalization to higher dimensions should be straightforward.

Furthermore, the relevant range for the mass of the Proca field depends on the physical problem at study. In Schwarzschild-AdS spacetime, the key parameters describing the interaction between the spacetime geometry and the Proca field are  $\mu r_h \sim \mu M^{1/(d-3)}$ , which is often called the gravitational coupling, and  $\mu L = \mu$  (in  $L = 1$  units). We try to give an overview of all of these regimes, focusing in particular on  $\mu r_h \lesssim 1$ ,  $\mu \lesssim 1$ . Be aware that it is always assumed there is no back-reaction of the Proca field in the metric, i.e., that the Proca field propagates in *fixed* Schwarzschild-AdS background. In Chapter 2, the energy-momentum tensor of the Proca field,  $T_{\mu\nu}$ , was found to be Eq. (2.5), and it was argued that linear perturbations in the Proca field do not contribute to  $T_{\mu\nu}$ . However, there are terms in  $T_{\mu\nu}$  which, despite second-order in  $A_\mu$ , are multiplied by the mass of the Proca field squared,  $\mu^2$ . This means that, for large values of the mass of the field, the physical relevance of the perturbations diminishes, as one needs to guarantee these are also small enough to counteract the mass factor. A quantitative bound for the mass of the field remains, however, elusive. In the next section, we study how Proca quasinormal modes are affected by varying the mass of the field. We then analyze the spectrum as a function of the black hole radius, the overtone number and the angular momentum number.

#### 4.4.1 Effect of the mass of the field on the quasinormal mode spectrum

##### Vector-type perturbations

The vector-type sector is described by Eq. (4.2) for both Maxwell and Proca field perturbations, so that asking what are the differences between the vector-type spectra of a Maxwell field and a Proca field propagating in Schwarzschild-AdS is qualitatively analogous to asking what are the differences between those of a massless scalar field and a massive one. In Table (4.1), we show the fundamental mode frequencies for  $l = 1$  vector-type Maxwell and Proca field perturbations, for different masses of the Proca field, in 4, 5, 6, 7-dimensional Schwarzschild-AdS black holes with sizes  $r_h = 100$ ,  $r_h = 1$  and  $r_h = 0.05$ .

$r_h$	$\mu$	$\omega (d = 4)$	$\omega (d = 5)$	$\omega (d = 6)$	$\omega (d = 7)$
100	0	0. - 150.048 <i>i</i>	200.026 - 199.995 <i>i</i>	299.458 - 200.486 <i>i</i>	383.691 - 199.894 <i>i</i>
	0.1	0. - 152.185 <i>i</i>	200.525 - 200.493 <i>i</i>	299.823 - 200.765 <i>i</i>	383.979 - 200.071 <i>i</i>
	0.2	0. - 158.505 <i>i</i>	202.007 - 201.975 <i>i</i>	300.914 - 201.596 <i>i</i>	384.839 - 200.602 <i>i</i>
	0.3	0. - 168.844 <i>i</i>	204.429 - 204.398 <i>i</i>	302.715 - 202.969 <i>i</i>	386.267 - 201.483 <i>i</i>
	0.4	0. - 183.251 <i>i</i>	207.729 - 207.698 <i>i</i>	305.205 - 204.868 <i>i</i>	388.252 - 202.707 <i>i</i>
	0.5	0. - 202.583 <i>i</i>	211.829 - 211.798 <i>i</i>	308.356 - 207.269 <i>i</i>	390.780 - 204.266 <i>i</i>
1	0	2.16302 - 1.69909 <i>i</i>	3.84177 - 1.62618 <i>i</i>	5.20392 - 1.53559 <i>i</i>	6.43969 - 1.45072 <i>i</i>
	0.1	2.17058 - 1.71095 <i>i</i>	3.84730 - 1.63091 <i>i</i>	5.20810 - 1.53813 <i>i</i>	6.44299 - 1.45229 <i>i</i>
	0.2	2.19254 - 1.74526 <i>i</i>	3.86377 - 1.64499 <i>i</i>	5.22058 - 1.54573 <i>i</i>	6.45286 - 1.45699 <i>i</i>
	0.3	2.22707 - 1.79879 <i>i</i>	3.89075 - 1.66805 <i>i</i>	5.24123 - 1.55828 <i>i</i>	6.46923 - 1.4648 <i>i</i>
	0.4	2.27191 - 1.86765 <i>i</i>	3.92761 - 1.69952 <i>i</i>	5.26981 - 1.57567 <i>i</i>	6.49202 - 1.47565 <i>i</i>
	0.5	2.32497 - 1.94823 <i>i</i>	3.97359 - 1.73872 <i>i</i>	5.30603 - 1.59769 <i>i</i>	6.52107 - 1.48949 <i>i</i>
0.05	0	2.93223 - 5.39171 $\times 10^{-5}$ <i>i</i>	4.11251 - 4.65094 $\times 10^{-6}$ <i>i</i>	4.99957 - 4.53425 $\times 10^{-7}$ <i>i</i>	5.99996 - 4.85953 $\times 10^{-8}$ <i>i</i>
	0.1	2.94163 - 5.46847 $\times 10^{-5}$ <i>i</i>	4.07167 - 4.45560 $\times 10^{-6}$ <i>i</i>	5.00290 - 4.54977 $\times 10^{-7}$ <i>i</i>	6.00246 - 4.87122 $\times 10^{-8}$ <i>i</i>
	0.2	2.96881 - 5.69458 $\times 10^{-5}$ <i>i</i>	4.03879 - 4.30233 $\times 10^{-6}$ <i>i</i>	5.01284 - 4.59635 $\times 10^{-7}$ <i>i</i>	6.00994 - 4.90633 $\times 10^{-8}$ <i>i</i>
	0.3	3.01112 - 6.05978 $\times 10^{-5}$ <i>i</i>	4.01466 - 4.19204 $\times 10^{-6}$ <i>i</i>	5.02927 - 4.67405 $\times 10^{-7}$ <i>i</i>	6.02234 - 4.96497 $\times 10^{-8}$ <i>i</i>
	0.4	3.01112 - 6.05978 $\times 10^{-5}$ <i>i</i>	3.99999 - 4.12551 $\times 10^{-6}$ <i>i</i>	5.05197 - 4.78298 $\times 10^{-7}$ <i>i</i>	6.03957 - 5.04733 $\times 10^{-8}$ <i>i</i>
	0.5	3.12875 - 7.16258 $\times 10^{-5}$ <i>i</i>	3.99493 - 4.10327 $\times 10^{-6}$ <i>i</i>	5.08069 - 4.92331 $\times 10^{-7}$ <i>i</i>	6.06151 - 5.15367 $\times 10^{-8}$ <i>i</i>

**Table 4.1:** Fundamental mode of  $l = 1$  vector-type Maxwell and Proca perturbations in 4, 5, 6, 7-dimensional Schwarzschild-AdS spacetime with  $r_h = 100$ ,  $r_h = 1$  and  $r_h = 0.05$ , for different values of the mass of the field.

Note that for  $r_h = 0.05$ , the frequencies are close to the ones for pure AdS, given in Eq. (3.15). This will be further investigated in Section 4.4.2. The frequencies for 4-dimensional Schwarzschild-AdS are close to the ones reported in [51]. We believe the discrepancies between values have to do with the poor convergence properties of the Horowitz-Hubeny method as the mass of the field increases (c.f. Figure 1 of [51] shows the convergence curve for  $\mu = 0.5$ ). The frequencies of Table (4.1) were computed by matching the numerical integrated solutions at an intermediate point and minimizing the Wronskian. This is specially important in  $d = 4$ , as the growing solution at infinity has an exponent close to zero for small masses of the field, c.f. Eq. (4.11). The impact of the mass of the field and the spacetime dimension on the spectrum will be studied in Section 4.4.1, along with scalar-type perturbations. As a prelude, note that both real and imaginary parts increase in magnitude as the mass of the field increases, in agreement with [42, 51].

### Monopole mode of the Proca field

As explained earlier, the monopole mode allows one to distinguish between the two scalar-type polarizations, since in this case only the non-electromagnetic polarization corresponds to a physical degree of freedom. We will thus start by analyzing this situation to better interpret the results for higher multipoles. Table (4.2) shows the quasinormal mode spectrum of monopole Proca perturbations in

4, 5, 6, 7-dimensional Schwarzschild-AdS, for different masses of the field and black hole sizes.

$r_h$	$\mu$	$\omega (d = 4)$	$\omega (d = 5)$	$\omega (d = 6)$	$\omega (d = 7)$
100	0.1	185.569 – 267.526 <i>i</i>	312.426 – 275.165 <i>i</i>	413.971 – 269.616 <i>i</i>	501.060 – 261.424 <i>i</i>
	0.2	187.346 – 270.819 <i>i</i>	313.801 – 276.650 <i>i</i>	415.038 – 270.457 <i>i</i>	501.916 – 261.962 <i>i</i>
	0.3	190.106 – 275.942 <i>i</i>	316.047 – 279.075 <i>i</i>	416.800 – 271.846 <i>i</i>	503.334 – 262.853 <i>i</i>
	0.4	193.636 – 282.504 <i>i</i>	319.103 – 282.376 <i>i</i>	419.234 – 273.765 <i>i</i>	505.304 – 264.092 <i>i</i>
	0.5	197.742 – 290.148 <i>i</i>	322.892 – 286.471 <i>i</i>	422.310 – 276.190 <i>i</i>	507.811 – 265.669 <i>i</i>
1	0.1	2.80724 – 2.68313 <i>i</i>	4.58507 – 2.55966 <i>i</i>	6.01308 – 2.35363 <i>i</i>	7.27221 – 2.16280 <i>i</i>
	0.2	2.83328 – 2.71753 <i>i</i>	4.60375 – 2.57442 <i>i</i>	6.02701 – 2.36168 <i>i</i>	7.28309 – 2.16779 <i>i</i>
	0.3	2.87379 – 2.77101 <i>i</i>	4.63430 – 2.59855 <i>i</i>	6.05003 – 2.37497 <i>i</i>	7.30115 – 2.17606 <i>i</i>
	0.4	2.92572 – 2.83946 <i>i</i>	4.67589 – 2.63137 <i>i</i>	6.08184 – 2.39332 <i>i</i>	7.32625 – 2.18756 <i>i</i>
	0.5	2.98623 – 2.91912 <i>i</i>	4.72755 – 2.67209 <i>i</i>	6.12207 – 2.41652 <i>i</i>	7.35822 – 2.20219 <i>i</i>
0.05	0.1	2.86292 – 1.94677 × 10 <sup>-2</sup> <i>i</i>	3.98937 – 1.75825 × 10 <sup>-3</sup> <i>i</i>	5.00162 – 1.81866 × 10 <sup>-4</sup> <i>i</i>	6.00231 – 1.94173 × 10 <sup>-5</sup> <i>i</i>
	0.2	2.88910 – 1.98707 × 10 <sup>-2</sup> <i>i</i>	4.00405 – 1.77507 × 10 <sup>-3</sup> <i>i</i>	5.01155 – 1.83002 × 10 <sup>-4</sup> <i>i</i>	6.00979 – 1.95086 × 10 <sup>-5</sup> <i>i</i>
	0.3	2.92988 – 2.05020 × 10 <sup>-2</sup> <i>i</i>	4.02805 – 1.80268 × 10 <sup>-3</sup> <i>i</i>	5.02797 – 1.84886 × 10 <sup>-4</sup> <i>i</i>	6.02219 – 1.96605 × 10 <sup>-5</sup> <i>i</i>
	0.4	2.98222 – 2.13182 × 10 <sup>-2</sup> <i>i</i>	4.06075 – 1.84049 × 10 <sup>-3</sup> <i>i</i>	5.05066 – 1.87503 × 10 <sup>-4</sup> <i>i</i>	6.03942 – 1.98727 × 10 <sup>-5</sup> <i>i</i>
	0.5	3.04330 – 2.22800 × 10 <sup>-2</sup> <i>i</i>	4.10136 – 1.88781 × 10 <sup>-3</sup> <i>i</i>	5.07935 – 1.90836 × 10 <sup>-4</sup> <i>i</i>	6.06136 – 2.01447 × 10 <sup>-5</sup> <i>i</i>

**Table 4.2:** Fundamental mode of  $l = 0$  Proca perturbations in 4, 5, 6, 7-dimensional Schwarzschild-AdS spacetime with  $r_h = 100$ ,  $r_h = 1$  and  $r_h = 0.05$ , for different values of the mass of the field.

As before, the frequencies approach those of pure AdS, c.f. Eq. (3.15), for small black holes. The results of Table (4.2) for  $d = 4$  may be compared with the ones obtained in [42]: overall there is an agreement between the results up to the fifth significant figure. The remaining discrepancies are attributed to the different methods used to compute the spectrum: [42] used Horowitz-Hubeny method while the results from Table (4.2) were obtained by numerical integration. Other aspects are similar to the ones observed for higher multipoles of scalar-type perturbations, and will be discussed in Section 4.4.1.

Although we did not present it in Table (4.2), we found there was a purely imaginary mode for all the dimensions studied. This was confirmed with Horowitz-Hubeny method. In particular, this mode was not reported in [42] for the 4-dimensional case. We chose not to present it here explicitly as we are not sure regarding its physical significance. Additionally, this mode was found to scale with the horizon radius, so that it does not correspond to the family of “special” modes discovered for vector-type gravitational perturbations in [32, 59, 60].

### Maxwell scalar-type perturbations

In the electromagnetic limit, the non-electromagnetic polarization becomes spurious due to the gauge freedom of the field, and the scalar-type sector is described by a single degree of freedom: the electromagnetic polarization. The frequencies for  $l = 1$  scalar-type electromagnetic perturbations are displayed in Table (4.3). In the small black hole limit, the results approach those of Eq. (3.19). For  $d = 5$ , the frequencies were found by imposing that the subdominant logarithmic term in Eq. (4.16) vanishes. Note,

$r_h$	$\omega (d = 4)$	$\omega (d = 5)$	$\omega (d = 6)$	$\omega (d = 7)$
100	$0. - 150.048i$	$200.010 - 200.000i$	$299.447 - 200.490i$	$383.681 - 199.896i$
1	$2.16302 - 1.69909i$	$2.66237 - 1.58299i$	$4.41406 - 1.68956i$	$5.73731 - 1.59713i$
0.05	$2.93223 - 5.39171 \times 10^{-5}i$	$2.99617 - 5.74442 \times 10^{-6}i$	$3.99948 - 1.65071 \times 10^{-6}i$	$4.99994 - 3.35996 \times 10^{-7}i$

**Table 4.3:** Fundamental mode frequencies of  $l = 1$  scalar-type electromagnetic perturbations in 4, 5, 6, 7-dimensional Schwarzschild-AdS for different black hole sizes.

however, that this is not required by the Dirichlet boundary condition, as this term also vanishes when the  $r \rightarrow \infty$  limit is taken. This is why the frequencies also approach the expression for  $d \geq 6$  spacetimes of Eq. (3.19). A more elaborate study still needs to be performed in order to establish the physically relevant boundary conditions in  $d = 5$  [19, 55]. Besides the results presented in Table (4.3), we found for  $d \geq 5$  an interesting purely imaginary mode which, unlike the other modes, scales with the inverse of the black hole radius. This could belong to the family of “special” modes reported numerically in [32, 59] and analytically in [60], and will be studied in Section 4.4.2

Note that scalar-type and vector-type Maxwell field modes are nearly isospectral in the large black hole regime for *all* spacetime dimensions. This is rather surprising, as the potentials Eqs. (4.2) and (4.5) show different behaviours for  $d > 4$ , even within this regime. We explore this in Appendix C following [3] (see also [32, 36]), and it turns out that, for large black holes, the scalar-type and vector-type potentials are “superpartner potentials”, which, added to the asymptotic behaviour of the solutions near spatial infinity, yield isospectral frequencies.

### Higher multipoles of scalar-type Proca perturbations

The mass of the field introduces a coupling between the two scalar-type degrees of freedom, which makes the analysis of the quasinormal mode spectrum more difficult. The solutions  $\omega$  for the eigenvalue problem Eq. (4.6) are now an admixture of modes corresponding to two different polarizations: the electromagnetic polarization and the non-electromagnetic polarization. The distinction between these two can be made in several ways. To begin with, the analysis leading to Eq. (2.62) suggests that, in the small mass limit, the electromagnetic and non-electromagnetic polarizations should approach, respectively, the (scalar-type) Maxwell field and the scalar field modes. The polarizations may thus be picked up by comparing these spectra in this limit. Scalar field perturbations in higher-dimensional Schwarzschild-AdS black holes were considered in [30], so we can apply the numerical methods studied in Section 4.3 to the potential presented in [30]. However, for large black holes, the dependence on  $l$  is weak and lower multipoles of non-electromagnetic polarized Proca perturbations may be picked up by simply comparing them with the monopole mode spectrum. On the other hand, and even though the boundary condition imposed at the horizon of Schwarzschild-AdS does not reduce to the regularity boundary condition imposed at the origin of pure AdS, the numerical results already obtained show that, for very small black holes, the Schwarzschild-AdS frequencies approach the pure AdS ones. This can be also used to distinguish the two scalar-type polarizations: we are expecting that in the  $r_h \rightarrow 0$  regime the spectra of electromagnetic and non-electromagnetic polarizations approach, respectively, the spectra of the (−) and (+) polarizations, given in Eq. (3.15). The quasinormal frequencies for  $l = 1$  scalar-type Proca perturbations are displayed in Tables (4.4) and (4.5), corresponding, respectively, to

electromagnetic and non-electromagnetic polarizations. These were computed for different masses of the field and different sizes of the black hole.

$r_h$	$\mu$	$\omega (d = 4)$	$\omega (d = 5)$	$\omega (d = 6)$	$\omega (d = 7)$
100	0.1	$0. - 152.097i$	$200.509 - 200.499i$	$299.812 - 200.768i$	$383.969 - 200.073i$
	0.2	$0. - 158.41i$	$201.990 - 201.980i$	$300.902 - 201.599i$	$384.830 - 200.604i$
	0.3	$0. - 168.74i$	$204.413 - 204.403i$	$302.704 - 202.972i$	$386.257 - 201.485i$
	0.4	$0. - 183.13i$	$207.714 - 207.703i$	$305.194 - 204.871i$	$388.242 - 202.709i$
	0.5	$0. - 202.42i$	$211.814 - 211.803i$	$308.345 - 207.272i$	$390.770 - 204.269i$
1	0.1	$1.55730 - 0.552855i$	$2.66878 - 1.59009i$	$4.41877 - 1.69234i$	$5.74090 - 1.59879i$
	0.2	$1.56804 - 0.584696i$	$2.68791 - 1.61115i$	$4.43286 - 1.70062i$	$5.75162 - 1.60373i$
	0.3	$1.58499 - 0.635019i$	$2.71949 - 1.64544i$	$4.45614 - 1.71432i$	$5.76942 - 1.61194i$
	0.4	$1.60693 - 0.700894i$	$2.76308 - 1.69187i$	$4.48836 - 1.73324i$	$5.79417 - 1.62335i$
	0.5	$1.63298 - 0.779491i$	$2.81810 - 1.74904i$	$4.52915 - 1.75717i$	$5.82571 - 1.63789i$
0.05	0.1	$1.98737 - 7.6215 \times 10^{-6}i$	$3.00114 - 5.79871 \times 10^{-6}i$	$4.00281 - 1.65889 \times 10^{-6}i$	$5.00243 - 3.37073 \times 10^{-7}i$
	0.2	$2.01476 - 8.3030 \times 10^{-6}i$	$3.01589 - 5.96205 \times 10^{-6}i$	$4.01275 - 1.68350 \times 10^{-6}i$	$5.00991 - 3.40312 \times 10^{-7}i$
	0.3	$2.05739 - 9.4465 \times 10^{-6}i$	$3.04000 - 6.23652 \times 10^{-6}i$	$4.02917 - 1.72478 \times 10^{-6}i$	$5.02231 - 3.45740 \times 10^{-7}i$
	0.4	$2.11204 - 1.10687 \times 10^{-5}i$	$3.07285 - 6.62548 \times 10^{-6}i$	$4.05187 - 1.78312 \times 10^{-6}i$	$5.03954 - 3.53397 \times 10^{-7}i$
	0.5	$2.17574 - 1.31993 \times 10^{-5}i$	$3.11366 - 7.13370 \times 10^{-6}i$	$4.08058 - 1.85907 \times 10^{-6}i$	$5.06149 - 3.63339 \times 10^{-7}i$

**Table 4.4:** Fundamental mode of the  $l = 1$  electromagnetic polarization of scalar-type Proca perturbations in 4, 5, 6, 7-dimensional Schwarzschild-AdS spacetime with  $r_h = 100$ ,  $r_h = 1$  and  $r_h = 0.05$ , for different values of the mass of the field.

$r_h$	$\mu$	$\omega (d = 4)$	$\omega (d = 5)$	$\omega (d = 6)$	$\omega (d = 7)$
100	0.1	$185.569 - 267.526i$	$312.433 - 275.163i$	$413.978 - 269.614i$	$501.067 - 261.422i$
	0.2	$187.346 - 270.819i$	$313.808 - 276.648i$	$415.045 - 270.455i$	$501.922 - 261.960i$
	0.3	$190.106 - 275.942i$	$316.054 - 279.073i$	$416.807 - 271.844i$	$503.340 - 262.852i$
	0.4	$193.636 - 282.504i$	$319.110 - 282.374i$	$419.241 - 273.763i$	$505.310 - 264.090i$
	0.5	$197.742 - 290.148i$	$322.899 - 286.469i$	$422.316 - 276.188i$	$507.817 - 265.667i$
1	0.1	$3.33864 - 2.50109i$	$5.09680 - 2.38187i$	$6.53418 - 2.18970i$	$7.80878 - 2.01206i$
	0.2	$3.36178 - 2.53441i$	$5.11406 - 2.39630i$	$6.54725 - 2.19759i$	$7.81908 - 2.01696i$
	0.3	$3.39782 - 2.58616i$	$5.14229 - 2.41988i$	$6.56884 - 2.21062i$	$7.83617 - 2.02509i$
	0.4	$3.44410 - 2.65233i$	$5.18076 - 2.45195i$	$6.59870 - 2.22862i$	$7.85993 - 2.03638i$
	0.5	$3.49815 - 2.72926i$	$5.22860 - 2.49174i$	$6.63649 - 2.25137i$	$7.89019 - 2.05076i$
0.05	0.1	$3.91824 - 4.75563 \times 10^{-5}i$	$4.99236 - 7.1501 \times 10^{-6}i$	$6.00264 - 8.725 \times 10^{-7}i$	$7.00244 - 9.888 \times 10^{-8}i$
	0.2	$3.94538 - 4.89806 \times 10^{-5}i$	$5.01207 - 7.2722 \times 10^{-6}i$	$6.01258 - 8.794 \times 10^{-7}i$	$7.00991 - 9.945 \times 10^{-8}i$
	0.3	$3.98765 - 5.12362 \times 10^{-5}i$	$5.03619 - 7.4219 \times 10^{-6}i$	$6.02901 - 8.909 \times 10^{-7}i$	$7.02231 - 1.004 \times 10^{-7}i$
	0.4	$4.04191 - 5.41980 \times 10^{-5}i$	$5.06904 - 7.6282 \times 10^{-6}i$	$6.05171 - 9.061 \times 10^{-7}i$	$7.03954 - 1.017 \times 10^{-7}i$
	0.5	$4.10524 - 5.77538 \times 10^{-5}i$	$5.10986 - 7.8886 \times 10^{-6}i$	$6.08042 - 9.275 \times 10^{-7}i$	$7.06149 - 1.035 \times 10^{-7}i$

**Table 4.5:** Fundamental mode of the  $l = 1$  non-electromagnetic polarization of scalar-type Proca perturbations in 4, 5, 6, 7-dimensional Schwarzschild-AdS spacetime with  $r_h = 100$ ,  $r_h = 1$  and  $r_h = 0.05$ , for different values of the mass of the field.

As expected, the frequencies approach the spectra of Eq. (3.15) in the small black hole regime, c.f. last rows of Tables (4.4) and (4.5). This however creates a difficulty in the distinction between the two polarizations, since the  $k + 1^{\text{th}}$  overtone with electromagnetic polarization is isospectral to the  $k^{\text{th}}$  overtone with non-electromagnetic polarization. Of course, a finite sized black hole breaks this isospectrality, but for very small black holes the degeneracy between the modes is very hard to spot numerically. In particular, for the modes computed, we needed to distinguish between the fundamental mode of the non-electromagnetic polarization and the first overtone of the electromagnetic polarization. Our strategy was to compute the first overtone of scalar-type Maxwell field perturbations and the fundamental mode of scalar field perturbations in this regime and then compare them with the two candidate Proca modes, for a small mass of the Proca field. The first overtone electromagnetically polarized corresponds to the first overtone of the electromagnetic perturbation, while the fundamental mode non-electromagnetically polarized corresponds to the fundamental mode of the scalar field perturbation. In  $d = 4$  this does not work, as the electromagnetic scalar-type frequencies in the small black hole regime approach  $\omega = 3$  instead of  $\omega = 2$ . In this case, the distinction was made by comparing the frequencies to the scalar field spectrum, while the electromagnetic polarization was picked up by exclusion.

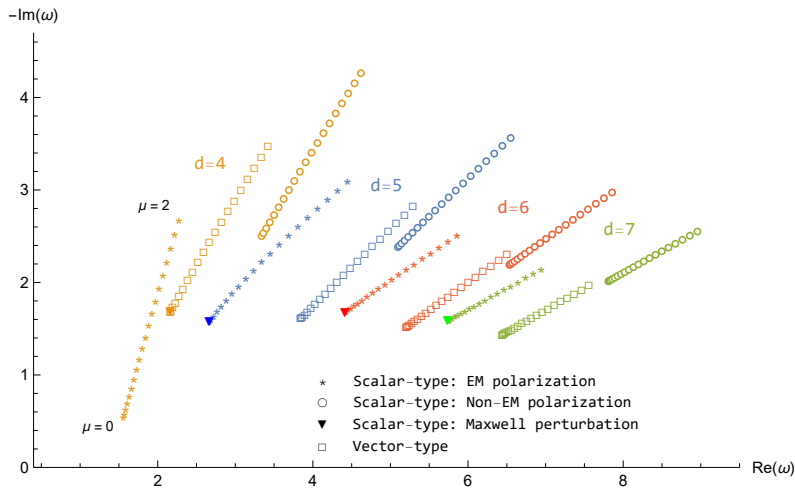


**Figure 4.7:** Effect of the field's mass ( $\mu \in [0.1, 2.0]$ ) on the fundamental quasinormal spectrum of vector-type and scalar-type  $l = 1$  Proca perturbations in 4, 5, 6, 7-dimensional Schwarzschild-AdS, with  $r_h = 1$ . We also plotted the results for a Maxwell perturbation, which should be compared with the Proca small mass limit.

Figure (4.7) summarizes the results obtained so far, for fundamental  $l = 1$  modes and  $r_h = 1$ . The qualitative effect of the Proca mass on the spectrum seems to be almost independent of the type of perturbation, specially for  $d > 4$ . Increasing the spacetime dimension suppresses this effect, as one expects from Eqs. (4.2) and (4.3): higher-dimensional Schwarzschild-AdS spacetimes already provide a mass term to the potential, proportional to  $(d - 4)(d - 2)$ . Note that, for  $d \geq 5$ , the electromagnetically polarized frequencies of the Proca field approach, in the small-mass limit, the ones for Maxwell field perturbations. This is in agreement with what one expects from Eq. (2.62). However, such behaviour does not happen in  $d = 4$ , where the Maxwell field modes can be viewed as the massless limit of vector-type perturbations, due to the isospectrality between scalar- and vector-type sectors. This is explained by the contrasting shapes of the vector-type effective potential when  $\mu = 0$  and when  $\mu \neq 0$ : for  $d > 4$ ,

going from a massless to a massive field changes smoothly the potential, whereas for  $d = 4$  the leading-order term in  $r$  disappears for  $\mu = 0$ , creating a “barrier-like potential” instead of a “box-like” one. We also compared the non-electromagnetic polarization spectrum with the spectrum for scalar field perturbations (see, e.g. [30]). In the small mass limit, these become nearly isospectral, as depicted in Fig. (4.8) for 7 dimensions, and in agreement with what one expects from Eq. (2.62).

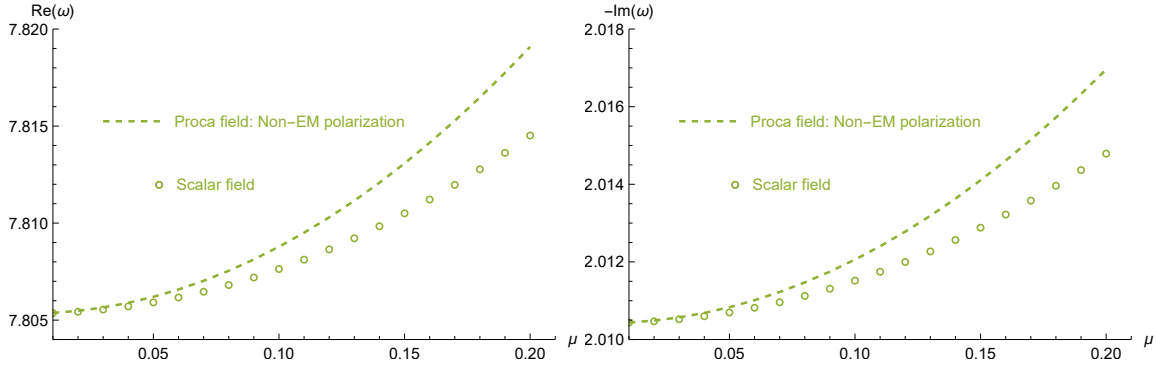


**Figure 4.8:** Comparison between the spectra for scalar field perturbations and for non-electromagnetically polarized Proca field perturbations in 7-dimensional Schwarzschild-AdS, with  $r_h = 1, l = 1$ . In the small-mass limit these are nearly isospectral, in agreement with Eq. (2.62).

Additionally, we found that the mass of the field seems to break the behaviour of the “special” modes found for scalar-type Maxwell perturbations. One should however perform a deeper analysis of these modes. Lastly, note that the isospectrality between scalar-type and vector-type modes in the large black hole regime, established in Appendix C for Maxwell field perturbations, seems to be maintained for vector-type and scalar-type electromagnetically polarized Proca field modes. This is quite a remarkable result, and was verified for larger black holes and larger masses of the field. As the scalar-type modes remain coupled in the large black hole regime, an analysis similar to the one done in Appendix C seems to be more difficult. This would be an interesting result to establish, as it could also hint for a decoupling in the scalar-type sector.

#### 4.4.2 Quasinormal mode spectrum as a function of the black hole radius

In this section we take a closer look on how the quasinormal mode spectrum varies with the size of the black hole. The qualitative behaviour in the different black hole regimes is independent of the perturbation parameters. We will restrict ourselves to the study of  $l = 2$  Proca perturbations, with field’s mass  $\mu = 0.2$ , in 5, 6, 7-dimensional Schwarzschild-AdS spacetime. Results for 4-dimensional Schwarzschild-AdS and other types of perturbations can be found in [30, 32, 34].

##### Large black hole regime

We start by studying the large black hole regime, where the imaginary part of the mode frequency has a direct application within the context of the AdS/CFT correspondence, as it is dual to the thermalization scale of the CFT. In [30], Horowitz and Hubeny showed that large Schwarzschild-AdS back holes obey a scaling symmetry such that the mode frequencies grow linearly with the radius of the horizon, that

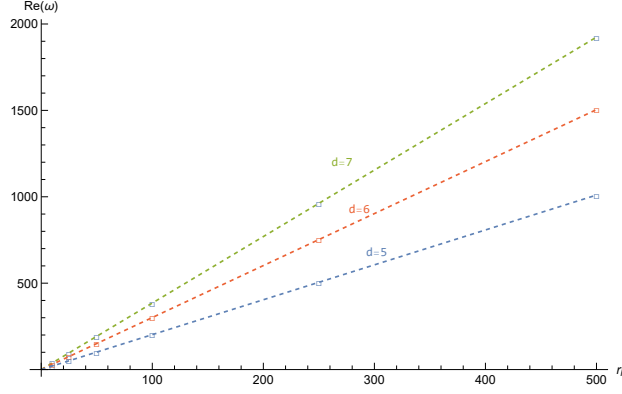


**Figure 4.9:** Fundamental quasinormal frequencies of  $l = 2$  vector-type Proca perturbations in 5, 6, 7-dimensional Schwarzschild-AdS spacetimes for a Proca field with mass  $\mu = 0.2$  as a function of the black hole radius, in the large black hole regime. For large black holes, the frequencies scale linearly with the radius of the horizon. Fit results: for  $d = 5$ ,  $\Re(\omega) = 2.01926r_h + 0.219492$ ; for  $d = 6$ ,  $\Re(\omega) = 3.00834r_h + 0.205195$ ; and for  $d = 7$ ,  $\Re(\omega) = 3.84754r_h + 0.214392$ .

is,  $\omega \sim r_h$ . The numerical results obtained for different radii in this regime, shown in Table (4.6) and Fig. (4.9), confirm this behaviour.

	$r_h$	Vector-type	Scalar-type (EM)	Scalar-type (Non-EM)
$d = 5$	500	1009.91 – 1009.90 <i>i</i>	1009.90 – 1009.90 <i>i</i>	1568.92 – 1383.26 <i>i</i>
	250	504.969 – 504.946 <i>i</i>	504.955 – 504.951 <i>i</i>	784.473 – 691.627 <i>i</i>
	100	202.027 – 201.968 <i>i</i>	201.990 – 201.980 <i>i</i>	313.820 – 276.644 <i>i</i>
	50	101.083 – 100.966 <i>i</i>	101.010 – 100.990 <i>i</i>	156.965 – 138.310 <i>i</i>
	25	50.6797 – 50.4471 <i>i</i>	50.5353 – 50.4951 <i>i</i>	78.5920 – 69.1315 <i>i</i>
	10	20.6542 – 20.0798 <i>i</i>	20.2959 – 20.1973 <i>i</i>	31.7420 – 27.5869 <i>i</i>
$d = 6$	500	1504.43 – 1008.01 <i>i</i>	1504.43 – 1008.01 <i>i</i>	2075.08 – 1352.31 <i>i</i>
	250	752.229 – 504.000 <i>i</i>	752.221 – 504.002 <i>i</i>	1037.55 – 676.150 <i>i</i>
	100	300.928 – 201.592 <i>i</i>	300.907 – 201.597 <i>i</i>	415.055 – 270.453 <i>i</i>
	50	150.529 – 100.781 <i>i</i>	150.487 – 100.792 <i>i</i>	207.587 – 135.213 <i>i</i>
	25	75.3933 – 50.3610 <i>i</i>	75.3102 – 50.3836 <i>i</i>	103.912 – 67.5802 <i>i</i>
	10	30.5160 – 20.0622 <i>i</i>	30.3099 – 20.1179 <i>i</i>	41.8956 – 26.9584 <i>i</i>
$d = 7$	500	1924.04 – 1003.04 <i>i</i>	1924.04 – 1003.04 <i>i</i>	2509.45 – 1309.83 <i>i</i>
	250	962.035 – 501.518 <i>i</i>	962.029 – 501.520 <i>i</i>	1254.74 – 654.914 <i>i</i>
	100	384.852 – 200.599 <i>i</i>	384.836 – 200.603 <i>i</i>	501.932 – 261.958 <i>i</i>
	50	192.493 – 100.285 <i>i</i>	192.461 – 100.293 <i>i</i>	251.031 – 130.964 <i>i</i>
	25	96.3813 – 50.1136 <i>i</i>	96.3176 – 50.1285 <i>i</i>	125.645 – 65.4537 <i>i</i>
	10	38.9276 – 19.9648 <i>i</i>	38.7697 – 20.0015 <i>i</i>	50.6197 – 26.1018 <i>i</i>

**Table 4.6:** Fundamental quasinormal mode frequencies of  $l = 2$  Proca field perturbations in 5, 6, 7-dimensional Schwarzschild-AdS, for a Proca field with mass  $\mu = 0.2$  and different black hole sizes, in the large black hole regime.

Note that the modes of Maxwell and Proca field perturbations in higher-dimensional large black holes

are no longer purely imaginary, as it happened in 4 dimensions [32, 51]. This primarily relates to the differences in the associated potential properties, although the modes always decay, whether oscillating ( $d > 4$ ) or not ( $d = 4$ ). In Fig. (4.9) we plotted the real part of the frequencies as a function of the black hole radius. Similar results can be found for the imaginary part. Within the AdS/CFT context, it is useful to express the frequencies as a function of the Hawking temperature,

$$T_H = \frac{f'(r_h)}{4\pi} = \frac{(d-1)r_h^2 + (d-3)L^2}{4\pi r_h L^2} \simeq \frac{(d-1)r_h}{4\pi L^2}, \quad (4.52)$$

where the last equality is for the large black hole regime. From this, one sees that the quasinormal frequencies also scale linearly with the Hawking temperature. An interesting exception to the  $r_h$  scaling happens for the “special” modes mentioned in Section 4.4.1, which scale with  $1/r_h$ : these were only found for scalar-type Maxwell perturbations in higher-dimensional Schwarzschild-AdS, and are presented in Fig. (4.10) as a function of the inverse of the black hole radius. We believe a study of these modes for Maxwell field perturbations in higher-dimensional settings is still missing. We also highlight once again the isospectrality between vector-type and electromagnetically polarized modes in this regime.

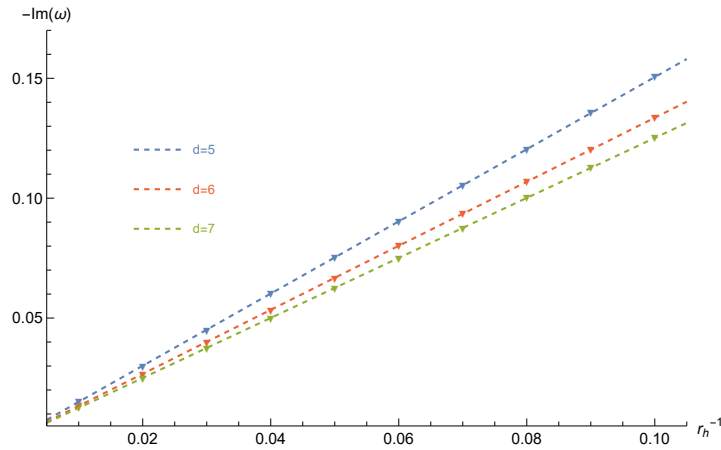


**Figure 4.10:** “Special” purely imaginary modes scaling with the inverse of the black hole radius, found for scalar-type Maxwell perturbations in 5, 6, 7-dimensional Schwarzschild-AdS. Fit results: for  $d = 5$ ,  $-\Im\omega = 1.50823r_h^{-1} - 9.47993 \times 10^{-5}$ ; for  $d = 6$ ,  $-\Im\omega = 1.33694r_h^{-1} - 2.14671 \times 10^{-4}$ ; and for  $d = 7$ ,  $-\Im\omega = 1.25203r_h^{-1} - 5.33241 \times 10^{-5}$ .

### Intermediate and small black hole regimes

For intermediate and small black holes, the interpretations within the context of the AdS/CFT correspondence are less clear [30, 36]. Nevertheless, it is important to study these regimes, as not only the behaviour of the effective potential is very different from the one for large black holes, but also because they provide simple backgrounds in which some analytical studies may be performed (we will come back to this in Section 4.5). The frequencies for intermediate and small black holes are shown in Table (4.7). These were computed by numerical integration, as Horowitz-Hubeny method in these regimes becomes impractical (see, however, [33]). For very small black holes (typically with characteristic modes with  $|\Im\omega| < 10^{-11}$ ) the poor convergence of the method only allows to estimate the order of magnitude

of the mode. We also present the frequencies for pure AdS, computed with Eq. (3.15). Additionally, Fig. (4.11) shows the evolution of the real part of the frequencies in the small black hole regime, for  $l = 2, \mu = 0.2$  Proca perturbations in a 5-dimensional Schwarzschild-AdS black hole. Similar results can be found for other dimensions.

	$r_h$	Vector-type	Scalar-type (EM)	Scalar-type (Non-EM)
$d = 5$	2	$5.85870 - 3.59632i$	$4.10661 - 3.61711i$	$7.90576 - 5.18245i$
	1	$4.71186 - 1.41105i$	$3.62825 - 0.900411i$	$5.81778 - 2.18450i$
	0.5	$4.63298 - 0.293471i$	$3.76967 - 0.136112i$	$5.46795 - 0.567694i$
	0.25	$4.92587 - 0.00400019i$	$3.96795 - 0.00131928i$	$5.70150 - 0.0636701i$
	0.1	$5.00759 - 1.38323 \times 10^{-6}i$	$4.01279 - 6.69931 \times 10^{-7}i$	$5.99879 - 3.67252 \times 10^{-6}i$
	0.01	$5.01969 - \sim 10^{-14}i$	$4.01974 - \sim 10^{-13}i$	$6.01960 - \sim 10^{-11}i$
	0	5.01980	4.01980	6.01980
	$d = 6$	2	$7.88651 - 3.60743i$	$7.01425 - 3.76222i$
1		$6.0056 - 1.35223i$	$4.92789 - 1.27903i$	$7.22317 - 2.00688i$
0.5		$5.77058 - 0.212875i$	$4.80185 - 0.173010i$	$6.61634 - 0.953938i$
0.25		$5.98038 - 0.00142972i$	$4.98573 - 0.00130714i$	$6.95226 - 0.00450034i$
0.1		$6.01148 - 3.67683 \times 10^{-7}i$	$5.01177 - 4.40212 \times 10^{-7}i$	$7.01008 - 9.42574 \times 10^{-7}i$
0.01		$6.01327 - \sim 10^{-15}i$	$5.01327 - \sim 10^{-13}i$	$7.01327 - \sim 10^{-11}i$
0		6.01327	5.01327	7.01327
$d = 7$		2	$9.71613 - 3.57472i$	$9.04742 - 3.69995i$
	1	$7.21079 - 1.28886i$	$6.27367 - 1.35943i$	$8.48599 - 1.84560i$
	0.5	$6.84854 - 0.158257i$	$5.85225 - 0.178768i$	$7.8153 - 0.854107i$
	0.25	$6.99751 - 0.000599454i$	$5.99607 - 0.00100992i$	$7.98665 - 0.00170896i$
	0.1	$7.00969 - 8.88417 \times 10^{-8}i$	$6.00967 - 1.90814 \times 10^{-7}i$	$8.00947 - 2.21802 \times 10^{-7}i$
	0.01	$7.00998 - \sim 10^{-17}i$	$6.00998 - \sim 10^{-13}i$	$8.00998 - \sim 10^{-12}i$
	0	7.00998	6.00998	8.00998

**Table 4.7:** Fundamental quasinormal mode frequencies of  $l = 2$  Proca perturbations in 5, 6, 7-dimensional Schwarzschild-AdS, for a Proca field with mass  $\mu = 0.2$  and different black hole sizes, in the intermediate and small black hole regimes. The values for  $r_h = 0$  are for pure AdS, computed with Eq. (3.15).

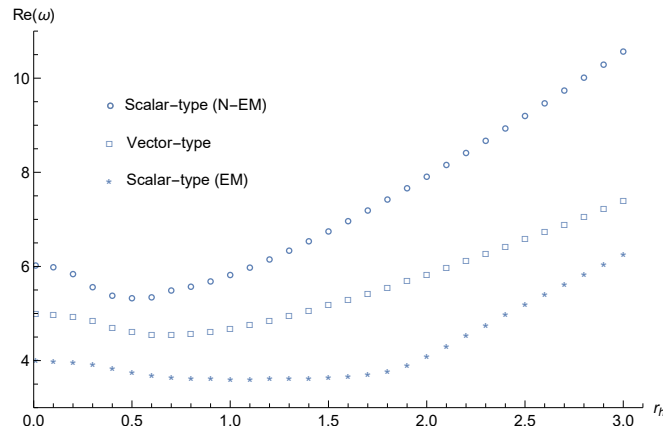


**Figure 4.11:** Real part of the quasinormal mode frequencies for  $l = 2, \mu = 0.2$ , Proca perturbations in 5-dimensional Schwarzschild-AdS spacetime in the small black hole regime. In the limit  $r_h \rightarrow 0$ , the frequencies approach those of pure AdS, given by Eq. (3.15).

Near  $r_h \sim 1$ , the frequencies start to deviate from the linear scaling found in the large black hole regime: their real part approaches a minimum for sufficiently small black holes, and, from there, it starts to increase, asymptoting the frequencies for pure AdS, given by Eq. (3.15), while the imaginary part tends to zero with an  $l$ -dependent functional form (this is explored in Section 4.5). The vanishing of the imaginary part in the very small black hole limit is intuitively clear: the modes only decay due to the absorption by the black hole, so one should expect purely oscillating normal modes when the black hole has negligible size. However, the fact that the frequencies approach those of pure AdS was not necessarily expected, as the purely ingoing boundary condition at  $r = r_h$  does not reduce to the regularity boundary condition at the origin imposed in pure AdS [30, 33]. On the other hand, the purely imaginary “special” modes of Maxwell scalar-type perturbations seem to become suppressed in the small black hole regime. Whether these modes disappear in this regime or this is simply a consequence of our numerical method still needs to be further investigated.

### 4.4.3 Higher overtones

While in the previous section we only showed results for the fundamental mode, our methods still allow an accurate determination of the first ( $k = 1$ ) and, sometimes, second ( $k = 2$ ) overtones of the spectrum. Yet,  $k \geq 2$  overtones converge very poorly cf. Fig. (4.6), and are thus very difficult to find using such methods. Table (4.8) shows the three lowest modes for  $l = 0, 1$  Proca field perturbations in 5, 6, 7-dimensional Schwarzschild-AdS with  $r_h = 1$ . We also investigated whether the mass of the field impacted the  $k = 0, 1$  modes differently. It is known that in Schwarzschild spacetimes the fundamental mode of monopole Proca perturbations behaves particularly differently from the other modes [42]. In Schwarzschild-AdS, such was not found, as Fig. (4.12) shows in 7 dimensions (similar results can be obtained for other dimensions as well).

		$l = 0$	$l = 1$		
			Vector-type	Scalar-type (EM)	Scalar-Type (Non-EM)
$d = 5$	$k = 0$	$4.72755 - 2.67209i$	$3.97359 - 1.73872i$	$2.81810 - 1.74904i$	$5.2286 - 2.49174i$
	$k = 1$	$7.55678 - 4.72454i$	$6.52350 - 3.83747i$	$5.71794 - 4.03211i$	$8.59081 - 6.07836i$
	$k = 2$	---	---	---	---
$d = 6$	$k = 0$	$6.12217 - 2.41656i$	$5.30603 - 1.59769i$	$4.52915 - 1.75717i$	$6.63649 - 2.25137i$
	$k = 1$	$9.37977 - 4.17408i$	$8.26224 - 3.38494i$	$7.71083 - 3.53869i$	$9.75569 - 4.05188i$
	$k = 2$	$12.6460 - 5.89531i$	$11.3652 - 5.11356i$	---	---
$d = 7$	$k = 0$	$7.35822 - 2.20219i$	$6.52107 - 1.48949i$	$5.82571 - 1.63789i$	$7.89019 - 2.05076i$
	$k = 1$	$10.8523 - 3.72975i$	$9.70370 - 3.03895i$	$9.20224 - 3.16690i$	$11.2431 - 3.61882i$
	$k = 2$	$14.3301 - 5.19102i$	$13.0310 - 4.51820i$	$12.6338 - 4.62355i$	---

**Table 4.8:** Lowest modes of  $l = 0, 1$  and  $\mu = 0.5$  Proca field perturbations in 5, 6, 7-dimensional Schwarzschild-AdS with  $r_h = 1$ . For the empty cells, none of the methods implemented converged.

While one expects the lowest modes to dominate the quasinormal ringing phase of a perturbed black hole, the  $|\omega| \rightarrow \infty$  limit has been studied in the context of quantum gravity, as in this regime the modes are thought to be related to the area quantization of black holes [61]. In particular, for Schwarzschild and Schwarzschild-de Sitter spacetimes, these modes are highly damped [27], and the spectrum in the asymptotic limit approaches  $\omega = \omega_{\text{off}} - ik\Delta\omega$  where  $\Delta\omega \in \mathbb{R}$  is called the gap term of the asymptotic spectrum and  $\omega_{\text{off}}$  is an offset term independent of  $k$ . In asymptotically AdS spacetimes, the asymp-

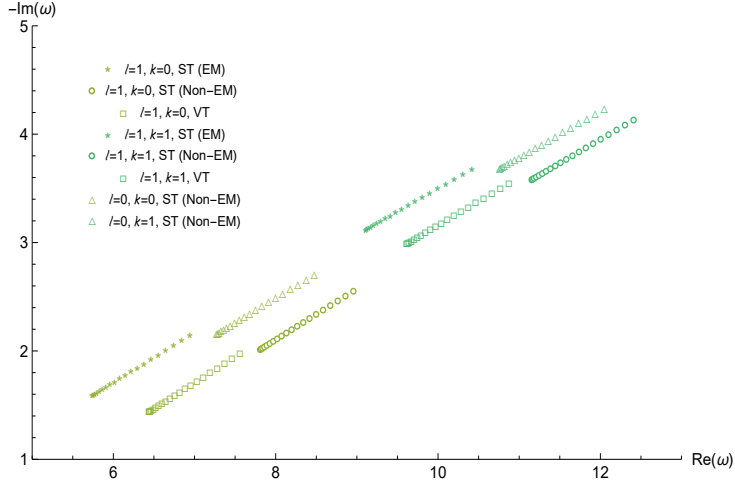


**Figure 4.12:** Effect of the field's mass ( $\mu \in [0.1, 2.0]$ ) on  $k = 0, 1$  and  $l = 0, 1$  Proca field modes, in 7-dimensional Schwarzschild-AdS, with  $r_h = 1$ . The mass of the field seems to have a similar effect on  $k = 0, 1$  overtones.

otic spectrum behaves differently, as it approaches  $\omega = \omega_{\text{off}} + k\Delta\omega$ , with  $\Delta\omega = \omega_R - i\omega_I \in \mathbb{C}$ , so that  $|\Im\mathfrak{m}(\omega)| \simeq |\Re\mathfrak{e}(\omega)|$  [32, 34]. Using a monodromy argument, [20] computed analytically the asymptotic quasinormal mode frequencies for various static and spherically symmetric spacetimes. Their study regarded scalar field and gravitational perturbations. [21, 62] generalized the results to electromagnetic perturbations. Whereas usually the limit  $|\omega| \rightarrow \infty$  is only reached when  $k \gg 1$ , for large Schwarzschild-AdS black holes the frequencies scale linearly with the size of the black hole, reaching quickly their asymptotic behaviour. Since the numerical methods we are using are only able to capture the lowest overtones, this proves to be very useful as a test to our numerical results. [21] showed that the quasinormal modes of scalar-type and vector-type Maxwell field perturbations in  $d > 5$  Schwarzschild-AdS obey, in the asymptotic limit,

$$\omega x_0 = \frac{\pi}{4}(d+1) + k\pi + \frac{1}{2i} \log \left( 2 \cos \frac{\pi j}{2} \right) \quad , \quad k \in \mathbb{N} \quad , \quad (4.53)$$

where  $j = \frac{2(d-3)}{d-2}$  and  $x_0 = x(+\infty)$ , with  $x(r)$  being the complex tortoise coordinate, resulting from the analytical continuation of Eq. (4.6) to the complex plane. Note that the asymptotic spectrum is independent of  $l$ . This happens since the  $l$ -dependent term in the potentials is suppressed at leading-order when one expands them near  $r = 0$  and  $r = \infty$  (note that, within the monodromy argument,  $r \in \mathbb{C}$ ). For  $d = 5$ , the asymptotic spectrum of vector-type perturbations is also given by Eq. (4.53), whereas the spectrum of scalar-type perturbations should be continuous [21]. For large Schwarzschild-AdS black holes one has [20]

$$x_0 = \frac{1}{4T_H \sin(\pi/(d-1))} e^{-i\pi/(d-1)} \quad , \quad (4.54)$$

where  $T_H$  is the Hawking temperature in Schwarzschild-AdS, given by Eq. (4.52). Substitution of  $x_0$  in

Eq. (4.53) leads to (in  $L = 1$  units)

$$\begin{aligned}\frac{\omega}{r_h} &= (4 - 4i) + (2 - 2i)k \quad , \quad d = 5 \quad , \\ \frac{\omega}{r_h} &= (5.44498 - 3.75563i) + (2.37764 - 1.72746i)k \quad , \quad d = 6 \quad , \\ \frac{\omega}{r_h} &= (6.61007 - 3.55102i) + (2.59808 - 1.50000i)k \quad , \quad d = 7 \quad .\end{aligned}\tag{4.55}$$

On the other hand, in  $d = 4$  one has  $j = 1$  and so Eq. (4.53) cannot be used. This has to do with the vanishing of the leading order term in the large  $r$  expansion of the potential. [62] found the sub-leading order expression for the quasinormal frequencies to be  $\frac{\Delta\omega}{r_h} = 1.299 - 2.25i - \frac{0.179+0.103i}{k}$ , whose gap term agrees with the numerical results of [34]. The fundamental, first and second overtones of  $l = 1$  vector-type and scalar-type electromagnetic perturbations in 5, 6, 7-dimensional Schwarzschild-AdS are presented in Table (4.9), for  $r_h = 100$ . For  $d = 6$ , the sinusoidal shape of the convergence curve (c.f. Fig. (4.4)) allowed to compute also the  $k = 3$  and  $k = 4$  modes using Horowitz-Hubeny method. A linear

	$k$	$\omega (d = 5)$	$\omega (d = 6)$	$\omega (d = 7)$
Vector-type	0	200.026 - 199.995 <i>i</i>	299.458 - 200.486 <i>i</i>	383.691 - 199.894 <i>i</i>
	1	400.031 - 399.970 <i>i</i>	541.138 - 374.618 <i>i</i>	651.862 - 352.717 <i>i</i>
	2	600.078 - 599.970 <i>i</i>	780.131 - 547.752 <i>i</i>	914.764 - 503.598 <i>i</i>
	3	—	1018.64 - 720.647 <i>i</i>	—
	4	—	1256.67 - 893.452 <i>i</i>	—
Scalar-type	0	200.010 - 200.000 <i>i</i>	299.447 - 200.490 <i>i</i>	383.681 - 199.896 <i>i</i>
	1	400.020 - 400.000 <i>i</i>	541.132 - 374.619 <i>i</i>	651.856 - 352.718 <i>i</i>
	2	599.999 - 600.002 <i>i</i>	780.164 - 547.738 <i>i</i>	914.759 - 503.599 <i>i</i>
	3	—	1018.55 - 720.655 <i>i</i>	—
	4	—	1256.68 - 893.495 <i>i</i>	—

**Table 4.9:** Fundamental, first and second overtones of  $l = 1$  vector-type and scalar-type Maxwell field perturbations in 5, 6, 7-dimensional Schwarzschild-AdS spacetime with  $r_h = 100$ . In 6-dimensional Schwarzschild-AdS, the convergence of Horowitz-Hubeny method allowed to find the  $k = 3, 4$  modes as well.

fit of the results of Table (4.9) for each dimension yields, for vector-type perturbations,

$$\begin{aligned}\frac{\omega}{r_h} &= (2.00019 - 1.99991i) + (2.00026 - 1.99987i)k \quad , \quad d = 5 \quad , \\ \frac{\omega}{r_h} &= (2.99906 - 2.00652i) + (2.39191 - 1.73196i)k \quad , \quad d = 6 \quad , \\ \frac{\omega}{r_h} &= (3.84569 - 2.00218i) + (2.65537 - 1.51852i)k \quad , \quad d = 7 \quad .\end{aligned}\tag{4.56}$$

Similar results can be obtained by fitting the scalar-type data, and by fitting different sized large black holes (a more rigorous analysis would be achieved by computing the modes for different large radii and performing a linear fit with variable  $r_h$ : the results obtained for  $r_h = 100$  were however satisfactory enough for what was pretended to show). Comparing Eq. (4.56) with Eq. (4.55), we see that the numerical gaps  $\Delta\omega_k = \omega_{k+1} - \omega_k$  are close to the ones predicted by Ortega in [21]. The deviations are mainly attributed to the fact that our numerical results only take into account the lowest overtones. However, note from Fig. (4.13) that the higher the overtone, the closest to the analytical prediction the gap is. Moreover, despite the disagreement between offsets, our results seem to be shifted by two over-

tones when compared with [21]. For scalar-type Maxwell field perturbations in  $d = 5$ , we imposed the vanishing of the subdominant logarithmic term in Eq. (4.16): that is why in this case the results can also be compared with the general  $d$  expression in Eq. (4.53).

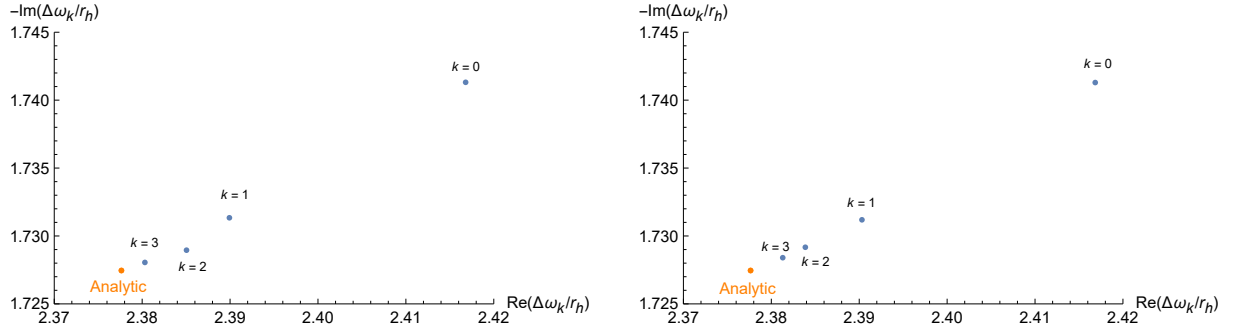


**Figure 4.13:** Numerical gaps for vector-type (left) and scalar-type (right) electromagnetic perturbations in 6-dimensional Schwarzschild-AdS. The higher the overtone, the closest the gap is to the one predicted in [21].

Although our results tend to agree with [21], its analytical formulas still need to be confirmed numerically, for example, by employing Leaver’s method of continued fractions [26], which is much more suitable to find higher overtones. Such analysis is way harder to implement (see, however, [57]), specially for higher-dimensional spacetimes with curvature, and is beyond the scope of our work. Furthermore, bear in mind that the asymptotic analysis done so far takes only into account Maxwell field perturbations. Indeed, studying only the lowest overtones is not sufficient to infer on the mass effect in the asymptotic limit. This is an interesting question to pose, as the mass term changes the number of degrees of freedom of the field and, with it, the structure of the scalar-type sector. Also, the mass of the Proca field does contribute to the leading-order asymptotic behaviour of the potential near spatial infinity. For the Proca monopole in 4-dimensional Schwarzschild-AdS, [42] showed numerically that the gap term of the asymptotic spectrum does not depend on the mass of the field. Are the spectrum gaps independent of the mass of the field in higher dimensions and for higher multipoles? Are these polarization-independent? Both questions should yield affirmative answers: note from Eq. (4.53) that the spectrum gap only depends on the spacetime-related parameters, through  $x_0$ , being completely independent of the perturbation-related parameters appearing in the potentials. On the other hand, the offset term should depend on the mass of the field, and, in principle, also on the polarization-type. These conclusions, however, can only be numerically supported with a larger sample of overtones.

#### 4.4.4 Dependence on $l$ and the eikonal limit

Another interesting feature of the quasinormal mode spectrum arises when one studies higher multipoles (so far, we have only focused on  $l = 0, 1, 2$  perturbations). In asymptotically AdS spacetimes, the evolution of the spectrum with  $l$  is specially important, as in the eikonal limit,  $l \gg 1$ , modes may be very long-lived [63–65]. These will in principle dominate the response of the perturbed black hole, and are thus physically relevant. On the one hand, the potentials ruling quasinormal modes in small and intermediate Schwarzschild-AdS black holes develop a well for sufficiently high  $l$ , allowing the existence of trapped modes in the potential barrier. Such is shown in Fig. (4.14), where we display the radial profile of

the effective potential for  $l = 1$ ,  $l = 60$  and  $l = 100$  vector-type Proca field perturbations in 7-dimensional Schwarzschild-AdS with  $r_h = 1$ .

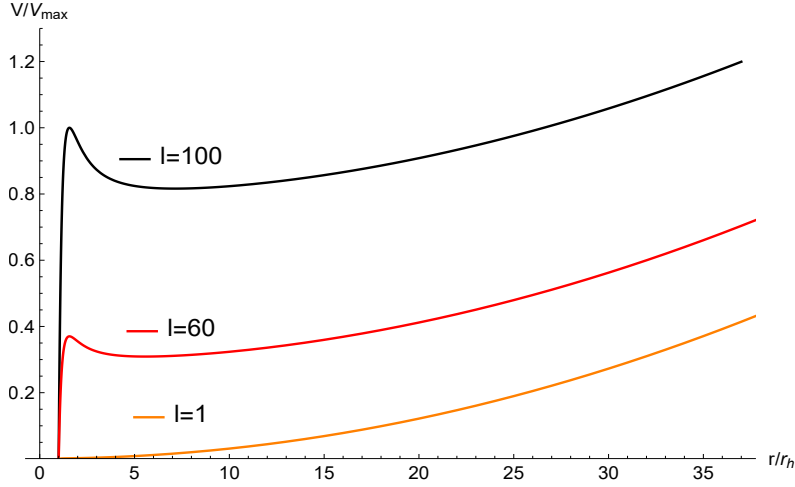


**Figure 4.14:** Radial profile of the effective potential for  $l = 1$ ,  $l = 60$  and  $l = 100$  vector-type Proca field perturbations, with  $\mu = 0.5$ , in 7-dimensional Schwarzschild-AdS spacetime with  $r_h = 1$ : for sufficiently large  $l$ , the potential develops a well, accommodating long-lived modes.

Note that the depth and width of the well increase with increasing  $l$ , so that one expects higher- $l$  modes to live longer (and thus, with smaller imaginary part frequencies, in magnitude). On the other hand, and despite not admitting such trapped modes, large Schwarzschild-AdS black holes were also proven to accommodate long-living modes in the eikonal limit for scalar field and gravitational perturbations [63, 64]. In this section, we investigate if such results can also be reproduced for Proca field perturbations.

### Large black hole regime

Using a WKB approach, [63] found that the dependence on  $l$  of scalar field quasinormal modes in large asymptotically AdS black holes should be, in the eikonal limit, (in  $L = 1$  units)

$$\omega = l + (\alpha_R - i\alpha_I) l^{-\beta} \quad , \quad (4.57)$$

where  $\alpha_R \in \mathbb{R}$ ,  $\alpha_I \in \mathbb{R}^+$  are parameters depending on the dimension of the spacetime, the radius of the black hole and the overtone number, and  $\beta = \frac{d-3}{d+1}$ . [64] confirmed numerically the results for tensor-type gravitational quasinormal modes (and thus, scalar field quasinormal modes, which are isospectral), and found that vector-type and scalar-type gravitational quasinormal modes also had the  $l$ -dependence of Eq. (4.57) (although different coefficients  $\alpha_R, \alpha_I$ ). We study if such happens for Proca field perturbations as well. In Table (4.10), we show the quasinormal mode frequencies of  $\mu = 0.5$  Proca field perturbations for different values of  $l$ , in the large black hole regime, with  $r_h = 100$  (observe that  $l$  should only influence the spectrum when  $l/r_h \gg 1$ : otherwise, as the  $l$ -dependent term in the potential goes as  $l^2/r^2$ , this term would always be suppressed by the others). In Fig. (4.15), we fitted the frequencies' imaginary parts to Eq. (4.57). The fit results obtained from the real and imaginary parts are compared with the analytical

predictions in Table (4.11).

	$l$	Vector-Type	Scalar-Type (EM)	Scalar-Type (Non-EM)
$d = 5$	10000	10032.2 – 53.9532 <i>i</i>	10015.4 – 24.9753 <i>i</i>	10051.6 – 87.2931 <i>i</i>
	15000	15028.3 – 47.1368 <i>i</i>	15013.6 – 21.7995 <i>i</i>	15045.2 – 76.2808 <i>i</i>
	20000	20025.8 – 42.8352 <i>i</i>	20012.4 – 19.7972 <i>i</i>	20041.1 – 69.2954 <i>i</i>
	25000	25024.0 – 39.7843 <i>i</i>	25011.6 – 18.3726 <i>i</i>	25038.3 – 64.2882 <i>i</i>
$d = 6$	10000	10037.0 – 44.3549 <i>i</i>	10020.4 – 23.7546 <i>i</i>	10056.1 – 68.2295 <i>i</i>
	15000	15031.3 – 37.2864 <i>i</i>	15017.4 – 19.9390 <i>i</i>	15047.4 – 57.3779 <i>i</i>
	20000	20027.9 – 32.9598 <i>i</i>	20015.6 – 17.6124 <i>i</i>	20042.1 – 50.7286 <i>i</i>
	25000	25025.5 – 29.9460 <i>i</i>	25014.3 – 15.9967 <i>i</i>	25038.4 – 46.1020 <i>i</i>
$d = 7$	10000	10041.4 – 39.2259 <i>i</i>	10025.2 – 23.1973 <i>i</i>	10060.0 – 57.7746 <i>i</i>
	15000	15034.2 – 32.0351 <i>i</i>	15021.0 – 18.9071 <i>i</i>	15049.4 – 47.2041 <i>i</i>
	20000	20029.9 – 27.7374 <i>i</i>	20018.4 – 16.3555 <i>i</i>	20043.1 – 40.8814 <i>i</i>
	25000	25026.9 – 24.8009 <i>i</i>	25016.7 – 14.6153 <i>i</i>	25038.7 – 36.5592 <i>i</i>

**Table 4.10:** Fundamental quasinormal mode frequencies of  $\mu = 0.5$  Proca perturbations in the eikonal limit for 5, 6, 7-dimensional Schwarzschild-AdS black holes with  $r_h = 100$ .

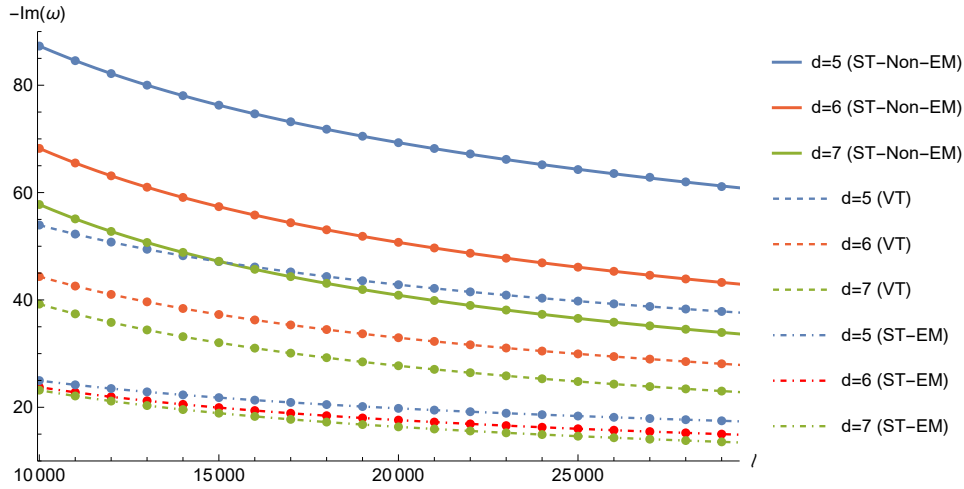


**Figure 4.15:** Imaginary part of fundamental quasinormal modes of  $\mu = 0.5$  Proca perturbations in the eikonal limit for 5, 6, 7-dimensional Schwarzschild-AdS black hole with  $r_h = 100$ . These were fitted to Eq. (4.57), showing an agreement with [63, 64].

	$\beta$ [63]	Vector-Type		Scalar-Type (EM)		Scalar-Type (Non-EM)	
		$\beta_R$	$\beta_I$	$\beta_R$	$\beta_I$	$\beta_R$	$\beta_I$
$d = 5$	0.33	0.32	0.33	0.31	0.33	0.33	0.33
$d = 6$	0.43	0.41	0.43	0.39	0.43	0.41	0.43
$d = 7$	0.50	0.46	0.50	0.45	0.50	0.50	0.50

**Table 4.11:** Values of  $\beta$  for the fundamental mode of  $\mu = 0.5$  Proca field perturbations in 5, 6, 7-dimensional Schwarzschild-AdS black holes with  $r_h = 100$ , computed from fitting the real ( $\beta_R$ ) and imaginary ( $\beta_I$ ) parts of the numerical results to Eq. (4.57). The analytical results of [63] for scalar field perturbations are also displayed.

Equation (4.57) not only shows good agreement with gravitational perturbations [64], but also with our numerical results for Proca field perturbations, specially when we fit the imaginary part of the frequencies. The fit to the real part of Eq. (4.57) gives less satisfactory results, which can be due to a real number offset between Eq. (4.57) and the numerical results, i.e.,  $\omega - \omega_0 = l + (\alpha_R - i\alpha_I)l^{-\beta}$ , although a larger sample of numerical data (and preferably obtained with a different procedure) is needed to exclude eventual numerical errors present. In particular, the results from Table (4.11), computed via numerical integration, could not be confirmed with Horowitz-Hubeny method, as the series solution shows poor convergence properties for  $l \gg r_h$ . This analysis however confirms the existence of long-lived Proca field modes within the large black hole regime, and hints for the universal functional dependence on  $l$ . It should be noted that, although  $\beta$  does not seem to depend on any parameter other than the dimension of the spacetime, we found that  $\alpha_R, \alpha_I$  do depend on the type of perturbation, as also observed in [64].

### Intermediate and small black hole regimes

In the intermediate and small black hole regimes, the damping of the mode is expected to decrease exponentially with  $l$  in the eikonal limit [63, 64]. We illustrate this for vector-type Proca field perturbations and a black hole with  $r_h = 1$ : Table (4.12) shows the quasinormal mode frequencies for different values of  $l$  and Fig. (4.16) shows a plot of the results, which agree with [63]. Similar results can be found for the scalar-type sector. The exponential decrease in damping impedes us from studying higher  $l$  values, as the numerical method starts to fail for sufficiently small imaginary parts.

$l$	$\omega (d = 5)$	$\omega (d = 6)$	$\omega (d = 7)$
10	$12.5682 - 5.83463 \times 10^{-1}i$	$13.6872 - 4.77965 \times 10^{-1}i$	$14.7665 - 4.22789 \times 10^{-1}i$
30	$32.8045 - 5.00076 \times 10^{-2}i$	$33.9362 - 8.98403 \times 10^{-3}i$	$34.9839 - 2.83059 \times 10^{-3}i$
50	$52.9598 - 7.46649 \times 10^{-4}i$	$54.0233 - 1.24031 \times 10^{-5}i$	$55.0364 - 1.15872 \times 10^{-6}i$
70	$73.0128 - 4.04631 \times 10^{-6}i$	$74.0473 - 8.46511 \times 10^{-9}i$	$75.0489 - 2.51485 \times 10^{-10}i$

**Table 4.12:** Fundamental mode of  $\mu = 0.5$  vector-type Proca perturbations in 5, 6, 7-dimensional Schwarzschild-AdS spacetime with  $r_h = 1$ , for different values of the angular momentum number  $l$ .

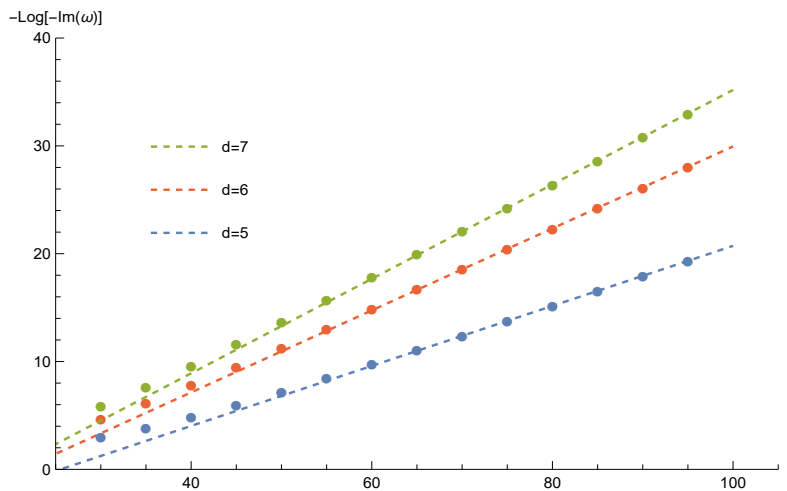


**Figure 4.16:** Imaginary part of fundamental modes for  $\mu = 0.5$  vector-type Proca perturbations in the eikonal limit,  $l \gg 1$ , in 5, 6, 7-dimensional Schwarzschild-AdS, with  $r_h = 1$ . For sufficiently large  $l$ , the mode damping becomes exponentially small with  $l$ .

A quick assessment of the potential Eq. (4.3) shows that the eikonal limit does not directly decouple the scalar-type modes. This would make the numerical treatment much more tractable, as one would not need to compare each mode with its analogue in the electromagnetic case by taking the massless limit (as explained earlier, the  $k + 1^{\text{th}}$  overtone of the electromagnetic polarization is very close to the  $k^{\text{th}}$  overtone of the non-electromagnetic polarization). Furthermore, it would also allow an analysis for  $d = 4$ . In this case, and for small masses of the field, the solution's behaviour at infinity according to Eq. (4.11) is  $u^{(\infty)} \sim c_1 r^{-1-\epsilon} + c_2 r^\epsilon$  with  $\epsilon \ll 1$ . The Dirichlet boundary condition yields  $c_2 = 0$ , which is very hard to solve numerically, specially for a coupled system, as  $r^\epsilon$  grows very slowly. For large values of angular momentum the numerical errors enhance, impeding one to find accurate solutions for the quasinormal modes.

We could not end this section without mentioning the developments made concerning the study of quasinormal modes in the eikonal limit for other spacetimes. In backgrounds allowing a purely outgoing wave solution at infinity, such as asymptotically flat and de Sitter spacetimes, quasinormal modes in the eikonal limit were shown to be related to the parameters describing particles trapped in unstable circular null geodesics [66–68]. Namely, the real part of the quasinormal mode is related to the angular velocity at the geodesic, while its imaginary part is determined by the instability timescale of the orbit. On the other hand, asymptotically AdS spacetimes do not allow, in general, a wave-like solution at infinity, so that such analogy between quasinormal modes and circular null geodesics cannot be directly inferred [66]. An extension of such procedure to AdS spacetimes could provide a deeper physical insight on the behaviour of quasinormal modes in this limit, as well as a possible way to decouple the Proca scalar-sector [68]. Also, it would be interesting to check if Maxwell scalar-type modes in  $d = 4, 6$ , which do allow the use of such boundary conditions, can be described by this “quasinormal mode/circular null geodesics correspondence”.

## 4.5 The long-wavelength approximation for small Schwarzschild-AdS black holes

In this section we investigate if it is possible to study analytically the quasinormal mode spectrum of Maxwell and Proca field perturbations in small Schwarzschild-AdS black holes, by matching asymptotic expansions of the solutions in the long wavelength approximation, which assumes that the radius of the black hole,  $r_h$ , is much smaller than the Compton wavelength of the field,  $1/\omega$ . This technique has often allowed to prove spacetime instabilities, by searching for mode frequencies with positive imaginary part, cf. [44, 69–74]. Our goal is to have results for the very small black hole regime, where even the numerical integration procedure begins to fail. Also, we investigate if the scalar-type Proca sector decouples within these approximations (we will see that it does not). A brief description of the method goes as follows. The spacetime is separated in two different regions: the near-region, verifying  $\frac{r-r_h}{L} \ll \frac{1}{\omega L}$  (hereafter we do not fix  $L$  for clarity); the far-region, for which  $\frac{r-r_h}{L} \gg \frac{r_h}{L}$ . The Schrödinger-like equation Eq. (4.6) is then solved analytically in both regions, by imposing the appropriate boundary conditions, and the

quasinormal mode spectrum is obtained by matching the near-region solution and the far-region solution at the overlap region  $\frac{r_h}{L} \ll \frac{r-r_h}{L} \ll \frac{1}{\omega L}$ , which is formed if the former assumptions are made.

## 4.5.1 Vector-type Proca and Maxwell field perturbations

### Near-region

In the near-region one can neglect the effect of the cosmological constant, so that the background is approximately Schwarzschild. Thus, it is useful to change coordinates to

$$z(r) \equiv 1 - \left(\frac{r_h}{r}\right)^{d-3}, \quad (4.58)$$

which maps the domain of interest  $r_h < r < \infty$  to  $0 < z < 1$ , with the event horizon at  $z = 0$  and spatial infinity at  $z = 1$ . In terms of  $z$ , the equation of motion for vector-type perturbations becomes

$$\begin{aligned} z(1-z) \frac{\partial^2 u_V^{\text{near}}}{\partial z^2} + \left(1-z \left(2 + \frac{1}{d-3}\right)\right) \frac{\partial u_V^{\text{near}}}{\partial z} + \\ + \frac{1}{(d-3)^2} \left( \frac{\omega^2 r^2}{z(1-z)} - \frac{(l+1)(l+d-4) + \mu^2 r^2}{1-z} - \frac{(d-4)(d-6)z}{4(1-z)} - \frac{(d-4)(d-3)}{2} \right) u_V^{\text{near}} = 0. \end{aligned} \quad (4.59)$$

The term  $\omega^2 r^2$  can be simplified as

$$\omega^2 r^2 = \omega^2 r_h^2 + 2\omega^2 r_h(r-r_h) + 2\omega^2(r-r_h)^2 \simeq \omega^2 r_h^2, \quad (4.60)$$

where the long-wavelength approximation was used. Additionally, assuming that  $\mu r_h \ll 1$  and that, in the near-region,  $\mu(r-r_h) \ll 1$ , one has  $\mu^2 r^2 \simeq \mu^2 r_h^2$ . This term may be neglected, as  $(l+1)(l+d-4)$  is at least of the order of unity (remember that for vector-type perturbations  $l \geq 1$ ). With these assumptions, Eq. (4.59) can be put in the standard hypergeometric equation form Eq. (B.1), by making the transformation

$$u_V^{\text{near}}(z) = z^\alpha (1-z)^\beta \Psi(z), \quad (4.61)$$

with

$$\begin{aligned} \alpha = -\frac{i\omega r_h}{d-3}, \quad \beta = \frac{2l+d-4}{2(d-3)}, \\ a = \frac{l+d-4-i\omega r_h}{d-3}, \quad b = \frac{l+d-2-i\omega r_h}{d-3}, \quad c = 1 - \frac{2i\omega}{d-3}. \end{aligned} \quad (4.62)$$

It follows from Appendix B that its solution near  $z = 0$  is

$$u_V^{\text{near}}(z) = c_1 z^\alpha + c_2 z^{\alpha+1-c} = c_1 z^{-i\omega r_h/(d-3)} + c_2 z^{i\omega r_h/(d-3)}, \quad (4.63)$$

where  $\lim_{z \rightarrow 0} F_1[a, b, c; z] = 1$  was used. The boundary condition at the horizon then yields  $c_2 = 0$  and

$$u_V^{\text{near}}(z) = c_1 z^\alpha (1-z)^\beta F_1[a, b, c; z]. \quad (4.64)$$

To obtain the solution in the overlap region, we take the limit  $z \rightarrow 1$  of Eq. (4.64). This is done by using the  $z \rightarrow 1 - z$  transformation rules Eqs. (B.5) and (B.6). If  $\frac{2l}{d-3}$  is not an integer, after taking the limit  $z \rightarrow 1$  one has

$$u_V^{\text{near}}(z) = c_1 \left( \frac{\Gamma \left[ 1 - \frac{2i\omega r_h}{d-3} \right] \Gamma \left[ -1 - \frac{2l}{d-3} \right]}{\Gamma \left[ \frac{1-l-i\omega r_h}{d-3} \right] \Gamma \left[ \frac{-1-l-i\omega r_h}{d-3} \right]} (1-z)^{\frac{2l+d-4}{2(d-3)}} + \frac{\Gamma \left[ 1 - \frac{2i\omega r_h}{d-3} \right] \Gamma \left[ 1 + \frac{2l}{d-3} \right]}{\Gamma \left[ \frac{l+d-4-i\omega r_h}{d-3} \right] \Gamma \left[ \frac{l+d-2-i\omega r_h}{d-3} \right]} (1-z)^{-\frac{2l+d-2}{2(d-3)}} \right), \quad (4.65)$$

or, in terms of  $r$ ,

$$u_V^{\text{near}}(r) = \frac{u_V^{\text{(near,1/r)}}}{r^{\frac{2l+d-4}{2}}} + u_V^{\text{(near,r)}} r^{\frac{2l+d-2}{2}}, \quad (4.66)$$

with

$$u_V^{\text{(near,1/r)}} = c_1 \frac{\Gamma \left[ 1 - \frac{2i\omega r_h}{d-3} \right] \Gamma \left[ -1 - \frac{2l}{d-3} \right]}{\Gamma \left[ \frac{1-l-i\omega r_h}{d-3} \right] \Gamma \left[ \frac{-1-l-i\omega r_h}{d-3} \right]} r_h^{\frac{2l+d-4}{2}}, \quad u_V^{\text{(near,r)}} = c_1 \frac{\Gamma \left[ 1 - \frac{2i\omega r_h}{d-3} \right] \Gamma \left[ 1 + \frac{2l}{d-3} \right]}{\Gamma \left[ \frac{l+d-4-i\omega r_h}{d-3} \right] \Gamma \left[ \frac{l+d-2-i\omega r_h}{d-3} \right]} r_h^{-\frac{2l+d-2}{2}}. \quad (4.67)$$

Note that Eq. (4.66) holds in the region  $r_h \ll r \ll 1/\omega$ . On the other hand, if  $\frac{2l}{d-3}$  is an integer, such that  $-1 - \frac{2l}{d-3} = -m$ , with  $m = 1, 2, \dots$ , the solution is instead

$$u_V^{\text{near}}(z) = c_1 \left( \frac{(-1)^{m+1} \Gamma[a+b-m]}{m! \Gamma[a-m] \Gamma[b-m]} (1-z)^{\frac{2l+d-4}{2(d-3)}} \log(1-z) + \frac{\Gamma \left[ 1 - \frac{2i\omega r_h}{d-3} \right] \Gamma \left[ 1 + \frac{2l}{d-3} \right]}{\Gamma \left[ \frac{l+d-4-i\omega r_h}{d-3} \right] \Gamma \left[ \frac{l+d-2-i\omega r_h}{d-3} \right]} (1-z)^{-\frac{2l+d-2}{2(d-3)}} \right), \quad (4.68)$$

or, in terms of  $r$ ,

$$u_V^{\text{near}}(r) = \frac{u_V^{\text{(near,1/r)}}}{r^{\frac{2l+d-4}{2}}} \log\left(\frac{r}{r_h}\right) + u_V^{\text{(near,r)}} r^{\frac{2l+d-2}{2}}, \quad (4.69)$$

with

$$u_V^{\text{(near,1/r)}} = c_1 \frac{(d-3)(-1)^m \Gamma \left[ 1 - \frac{2i\omega r_h}{d-3} \right]}{m! \Gamma \left[ \frac{1-l-i\omega r_h}{d-3} \right] \Gamma \left[ \frac{-1-l-i\omega r_h}{d-3} \right]} r_h^{\frac{2l+d-4}{2}}, \quad (4.70)$$

and  $u_V^{\text{(near,r)}}$  is still given by Eq. (4.67). Equations (4.66) and (4.69) are to be matched with the corresponding solutions from the far-region, which we compute next.

## Far-region

In the far-region, one can neglect the effect of the black hole, so that the background is approximately pure AdS. This case was already discussed in Chapter 3, although now the solution only holds in the  $r \gg r_h$  region. So, while the equations of motion and the boundary condition at infinity are the same as in pure AdS, instead of applying the regularity boundary condition at the origin, one takes the limit to the overlap region to perform the matching. For clarity, we rewrite the equation of motion for vector-type perturbations in terms of  $\xi$ , defined as

$$\xi(r) \equiv \frac{1}{1+r^2/L^2}, \quad (4.71)$$

so that the region of interest  $r_h < r < \infty$  gets mapped to  $0 < \xi < 1$ , this time with  $\xi = 0$  corresponding to spatial infinity and  $\xi = 1$  corresponding to the horizon. This will spare us from using an additional  $\xi \rightarrow 1/\xi$  transformation of the hypergeometric function. The equation of motion is

$$\xi(1-\xi)\frac{\partial^2 u_V^{\text{far}}}{\partial \xi^2} + \left(\frac{1}{2} - \xi\right)\frac{\partial u_V^{\text{far}}}{\partial \xi} + \left(\frac{\omega^2 L^2}{4} - \frac{(2l+d-4)(2l+d-2)}{16(1-\xi)} - \frac{1}{4\xi}\left(\mu^2 L^2 + \frac{(d-4)(d-2)}{4}\right)\right)u_V^{\text{far}} = 0 \quad , \quad (4.72)$$

which may be written as the usual hypergeometric differential equation by performing

$$u_V^{\text{far}}(\xi) = \xi^\alpha (1-\xi)^\beta \Psi(\xi) \quad , \quad (4.73)$$

with

$$\begin{aligned} \alpha &= \frac{1}{4} \left(1 + \sqrt{(d-3)^2 + 4\mu^2 L^2}\right) \quad , \quad \beta = \frac{2l+d-2}{4} \quad , \\ a &= \frac{1}{4} \left(\sqrt{(d-3)^2 + 4\mu^2 L^2} + 2l+d-1+2\omega L\right) \quad , \quad b = \frac{1}{4} \left(\sqrt{(d-3)^2 + 4\mu^2 L^2} + 2l+d-1-2\omega L\right) \quad , \\ c &= 1 + \frac{1}{2} \sqrt{(d-3)^2 + 4\mu^2 L^2} \quad . \end{aligned} \quad (4.74)$$

In this case,  $c$  may be an integer and one needs to do a separate study for integer and non-integer  $c$ . When  $c$  is non-integer, the solution near  $\xi = 0$  (spatial infinity) is given by Eq. (B.2) with the appropriate substitutions. Performing the  $\xi \rightarrow 0$  limit one gets

$$u_V^{\text{far}}(\xi) = k_1 \xi^{\frac{1}{4}} \left(1 - \sqrt{(d-3)^2 + 4\mu^2 L^2}\right) + k_2 \xi^{\frac{1}{4}} \left(1 + \sqrt{(d-3)^2 + 4\mu^2 L^2}\right) \quad , \quad (4.75)$$

and so  $k_2 = 0$  in order to satisfy the Dirichlet boundary condition. Thus,

$$u_V^{\text{far}}(\xi) = k_1 \xi^\alpha (1-\xi)^\beta F_1[a, b, c; \xi] \quad . \quad (4.76)$$

For integer  $c = m+1$ , with  $m = 1, 2, 3, \dots$ , one can show that Eq. (4.76) is also the only solution satisfying the Dirichlet boundary condition (see Appendix B). The solution in the overlap region is obtained by taking the  $\xi \rightarrow 1$  limit of Eq. (4.76). If  $\frac{1}{2}(3-d-2l)$  is non-integer, that is, if  $d$  is even, performing the  $\xi \rightarrow 1-\xi$  transformation and taking the  $\xi \rightarrow 1$  limit yields

$$\begin{aligned} u_V^{\text{far}}(\xi) &= k_1 \left( \frac{\Gamma\left[1 + \frac{1}{2}\sqrt{(d-3)^2 + 4\mu^2 L^2}\right] \Gamma\left[-l - \frac{d-3}{2}\right]}{\Gamma\left[\frac{5-d-2l + \sqrt{(d-3)^2 + 4\mu^2 L^2} + 2\omega L}{4}\right] \Gamma\left[\frac{5-d-2l + \sqrt{(d-3)^2 + 4\mu^2 L^2} - 2\omega L}{4}\right]} (1-\xi)^{\frac{2l+d-2}{4}} + \right. \\ &\quad \left. + \frac{\Gamma\left[1 + \frac{1}{2}\sqrt{(d-3)^2 + 4\mu^2 L^2}\right] \Gamma\left[l + \frac{d-3}{2}\right]}{\Gamma\left[\frac{2l+d-1 + \sqrt{(d-3)^2 + 4\mu^2 L^2} + 2\omega L}{4}\right] \Gamma\left[\frac{2l+d-1 + \sqrt{(d-3)^2 + 4\mu^2 L^2} - 2\omega L}{4}\right]} (1-\xi)^{-\frac{2l+d-4}{4}} \right) \quad , \end{aligned} \quad (4.77)$$

or, in terms of  $r$ ,

$$u_V^{\text{far}}(r) = \frac{u_V^{\text{far},1/r}}{r^{\frac{2l+d-4}{2}}} + u_V^{\text{far},r} r^{\frac{2l+d-2}{2}} \quad , \quad (4.78)$$

with

$$\begin{aligned}
u_V^{(\text{far},1/r)} &= \frac{k_1 \Gamma \left[ 1 + \frac{1}{2} \sqrt{(d-3)^2 + 4\mu^2 L^2} \right] \Gamma \left[ l + \frac{d-3}{2} \right]}{\Gamma \left[ \frac{2l+d-1+\sqrt{(d-3)^2+4\mu^2 L^2+2\omega L}}{4} \right] \Gamma \left[ \frac{2l+d-1+\sqrt{(d-3)^2+4\mu^2 L^2-2\omega L}}{4} \right]} L^{\frac{2l+d-4}{2}}, \\
u_V^{(\text{far},r)} &= \frac{k_1 \Gamma \left[ 1 + \frac{1}{2} \sqrt{(d-3)^2 + 4\mu^2 L^2} \right] \Gamma \left[ -l - \frac{d-3}{2} \right]}{\Gamma \left[ \frac{5-d-2l+\sqrt{(d-3)^2+4\mu^2 L^2+2\omega L}}{4} \right] \Gamma \left[ \frac{5-d-2l+\sqrt{(d-3)^2+4\mu^2 L^2-2\omega L}}{4} \right]} L^{-\frac{2l+d-2}{2}}.
\end{aligned} \tag{4.79}$$

Equation (4.78) holds in the region  $r_h \ll r - r_h \ll \frac{L^2}{2r_h}$ . On the other hand, if  $\frac{1}{2}(3-d-2l)$  is an integer, such that  $-l - \frac{d-3}{2} = -m$ , with  $m = 1, 2, 3, \dots$ , that is, if  $d$  is odd, one has

$$u_{\text{far}}(r) = \frac{u_V^{(\text{far},1/r)}}{r^{\frac{2l+d-4}{2}}} + u_V^{(\text{far},r)} r^{\frac{2l+d-2}{2}} \log\left(\frac{r}{L}\right), \tag{4.80}$$

with

$$u_V^{(\text{far},r)} = k_1 \frac{2(-1)^{m+1} \Gamma \left[ 1 + \frac{1}{2} \sqrt{(d-3)^2 + 4\mu^2 L^2} \right]}{m! \Gamma \left[ \frac{5-d-2l+\sqrt{(d-3)^2+4\mu^2 L^2+2\omega L}}{4} \right] \Gamma \left[ \frac{5-d-2l+\sqrt{(d-3)^2+4\mu^2 L^2-2\omega L}}{4} \right]} L^{-\frac{2l+d-2}{2}}, \tag{4.81}$$

and  $u_V^{(\text{far},1/r)}$  given by Eq. (4.79). The solutions originating in the far-region are then in the overlap region described either by Eq. (4.78) or Eq. (4.80).

## Matching

For the functional matching to be possible, the near-region and far-region solutions need to have the same functional dependence on  $r$  in the overlap region. Examining Eqs. (4.66), (4.69), (4.78) and (4.80), one sees that the near-region and far-region solutions only have a common functional dependence when both  $\frac{2l}{d-3}$  is non-integer and  $d$  is even. Otherwise, the logarithmic terms give different functional contributions. We hereafter focus on non-integer  $\frac{2l}{d-3}$  and even  $d$ . Since the near- and far-regions hold, respectively, in  $0 \ll r - r_h \ll 1/\omega$  and  $r_h \ll r - r_h \ll \frac{L^2}{2r_h}$ , the overlap region is given by  $r_h \ll r - r_h \ll \min\left(1/\omega, \frac{L^2}{2r_h}\right)$ . In this case, one can match Eq. (4.66) with Eq. (4.78), yielding

$$\begin{aligned}
& \frac{\Gamma \left[ -1 - \frac{2l}{d-3} \right] \Gamma \left[ -l - \frac{d-3}{2} \right]}{\Gamma \left[ \frac{1-l-i\omega r_h}{d-3} \right] \Gamma \left[ \frac{-1-l-i\omega r_h}{d-3} \right] \Gamma \left[ \frac{5-d-2l+\sqrt{(d-3)^2+4\mu^2 L^2+2\omega L}}{4} \right] \Gamma \left[ \frac{5-d-2l+\sqrt{(d-3)^2+4\mu^2 L^2-2\omega L}}{4} \right]} \left(\frac{r_h}{L}\right)^{2l+d-3} = \\
& = \frac{\Gamma \left[ 1 + \frac{2l}{d-3} \right] \Gamma \left[ l + \frac{d-3}{2} \right]}{\Gamma \left[ \frac{l+d-4-i\omega r_h}{d-3} \right] \Gamma \left[ \frac{l+d-2-i\omega r_h}{d-3} \right] \Gamma \left[ \frac{2l+d-1+\sqrt{(d-3)^2+4\mu^2 L^2+2\omega L}}{4} \right] \Gamma \left[ \frac{2l+d-1+\sqrt{(d-3)^2+4\mu^2 L^2-2\omega L}}{4} \right]}.
\end{aligned} \tag{4.82}$$

Equation (4.82) can then be solved for  $\omega$ , which gives the quasinormal mode spectrum. Due to the cumbersome form of the matching condition, one can only solve analytically Eq. (4.82) by performing some approximations. In the far-region, we have already established that the spacetime can be regarded

as pure AdS. Since  $r_h/L \ll 1$  and given the numerical results obtained, we expect that the presence of the black hole will change the frequencies from the pure AdS ones by a small imaginary part,  $\delta$ , allowing to write them as

$$\omega = \omega_{\text{AdS}} + i\delta \quad , \quad |\delta| \ll |\omega_{\text{AdS}}| \quad . \quad (4.83)$$

The stability study of Section 4.2.3 implies  $\delta < 0$ , which can be used as a sanity check. Substituting Eq. (3.15) with  $S = V$  in Eq. (4.83), the relevant gamma functions are transformed to

$$\begin{aligned} \Gamma \left[ \frac{5 - d - 2l + \sqrt{(d-3)^2 + 4\mu^2 L^2} + 2\omega L}{4} \right] &= \Gamma \left[ 1 + k + \frac{1}{2} \sqrt{(d-3)^2 + 4\mu^2 L^2} + i \frac{\delta L}{2} \right] \simeq \\ &\simeq \Gamma \left[ 1 + k + \frac{1}{2} \sqrt{(d-3)^2 + 4\mu^2 L^2} \right] \quad , \end{aligned} \quad (4.84)$$

$$\Gamma \left[ \frac{5 - d - 2l + \sqrt{(d-3)^2 + 4\mu^2 L^2} - 2\omega L}{4} \right] = \Gamma \left[ -k - l - \frac{d-3}{2} - i \frac{\delta L}{2} \right] \simeq \Gamma \left[ -k - l - \frac{d-3}{2} \right] \quad , \quad (4.85)$$

$$\begin{aligned} \Gamma \left[ \frac{2l + d - 1 + \sqrt{(d-3)^2 + 4\mu^2 L^2} + 2\omega L}{4} \right] &= \Gamma \left[ k + l + \frac{d-1}{2} + \frac{1}{2} \sqrt{(d-3)^2 + 4\mu^2 L^2} + i \frac{\delta L}{2} \right] \simeq \\ &\simeq \Gamma \left[ k + l + \frac{d-1}{2} + \frac{1}{2} \sqrt{(d-3)^2 + 4\mu^2 L^2} \right] \quad , \end{aligned} \quad (4.86)$$

$$\frac{1}{\Gamma \left[ \frac{2l + d - 1 + \sqrt{(d-3)^2 + 4\mu^2 L^2} - 2\omega L}{4} \right]} = \frac{1}{\Gamma \left[ -k - i \frac{\delta L}{2} \right]} \simeq i(-1)^{k+1} k! \frac{\delta L}{2} \quad , \quad (4.87)$$

where we used

$$\begin{aligned} \Gamma[z + \epsilon] &\simeq \Gamma[z] \quad , \quad z \notin \mathbb{Z}_{\leq 0} \quad , \\ \lim_{z \rightarrow -k} \frac{1}{\Gamma[z + \epsilon]} &\simeq \lim_{z \rightarrow -k} -\frac{\psi[z]}{\Gamma[z]} \epsilon = (-1)^k k! \epsilon \quad . \end{aligned} \quad (4.88)$$

Substituting in Eq. (4.82), and doing the same for the gamma functions with arguments containing  $\omega r_h$  terms, yields

$$\begin{aligned} \delta L &= \frac{2i(-1)^k}{k!} \frac{\Gamma \left[ -1 - \frac{2l}{d-3} \right] \Gamma \left[ -l - \frac{d-3}{2} \right]}{\Gamma \left[ 1 + \frac{2l}{d-3} \right] \Gamma \left[ l + \frac{d-3}{2} \right]} \times \frac{\Gamma \left[ \frac{l+d-4-i\omega r_h}{d-3} \right] \Gamma \left[ \frac{l+d-2-i\omega r_h}{d-3} \right]}{\Gamma \left[ \frac{1-l-i\omega r_h}{d-3} \right] \Gamma \left[ \frac{-1-l-i\omega r_h}{d-3} \right]} \times \\ &\times \frac{\Gamma \left[ k + l + \frac{d-1}{2} + \frac{1}{2} \sqrt{(d-3)^2 + 4\mu^2 L^2} \right]}{\Gamma \left[ k + 1 + \frac{1}{2} \sqrt{(d-3)^2 + 4\mu^2 L^2} \right] \Gamma \left[ -k - l - \frac{d-3}{2} \right]} \left( \frac{r_h}{L} \right)^{2l+d-3} \quad . \end{aligned} \quad (4.89)$$

Since  $\frac{1-l}{d-3}$  and  $-\frac{1+l}{d-3}$  are allowed to take non-positive integer values, one needs to be careful again when performing the expansion of these gamma functions. Note that if  $\frac{1-l}{d-3}$  is integer, then  $\frac{-1-l}{d-3}$  is not and vice-versa. This is because  $\frac{2}{d-3}$  is never integer, as this would imply  $d = 4$  or  $d = 5$  (none of these two cases can be studied with this method since, for  $d = 4$ ,  $\frac{2l}{d-3}$  is always integer, and  $d = 5$  is an odd dimension). Thus, we only need to consider three cases: when  $\frac{1-l}{d-3}$  is integer; when  $\frac{-1-l}{d-3}$  is integer; when none of them are integers. For integer  $\frac{1-l}{d-3} = -p$ , with  $p = 0, 1, 2, \dots$ , one has, after simplifying the

negative arguments in the gamma functions,

$$\delta = -\frac{2p!}{k!} \frac{(l+1)^2 \Gamma \left[ k+l + \frac{d-1}{2} + \frac{1}{2} \sqrt{(d-3)^2 + 4\mu^2 L^2} \right] \Gamma^2 \left[ \frac{l+1}{d-3} \right] \Gamma \left[ \frac{l+d-4}{d-3} \right] \prod_{j=1}^k \left( l + \frac{d-3}{2} + j \right)}{(2l+d-3)(d-3)^2 \Gamma \left[ k+1 + \frac{1}{2} \sqrt{(d-3)^2 + 4\mu^2 L^2} \right] \Gamma^2 \left[ 1 + \frac{2l}{d-3} \right] \Gamma \left[ l + \frac{d-3}{2} \right]} \times \left( \frac{r_h}{L} \right)^{2l+d-2} \omega_{\text{AdS}} , \quad (4.90)$$

which is manifestly negative as for  $z > 0$ ,  $\Gamma[z] > 0$ . This is in agreement with the stability study from Section 4.2.3, where we proved stability for Schwarzschild-AdS black holes against vector-type Proca and Maxwell field perturbations. In principle, we could test the validity of Eq. (4.90) by comparing it with the numerical results obtained by numerical integration. However, for frequencies with sufficiently small imaginary part (typically  $|\Im(\omega)| \lesssim 10^{-11}$ ), the solutions obtained from numerically integrating the equation of motion oscillate substantially when one changes the initial guess or the domain of integration. As we are dealing with small black holes, and since the magnitude of the imaginary part of the frequencies decreases as  $(r_h/L)^{2l+d-2}$ , we cannot obtain accurate numerical results in the majority of the cases (for a black hole with size  $r_h = 0.01$ , the largest imaginary parts are of the order  $\sim 10^{-11}$ ). Thus, numerical verification of Eq. (4.90) is still needed, for example, using the Breit-Wigner resonance method approached in [39, 65]. Additionally, note that Eq. (4.90) only covers the cases:  $l = 1, d-2, 2d-5, 3d-8, \dots$ . In Table (4.13) we present the analytical results for several allowed parameters and the corresponding numerical results with the available precision, for  $r_h = 0.1$  and  $r_h = 0.01$ .

$r_h$	Parameters	$\delta$ (Analytical)	$\delta$ (Numerical)
0.1	$d = 6, l = 1, \mu = 0$	$-2.71624 \times 10^{-5}$	$-3.44092 \times 10^{-5}$
	$d = 6, l = 1, \mu = 0.5$	$-2.94359 \times 10^{-5}$	$-3.75448 \times 10^{-5}$
	$d = 6, l = 4, \mu = 0.5$	$-1.66287 \times 10^{-11}$	$-2.85 \times 10^{-11}$
	$d = 8, l = 1, \mu = 0.5$	$-1.36372 \times 10^{-6}$	$-1.47671 \times 10^{-6}$
0.01	$d = 6, l = 1, \mu = 0$	$-2.71624 \times 10^{-11}$	$-2.7239 \times 10^{-11}$
	$d = 6, l = 1, \mu = 0.5$	$-2.94359 \times 10^{-11}$	$-2.9522 \times 10^{-11}$
	$d = 6, l = 4, \mu = 0.5$	$-1.66287 \times 10^{-23}$	—
	$d = 8, l = 1, \mu = 0.5$	$-1.36372 \times 10^{-14}$	$-1.4 \times 10^{-14}$

**Table 4.13:** Imaginary part of vector-type quasinormal frequencies for some of the allowed values of  $d, l, \mu$ , for black holes with sizes  $r_h = 0.1$  and  $r_h = 0.01$ . The analytical results were computed from Eq. (4.90).

Similarly, for integer  $-\frac{1+l}{d-3} = -q$ , with  $q = 0, 1, 2, \dots$ , one has

$$\delta = -\frac{2q!}{k!} \frac{(l-1)^2 \Gamma \left[ k+l + \frac{d-1}{2} + \frac{1}{2} \sqrt{(d-3)^2 + 4\mu^2 L^2} \right] \Gamma^2 \left[ \frac{l-1}{d-3} \right] \Gamma \left[ \frac{l+d-2}{d-3} \right] \prod_{j=1}^k \left( l + \frac{d-3}{2} + j \right)}{(2l+d-3)(d-3)^2 \Gamma \left[ k+1 + \frac{1}{2} \sqrt{(d-3)^2 + 4\mu^2 L^2} \right] \Gamma^2 \left[ 1 + \frac{2l}{d-3} \right] \Gamma \left[ l + \frac{d-3}{2} \right]} \times \left( \frac{r_h}{L} \right)^{2l+d-2} \omega_{\text{AdS}} , \quad (4.91)$$

which covers the cases  $l = d - 4, 2d - 7, 3d - 10, \dots$ . Analytical and numerical results are shown in Table (4.14).

$r_h$	Parameters	$\delta$ (Analytical)	$\delta$ (Numerical)
0.1	$d = 6, l = 2, \mu = 0$	$-2.61924 \times 10^{-7}$	$-3.61579 \times 10^{-7}$
	$d = 6, l = 2, \mu = 0.5$	$-2.87685 \times 10^{-7}$	$-4.00185 \times 10^{-7}$
	$d = 6, l = 5, \mu = 0.5$	$-1.09237 \times 10^{-13}$	$-2.1035 \times 10^{-13}$
	$d = 8, l = 4, \mu = 0.5$	$-2.42402 \times 10^{-12}$	$-2.9644 \times 10^{-12}$
0.01	$d = 6, l = 2, \mu = 0$	$-2.61924 \times 10^{-15}$	$-3 \times 10^{-15}$
	$d = 6, l = 2, \mu = 0.5$	$-2.87685 \times 10^{-15}$	$-3 \times 10^{-15}$
	$d = 6, l = 5, \mu = 0.5$	$-1.09237 \times 10^{-27}$	–
	$d = 8, l = 4, \mu = 0.5$	$-2.42402 \times 10^{-26}$	–

**Table 4.14:** Imaginary part of vector-type quasinormal frequencies for some of the allowed values of  $d, l, \mu$ , for black holes with sizes  $r_h = 0.1$  and  $r_h = 0.01$ . The analytical results were computed from Eq. (4.91).

When none of  $-\frac{l+1}{d-3}$  and  $-\frac{l-1}{d-3}$  are integers, none of the gamma functions in Eq. (4.89) vanishes at leading-order, so that

$$\frac{\Gamma\left[\frac{l+d-4-i\omega r_h}{d-3}\right] \Gamma\left[\frac{l+d-2-i\omega r_h}{d-3}\right]}{\Gamma\left[\frac{1-l-i\omega r_h}{d-3}\right] \Gamma\left[\frac{-1-l-i\omega r_h}{d-3}\right]} \simeq \frac{\Gamma\left[\frac{l+d-4}{d-3}\right] \Gamma\left[\frac{l+d-2}{d-3}\right]}{\Gamma\left[\frac{1-l}{d-3}\right] \Gamma\left[\frac{-l+1}{d-3}\right]} \left(1 + \frac{i\pi\omega}{d-3} \left(\cot\left(\frac{\pi(l-1)}{d-3}\right) + \cot\left(\frac{\pi(l+1)}{d-3}\right)\right)\right), \quad (4.92)$$

and the leading-order term of  $\delta$  gives a correction to the real part of  $\omega$ . The decay is given by the real part of  $\delta$  (corresponding to the next-to-leading-order term in the gamma expansion)

$$\Re\epsilon(\delta) = -\frac{2}{k!} \frac{(l-1)^2(l+1)^2 \Gamma\left[k+l+\frac{d-1}{2} + \frac{1}{2}\sqrt{(d-3)^2+4\mu^2 L^2}\right] \Gamma^2\left[\frac{l+1}{d-3}\right] \Gamma^2\left[\frac{l-1}{d-3}\right] \prod_{j=1}^k \left(l+\frac{d-3}{2}+j\right)}{(2l+d-3)(d-3)^4 \Gamma\left[k+1+\frac{1}{2}\sqrt{(d-3)^2+4\mu^2 L^2}\right] \Gamma^2\left[1+\frac{2l}{d-3}\right] \Gamma\left[l+\frac{d-3}{2}\right]} \times \left(\frac{r_h}{L}\right)^{2l+d-2} \omega_{\text{AdS}}, \quad (4.93)$$

so that  $\Re\epsilon(\delta) < 0$ . This covers the cases not covered by Eqs. (4.90) and (4.91), keeping always in mind that  $\frac{2l}{d-3}$  cannot be integer. Thus, for example, for  $d = 6, l = 3, 6, 9, \dots$ ,  $\frac{2l}{d-3}$  is integer and the method does not work. Analytical and numerical results for some of the allowed values of  $l$  in  $d = 8$  and  $d = 10$  are presented in Table (4.15).

$r_h$	Parameters	$\Re\epsilon(\delta)$ (Analytical)	$\Re\epsilon(\delta)$ (Numerical)
0.1	$d = 8, l = 2, \mu = 0.5$	$-1.89267 \times 10^{-8}$	$-2.12663 \times 10^{-8}$
	$d = 8, l = 3, \mu = 0.5$	$-2.25788 \times 10^{-10}$	$-2.64183 \times 10^{-10}$
	$d = 10, l = 2, \mu = 0.5$	$-9.71194 \times 10^{-10}$	$-1.00734 \times 10^{-9}$
	$d = 10, l = 3, \mu = 0.5$	$-1.36078 \times 10^{-11}$	$-1.44325 \times 10^{-11}$
0.01	$d = 8, l = 2, \mu = 0.5$	$-1.89267 \times 10^{-18}$	—
	$d = 8, l = 3, \mu = 0.5$	$-2.25788 \times 10^{-22}$	—
	$d = 10, l = 2, \mu = 0.5$	$-9.71194 \times 10^{-22}$	—
	$d = 10, l = 3, \mu = 0.5$	$-1.36078 \times 10^{-25}$	—

**Table 4.15:** Imaginary part of vector-type quasinormal frequencies for some of the allowed values of  $d, l, \mu$ , for black holes with sizes  $r_h = 0.1$  and  $r_h = 0.01$ . The analytical results were computed from Eq. (4.93).

The agreement between analytical and numerical results highly depends on the black hole size used. Ideally, if one was able to find accurate numerical results for  $r_h \lesssim 0.01$ , one could test the analytical method by fitting the numerical results to  $\delta = -A(r_h/L)^B$  and comparing  $A, B$  with the ones predicted by the corresponding analytical expressions Eqs. (4.90), (4.91) and (4.93). As discussed above, our numerical results are only accurate for  $|\Im m(\omega)| \gtrsim 10^{-11}$ , making this technique unreliable for the parameters studied. Note, however, that the numerically accurate values obtained for  $r_h = 0.1$  already agree in the order of magnitude with the analytical results. Such an agreement was not expected, as in this case  $r_h \omega \simeq 1$  ( $\omega$  is order  $10^1$  for the cases studied), and the overlap region is very small. Moreover, the numerical results available for  $r_h = 0.01$  confirm this agreement, with the frequencies deviating from the analytical predictions only in the second decimal place.

On a final observation, bear in mind that the analytical method developed is quite restrictive, as it only works for even  $d$ . Indeed, for odd  $d$ , the functional form of the near- and far-region solutions is not the same, preventing us from matching them at the overlap region. A possible way to overcome this would be to match the near- and far-region solutions and its first derivatives at a suitable point in the domain, although the lack of a prescription to choose the matching point leads to unreliable results for the imaginary part of the frequencies [72]. A different analytical procedure seems to be needed in order to study the spectrum of odd dimensional spacetimes (and certain combinations of  $l$  and  $d$ ).

## 4.5.2 Monopole Proca field perturbations

### Near-region

One can perform the same analysis for the monopole mode of scalar-type Proca field perturbations. Writing Eq. (4.6) with effective potential given by Eq. (4.4), one has, in terms of  $z$ ,

$$z(1-z)\frac{\partial^2 u_{l=0}^{\text{near}}}{\partial z^2} + \left(1-z\left(2+\frac{1}{d-3}\right)\right)\frac{\partial u_{l=0}^{\text{near}}}{\partial z} + \frac{1}{(d-3)^2}\left(\frac{\omega^2 r_h^2}{z(1-z)} - \frac{d(d-2)z}{4(1-z)} + \frac{(d-2)(d-3)}{2} - \frac{\mu^2 r_h^2}{1-z}\right)u_{l=0}^{\text{near}} = 0 \quad . \quad (4.94)$$

The mass term may be neglected by making  $\frac{(d-2)(d-3)}{2} = \frac{(d-2)(d-3)}{2(1-z)} - \frac{(d-2)(d-3)z}{2(1-z)}$ . Performing Eq. (4.61) one arrives at the standard hypergeometric differential equation with

$$\alpha = -\frac{i\omega r_h}{d-3}, \quad \beta = \frac{d-2}{2(d-3)}, \quad (4.95)$$

$$a = \frac{2d-4-i\omega r_h}{d-3}, \quad b = -\frac{i\omega r_h}{d-3}, \quad c = 1 - \frac{2i\omega}{d-3} \quad .$$

Imposing the boundary condition at the horizon and taking the  $z \rightarrow 1$  limit as before one has, in the overlap region,

$$u_{l=0}^{\text{near}}(r) = \frac{u_{l=0}^{\text{(near,1/r)}}}{r^{\frac{d-2}{2}}} + u_{l=0}^{\text{(near,r)}} r^{\frac{d}{2}}, \quad (4.96)$$

with

$$u_{l=0}^{\text{(near,1/r)}} = c_1 \frac{\Gamma\left[1 - \frac{2i\omega r_h}{d-3}\right] \Gamma\left[-1 - \frac{2}{d-3}\right]}{\Gamma\left[1 - \frac{i\omega r_h}{d-3}\right] \Gamma\left[\frac{1-d-i\omega r_h}{d-3}\right]} r_h^{\frac{d-2}{2}}, \quad u_{l=0}^{\text{(near,r)}} = c_1 \frac{\Gamma\left[1 - \frac{2i\omega r_h}{d-3}\right] \Gamma\left[1 + \frac{2}{d-3}\right]}{\Gamma\left[\frac{2d-4-i\omega r_h}{d-3}\right] \Gamma\left[\frac{-i\omega r_h}{d-3}\right]} r_h^{-\frac{d}{2}} \quad . \quad (4.97)$$

Equation (4.96) holds for  $d \geq 6$ . For  $d = 4$  and  $d = 5$ , Eq. (4.96) contains a logarithmic term multiplying  $r^{-\frac{d-2}{2}}$ , as  $\frac{2}{d-3}$  is integer.

### Far-region

In the far-region, the vector-type effective potential Eq. (4.2) with  $l = 1$  is reduced to the monopole effective potential Eq. (4.4), so that the results can be readily obtained by substituting  $l = 1$  in the expressions already obtained for vector-type perturbations. Thus, for even  $d$ , the solution is Eq. (4.78) with Eq. (4.79) after setting  $l = 1$ , while for odd  $d$  there is a logarithmic term multiplying  $r^{\frac{d}{2}}$ .

## Matching

The functional matching is only possible when  $d$  is even and  $d \neq 4$ . In this case, the matching condition is

$$\begin{aligned} & \frac{\Gamma\left[-1 - \frac{2}{d-3}\right] \Gamma\left[-1 - \frac{d-3}{2}\right]}{\Gamma\left[\frac{1-d-i\omega r_h}{d-3}\right] \Gamma\left[1 - \frac{i\omega r_h}{d-3}\right] \Gamma\left[\frac{3-d+\sqrt{(d-3)^2+4\mu^2 L^2+2\omega L}}{4}\right] \Gamma\left[\frac{3-d+\sqrt{(d-3)^2+4\mu^2 L^2-2\omega L}}{4}\right]} \left(\frac{r_h}{L}\right)^{d-1} = \\ & = \frac{\Gamma\left[1 + \frac{2}{d-3}\right] \Gamma\left[1 + \frac{d-3}{2}\right]}{\Gamma\left[\frac{2d-4-i\omega r_h}{d-3}\right] \Gamma\left[\frac{-i\omega r_h}{d-3}\right] \Gamma\left[\frac{1+d+\sqrt{(d-3)^2+4\mu^2 L^2+2\omega L}}{4}\right] \Gamma\left[\frac{1+d+\sqrt{(d-3)^2+4\mu^2 L^2-2\omega L}}{4}\right]} . \end{aligned} \quad (4.98)$$

Assuming Eq. (4.83) with  $\omega_{\text{AdS}}$  given by Eq. (3.15), substituting in Eq. (4.98) and expanding the Gamma functions in the same way as we did for vector-type perturbations, we arrive at

$$\begin{aligned} \delta = & - \frac{2\pi^2(d-3)^2 \Gamma\left[\frac{1}{2}\left(d+1+2k+\sqrt{(d-3)^2+4\mu^2 L^2}\right)\right] \prod_{j=1}^k \left(\frac{d-1}{2} + j\right)}{(d-1)k! \sin^2\left(\frac{2\pi}{d-3}\right) \Gamma^2\left[1 + \frac{2}{d-3}\right] \Gamma^2\left[\frac{1-d}{d-3}\right] \Gamma\left[\frac{d-1}{2}\right] \Gamma\left[1+k+\frac{1}{2}\sqrt{(d-3)^2+4\mu^2 L^2}\right]} \times \\ & \times \left(\frac{r_h}{L}\right)^{d-2} \frac{1}{\omega_{\text{AdS}} L^2} , \end{aligned} \quad (4.99)$$

which, again, is manifestly negative in agreement with the studies of Section 4.2.3. Since in this case the dependence on  $r_h$  is only  $r_h^{d-2}$ , it is possible to obtain numerical results with the desired accuracy for smaller black holes. For example, for  $d = 6$  and a black hole with size  $r_h = 0.001$ ,  $\delta$  should be order  $10^{-11}$ , which is more or less the limit of accuracy of our numerical results. Of course, for higher  $d$ ,  $\delta$  decreases in magnitude and more accurate numerical results are needed. Analytical and numerical results are shown in Table (4.16). The numerical values for  $\delta$  tend to agree with the analytical ones as

$r_h$	Parameters	$\delta$ (Analytical)	$\delta$ (Numerical)
0.1	$d = 6, \mu = 0.5$	$-2.85033 \times 10^{-3}$	$-3.57515 \times 10^{-3}$
	$d = 6, \mu = 2$	$-4.52707 \times 10^{-3}$	$-6.12516 \times 10^{-3}$
	$d = 8, \mu = 0.5$	$-1.34463 \times 10^{-4}$	$-1.43570 \times 10^{-4}$
	$d = 8, \mu = 2$	$-1.95524 \times 10^{-4}$	$-2.12290 \times 10^{-4}$
0.01	$d = 6, \mu = 0.5$	$-2.85033 \times 10^{-7}$	$-2.85907 \times 10^{-7}$
	$d = 6, \mu = 2$	$-4.52707 \times 10^{-7}$	$-4.54601 \times 10^{-7}$
	$d = 8, \mu = 0.5$	$-1.34463 \times 10^{-10}$	$-1.34567 \times 10^{-10}$
	$d = 8, \mu = 2$	$-1.95524 \times 10^{-10}$	$-1.95711 \times 10^{-10}$
0.001	$d = 6, \mu = 0.5$	$-2.85033 \times 10^{-11}$	$-2.85045 \times 10^{-11}$
	$d = 6, \mu = 2$	$-4.52707 \times 10^{-11}$	$-4.52734 \times 10^{-11}$
	$d = 8, \mu = 0.5$	$-1.34463 \times 10^{-16}$	—
	$d = 8, \mu = 2$	$-1.95524 \times 10^{-16}$	—

**Table 4.16:** Imaginary part of monopole quasinormal frequencies for some of the allowed values of  $d, \mu$ , for black holes with sizes  $r_h = 0.1, r_h = 0.01$  and  $r_h = 0.001$ . The analytical results were computed from Eq. (4.99).

one decreases  $r_h$ . In particular, for  $r_h = 0.001$ , they are the same up to the fourth significant figure. Interestingly, note that the damping of the monopole mode goes as  $\delta \sim \omega_{\text{AdS}}^{-1}$ , while for vector-type

perturbations one has  $\delta \sim \omega_{\text{AdS}}$ .

### 4.5.3 Scalar-type Maxwell field perturbations

#### Near-region

The equation of motion for Maxwell scalar-type perturbations in the near-region is

$$z(1-z)\frac{\partial^2 u_{\text{EM}}^{\text{near}}}{\partial z^2} + \left(1-z\left(2+\frac{1}{d-3}\right)\right)\frac{\partial u_{\text{EM}}^{\text{near}}}{\partial z} + \frac{1}{(d-3)^2}\left(\frac{\omega^2 r_h^2}{z(1-z)} - \frac{l(l+d-3)}{1-z} - \frac{(d-2)(d-4)z}{4(1-z)} + \frac{(d-4)(d-3)}{2}\right)u_{\text{EM}}^{\text{near}} = 0 \quad . \quad (4.100)$$

Using Eq. (4.61) leads to the standard hypergeometric differential equation with

$$\alpha = -\frac{i\omega r_h}{d-3} \quad , \quad \beta = \frac{2l+d-4}{2(d-3)} \quad , \quad (4.101)$$

$$a = \frac{l-i\omega r_h}{d-3} \quad , \quad b = 2 + \frac{l-i\omega r_h}{d-3} \quad , \quad c = 1 - \frac{2i\omega}{d-3} \quad .$$

If  $\frac{2l}{d-3}$  is non-integer, after imposing the boundary condition at the horizon and taking the  $z \rightarrow 1$ , the solution in the overlap region yields

$$u_{\text{EM}}^{\text{near}}(r) = \frac{u_{\text{EM}}^{(\text{near},1/r)}}{r^{\frac{2l+d-4}{2}}} + u_{\text{EM}}^{(\text{near},r)} r^{\frac{2l+d-2}{2}} \quad , \quad (4.102)$$

with

$$u_{\text{EM}}^{(\text{near},1/r)} = c_1 \frac{\Gamma\left[1 - \frac{2i\omega r_h}{d-3}\right] \Gamma\left[-1 - \frac{2l}{d-3}\right]}{\Gamma\left[1 - \frac{l+i\omega r_h}{d-3}\right] \Gamma\left[-1 - \frac{l+i\omega r_h}{d-3}\right]} r_h^{\frac{2l+d-4}{2}} \quad , \quad u_{\text{EM}}^{(\text{near},r)} = c_1 \frac{\Gamma\left[1 - \frac{2i\omega r_h}{d-3}\right] \Gamma\left[1 + \frac{2l}{d-3}\right]}{\Gamma\left[\frac{l-i\omega r_h}{d-3}\right] \Gamma\left[2 + \frac{l-i\omega r_h}{d-3}\right]} r_h^{-\frac{2l+d-2}{2}} \quad . \quad (4.103)$$

On the other hand, if  $\frac{2l}{d-3}$  is integer, the solution acquires a logarithmic term multiplying  $r^{-\frac{2l+d-4}{2}}$ .

#### Far-region

In the far-region, the equation of motion is written as

$$\xi(1-\xi)\frac{\partial^2 u_{\text{EM}}^{\text{far}}}{\partial \xi^2} + \left(\frac{1}{2} - \xi\right)\frac{\partial u_{\text{EM}}^{\text{far}}}{\partial \xi} + \left(\frac{\omega^2 L^2}{4} - \frac{l(l+d-3)}{4(1-\xi)} - \frac{(d-2)(d-4)}{16\xi(1-\xi)} + \frac{d-4}{4\xi}\right)u_{\text{EM}}^{\text{far}} = 0 \quad , \quad (4.104)$$

and performing the usual transformation yields the hypergeometric differential equation with

$$\alpha = \frac{d-4}{4} \quad , \quad \beta = \frac{2l+d-2}{4} \quad , \quad (4.105)$$

$$a = \frac{l+d-3+\omega L}{2} \quad , \quad b = \frac{l+d-3-\omega L}{2} \quad , \quad c = \frac{d-3}{2} \quad .$$

We have already seen that the solutions obeying the Dirichlet boundary condition at infinity are

$$u_{\text{EM}}^{\text{far}}(\xi) = \begin{cases} k_1 \xi^{\frac{1}{2}} (1 - \xi)^{\frac{l+1}{2}} F_1 [1 + a - c, 1 + b - c, 2 - c, \xi] & d = 4 \\ \xi^{\frac{1}{4}} (1 - \xi)^{\frac{2l+3}{4}} (k_1 F_1 [a, b, c, \xi] + k_2 \log(\xi) F_1 [1 + a - c, 1 + b - c, 2 - c, \xi]) & d = 5 \\ k_1 \xi^{\frac{d-4}{4}} (1 - \xi)^{\frac{2l+d-2}{4}} F_1 [a, b, c, \xi] & d \geq 6 \end{cases} . \quad (4.106)$$

For  $d \geq 6$ , after proceeding with the  $\xi \rightarrow 1 - \xi$  transformation and taking the  $\xi \rightarrow 1$  limit, one has, in the overlap region, for even  $d$ ,

$$u_{\text{EM}}^{\text{far}}(r) = \frac{u_{\text{EM}}^{(\text{far},1/r)}}{r^{\frac{2l+d-4}{2}}} + u_{\text{EM}}^{(\text{far},r)} r^{\frac{2l+d-2}{2}} , \quad (4.107)$$

with

$$u_{\text{EM}}^{(\text{far},1/r)} = \frac{k_1 \Gamma \left[ \frac{d-3}{2} \right] \Gamma \left[ l + \frac{d-3}{2} \right]}{\Gamma \left[ \frac{l+d-3+\omega L}{2} \right] \Gamma \left[ \frac{l+d-3-\omega L}{2} \right]} L^{\frac{2l+d-4}{2}} , \quad u_{\text{EM}}^{(\text{far},r)} = \frac{k_1 \Gamma \left[ \frac{d-3}{2} \right] \Gamma \left[ -l - \frac{d-3}{2} \right]}{\Gamma \left[ -\frac{l+\omega L}{2} \right] \Gamma \left[ -\frac{l-\omega L}{2} \right]} L^{-\frac{2l+d-2}{2}} , \quad (4.108)$$

while for odd  $d$  the same calculation leads to a logarithmic term multiplying  $r^{\frac{2l+d-2}{2}}$ . For  $d = 4$  a similar analysis yields Eq. (4.107), although the pre-factors change. We do not show them here since the matching cannot be done for  $d = 4$  ( $\frac{2l}{d-3}$  is integer). For  $d = 5$ , the usual requirement of the vanishing of the logarithmic term in Eq. (4.106) implies a logarithmic term multiplying  $r^{\frac{2l+3}{2}}$  in Eq. (4.107).

## Matching

As for vector-type perturbations, the functional matching is only possible when  $d$  is even and  $\frac{2l}{d-3}$  is non-integer. Carrying on the same calculations as before leads to

$$\Re(\delta) = -\frac{2}{k!} \frac{\Gamma[l+k+d-3] \Gamma^2 \left[ 2 + \frac{l}{d-3} \right] \Gamma^2 \left[ \frac{l}{d-3} \right] \prod_{j=1}^k \left( l + \frac{d-3}{2} + j \right)}{(2l+d-3) \Gamma^2 \left[ 1 + \frac{2l}{d-3} \right] \Gamma \left[ l + \frac{d-3}{2} \right] \Gamma \left[ k + \frac{d-3}{2} \right]} \times \left( \frac{r_h}{L} \right)^{2l+d-2} \omega_{\text{AdS}} , \quad (4.109)$$

where  $\omega_{\text{AdS}}$  is given by Eq. (3.19) and we expanded the next-to-leading order in  $\omega r_h$  since the leading-order term gives an imaginary contribution to  $\delta$  (and thus corrects the real part of  $\omega$ ). A comparison between numerical and analytical results is displayed in Table (4.17).

$r_h$	Parameters	$\Re(\delta)$ (Analytical)	$\Re(\delta)$ (Numerical)
0.1	$d = 6, l = 1$	$-1.01729 \times 10^{-4}$	$-1.15610 \times 10^{-4}$
	$d = 6, l = 4$	$-7.55262 \times 10^{-12}$	$-1.153 \times 10^{-11}$
	$d = 8, l = 1$	$-1.51335 \times 10^{-5}$	$-1.34251 \times 10^{-5}$
	$d = 10, l = 1$	$-1.40309 \times 10^{-6}$	$-9.85025 \times 10^{-7}$
0.01	$d = 6, l = 1$	$-1.01729 \times 10^{-10}$	$-1.01899 \times 10^{-10}$
	$d = 6, l = 4$	$-7.55262 \times 10^{-24}$	—
	$d = 8, l = 1$	$-1.51335 \times 10^{-13}$	$-1.51 \times 10^{-13}$
	$d = 10, l = 1$	$-1.40309 \times 10^{-16}$	$-1.4 \times 10^{-16}$

**Table 4.17:** Imaginary part of scalar-type electromagnetic quasinormal frequencies for some of the allowed values of  $d, l$ , for black holes with sizes  $r_h = 0.1$  and  $r_h = 0.01$ . The analytical results were computed from Eq. (4.109).

#### 4.5.4 Higher multipoles of scalar-type Proca field perturbations

For higher multipole scalar-type Proca field perturbations, the coupling between the modes makes the analytical matching procedure more involved. We have seen in Chapter 3 that in pure AdS the two scalar-type modes decouple. This means that one can find the behaviour of the two decoupled modes in the overlap region by taking the limit of the far-region solutions. Indeed, the far-region solutions obey

$$\begin{aligned} & \xi(1-\xi)\frac{\partial^2 u_{(\pm)}^{\text{far}}}{\partial \xi^2} + \left(\frac{1}{2} - \xi\right)\frac{\partial u_{(\pm)}^{\text{far}}}{\partial \xi} + \\ & + \left(\frac{\omega^2 L^2}{4} - \frac{(2j_{(\pm)} + d - 4)(2j_{(\pm)} + d - 2)}{16(1-\xi)} - \frac{1}{4\xi}\left(\mu^2 L^2 + \frac{(d-4)(d-2)}{4}\right)\right) u_{(\pm)}^{\text{far}} = 0 \quad , \end{aligned} \quad (4.110)$$

with  $j_{(\pm)} = l \pm 1$ . As already mentioned in Chapter 3, this is the same equation as Eq. (4.72) with  $j_V = l$ , resembling the spin-orbit interaction between the spin of the field and the orbital angular momentum of each multipole. Thus, the behaviour of the solutions in the overlap region can be readily obtained from Eq. (4.78) and Eq. (4.79) substituting  $l$  by  $l \pm 1$  (for simplicity and concreteness, we are already assuming that  $d$  is even and  $2l/(d-3)$  is non-integer). Writing explicitly for clarity,

$$u_{(\pm)}^{\text{far}}(r) = u_{(\pm)}^{(\text{far},1/r)} r^{-\frac{2(l\pm 1)+d-4}{2}} + u_{(\pm)}^{(\text{far},r)} r^{\frac{2(l\pm 1)+d-2}{2}} \quad , \quad (4.111)$$

where  $u_{(\pm)}^{(\text{far},1/r)}$ ,  $u_{(\pm)}^{(\text{far},r)}$  are given by Eq. (4.79) substituting  $l$  by  $l \pm 1$ . Note that there are two different constants of integration:  $k_{(+)}$  and  $k_{(-)}$ . One may then use Eq. (3.8) to write Eq. (4.111) in terms of  $u_2, u_3$ , as

$$\begin{aligned} u_2^{\text{far}}(r) &= u_{(+)}^{(\text{far},1/r)} r^{-\frac{2l+d-2}{2}} + u_{(-)}^{(\text{far},1/r)} r^{-\frac{2l+d-6}{2}} + u_{(+)}^{(\text{far},r)} r^{\frac{2l+d}{2}} + u_{(-)}^{(\text{far},r)} r^{\frac{2l+d-4}{2}} \quad , \\ u_3^{\text{far}}(r) &= -l u_{(+)}^{(\text{far},1/r)} r^{-\frac{2l+d-2}{2}} + (l+d-3) u_{(-)}^{(\text{far},1/r)} r^{-\frac{2l+d-6}{2}} - l u_{(+)}^{(\text{far},r)} r^{\frac{2l+d}{2}} + (l+d-3) u_{(-)}^{(\text{far},r)} r^{\frac{2l+d-4}{2}} \quad . \end{aligned} \quad (4.112)$$

Moreover, using the definition Eq. (2.53) one gets

$$u_{\text{EM}} = \frac{u_2}{r} - \frac{f r^{\frac{d-4}{2}}}{l(l+d-3)} \partial_r \left( u_3 r^{-\frac{d-4}{2}} \right) \quad , \quad (4.113)$$

so that

$$u_{\text{EM}}^{\text{far}}(r) = \frac{2l+d-5}{l} u_{(-)}^{(\text{far},1/r)} r^{-\frac{2l+d-4}{2}} + \frac{2l+d-1}{l+d-3} u_{(+)}^{(\text{far},r)} r^{\frac{2l+d-2}{2}} \quad . \quad (4.114)$$

On the other hand, in the near-region, it is not possible to decouple the equations of motion, even within the approximations we are performing. If we knew how the decoupled modes behave in this region, we would just need to match these with Eq. (4.111) and extract the two frequencies  $\delta_{(\pm)}$  from the matching condition, as we did before. Although this is not possible, we can try to match the solutions assuming that the factorization in Eq. (2.62) holds, i.e., the scalar-type Proca field modes with electromagnetic and non-electromagnetic polarizations approach the (scalar-type) Maxwell field and scalar field modes, respectively. Assuming this,  $ru_3$  obeys the Klein-Gordon equation and we find that the solutions for  $u_3$

in the overlap region behave as

$$u_3^{\text{near}}(r) = u_3^{(\text{near},1/r)} r^{-\frac{2l+d-2}{2}} + u_3^{(\text{near},r)} r^{\frac{2l+d-4}{2}}, \quad (4.115)$$

with

$$u_3^{(\text{near},1/r)} = k_3 \frac{\Gamma\left[1 - \frac{2i\omega_3 r_h}{d-3}\right] \Gamma\left[-1 - \frac{2l}{d-3}\right]}{\Gamma^2\left[\frac{-l-i\omega_3 r_h}{d-3}\right]} r_h^{\frac{2l+d-4}{2}}, \quad (4.116)$$

$$u_3^{(\text{near},r)} = k_3 \frac{\Gamma\left[1 - \frac{2i\omega_3 r_h}{d-3}\right] \Gamma\left[1 + \frac{2l}{d-3}\right]}{\Gamma^2\left[\frac{l+d-3-i\omega_3 r_h}{d-3}\right]} r_h^{-\frac{2l+d-2}{2}}.$$

Similarly, Eq. (4.102) yields the behaviour of the Proca electromagnetic polarization in the overlap region

$$u_{\text{EM}}^{\text{near}}(r) = u_{\text{EM}}^{(\text{near},1/r)} r^{-\frac{2l+d-4}{2}} + u_{\text{EM}}^{(\text{near},r)} r^{\frac{2l+d-2}{2}}, \quad (4.117)$$

with  $u_{\text{EM}}^{(\text{near},1/r)}$ ,  $u_{\text{EM}}^{(\text{near},r)}$  given by Eq. (4.103). Note that while the electromagnetically polarized mode has the same functional dependence in both regions, the non-electromagnetically polarized mode has two additional power terms in the far-region that do not appear in the near-region. This is because, in the near-region, we are solving a second-order differential equation for  $u_3$ , instead of the fourth-order differential equation that describes the coupled system, resulting from substituting Eq. (2.46) in Eq. (2.45) and writing Eq. (2.45) as an equation for  $u_3$  only. If we match only the same functional terms of Eq. (4.112) and Eq. (4.115) and of Eq. (4.114) and Eq. (4.117), and assume that  $\omega_{(\text{EM})} = \omega_{(-)} = \omega_{(-)}^{\text{AdS}} + i\delta_{(-)}$ ,  $\omega_3 = \omega_{(+)} = \omega_{(+)}^{\text{AdS}} + i\delta_{(+)}$ , we get a single matching condition relating  $\delta_{(-)}$  and  $\delta_{(+)}$ . Still, in order to determine each one, we would need another matching condition of the same sort. If we were able to solve the fourth-order differential equation for  $u_3$ , and if the resulting terms power terms were the same as the ones appearing in Eq. (4.115), an additional matching condition would appear, allowing to determine both  $\delta_{(-)}$  and  $\delta_{(+)}$ . However, a solution to the fourth-order differential equation does not seem to be obvious, even within the approximations performed.

To summarize, the non-trivial coupling between the two scalar-type degrees of freedom in the near-region does not allow an analytical matching procedure as the one done for decoupled perturbations. Equations (4.112), (4.114), (4.115) and (4.117) illustrate this behaviour, with the modes in the near-region being linear combinations of the  $(\pm)$  modes appearing in the far-region. Although a relation between the two frequencies  $\delta_{(\pm)}$  can be achieved, one would need to solve an increased-order differential equation for  $u_3$  to extract the missing relation between  $\delta_{(+)}$  and  $\delta_{(-)}$ , which does not seem to be possible. We conclude by mentioning that, although very restrictive and seemingly unable to describe the scalar-type sector of Proca field perturbations, this method improved our understanding in the following aspects: for small black holes, the mode damping decreases with the black hole radius as  $(r_h/L)^{2l+d-2}$ , in agreement with previous studies [52, 65]; numerical and analytical results agree up to the third significant figure for black holes with  $r_h/L = 0.01$  and up to the fourth significant figure for black holes with  $r_h/L = 0.001$ ; the coupling between the Proca scalar-type modes is non-trivial even within the small black hole regime and long-wavelength approximation.

# Chapter 5

## Conclusion

### 5.1 Achievements

In this work, the formalism developed in [12–14, 46, 47] was used to study Proca field perturbations in spaces with warped product topology  $\mathcal{M}^d = \mathcal{N}^m \times \mathcal{K}^n$ . We showed that if the Proca field is decomposed according to its tensorial behaviour on  $\mathcal{K}^n$ , the Proca equations give rise to two completely separated sectors: the vector-type sector, described by a second-order differential equation for one variable, which covers  $n - 1$  decoupled degrees of freedom of the field; the scalar-type sector, described by a system of  $m$  second-order coupled differential equations for  $m$  variables, which cover the remaining  $m$  (dynamical) degrees of freedom of the field. This procedure was further developed in  $(d = 2 + n)$ -dimensional spherically symmetric spacetimes, by expanding the vector-type (scalar-type) variables in vector (scalar)  $n$ -dimensional spherical harmonics. After such expansion, the Proca field equations simplified to a set of three wave-like equations: a single decoupled wave equation describing the vector-type degrees of freedom and two coupled wave equations describing the scalar-type degrees of freedom. The Maxwell field equations were also obtained by carefully taking the massless limit of the Proca field: in this case, one scalar-type degree of freedom becomes pure-gauge, so that the scalar-type sector is also decoupled.

The remainder of the thesis was devoted to the study of Proca field (quasi)normal modes in  $d$ -dimensional AdS and Schwarzschild-AdS spacetimes. In AdS, we showed that the Proca scalar-type sector can be decoupled analytically and we found the exact normal mode solutions for the Proca field by imposing Dirichlet boundary conditions at spatial infinity. The modes are splitted according to their total angular momentum number, resembling a spin-orbit interaction between the spin of the Proca field and the angular momentum of each mode [44]. Within this picture, vector-type modes have spin projection 0, whereas scalar-type modes have spin projections  $\pm 1$ , in accordance with the angular momentum addition rules for a spin-1 field. The results agreed with [45] for  $d = 4$  and generalized its study to higher-dimensional AdS. Moreover, the Maxwell field normal modes were obtained, agreeing with [20, 21].

In Schwarzschild-AdS, such exact solutions cannot be found. Moreover, the Proca field scalar-type degrees of freedom do not trivially decouple. We showed, however, that these can be distinguished in the massless limit, where the degree of freedom that becomes pure-gauge satisfies the Klein-Gordon field

equation and the degree of freedom that remains physical satisfies the scalar-type Maxwell field equation. The former degree of freedom was defined as having non-electromagnetic polarization, whereas the latter as having electromagnetic polarization. Although an exact solution for the modes could not be found, its stability was studied analytically using the S-deformation technique [13, 35]. Schwarzschild-AdS was proved to be stable against vector-type Proca and Maxwell field perturbations, scalar-type Maxwell field perturbations and monopole Proca field perturbations. Stability against higher multipoles of scalar-type Proca field perturbations could not be proved due to the non-hermitian nature of the mode coupling. The quasinormal mode frequency spectrum of Proca field perturbations in  $d = 4, 5, 6, 7$ -dimensional Schwarzschild-AdS spacetimes was obtained numerically with two different techniques: by using the Horowitz-Hubeny method and by integrating the equations of motion. The latter proved to be more reliable and allowed to study the small black hole regime, for which Horowitz-Hubeny method showed poor convergence properties. A summary of the main results from the numerical study goes as follows:

- Both the real and imaginary parts of the frequencies increase in magnitude as the mass of the field increases, in agreement with [42, 51].
- In the small-mass limit, scalar-type modes with electromagnetic and non-electromagnetic polarizations approach, respectively, scalar-type Maxwell field modes and scalar field modes, as expected.
- In the large black hole regime, most frequencies scale linearly with the black hole radius, as found in [30]. An exception was found for scalar-type Maxwell field perturbations in  $d \geq 5$  spacetimes, whose spectrum also seems to contain “special” purely imaginary modes that scale with the inverse of the black hole radius.
- Also for large black holes, Maxwell field scalar-type and vector-type modes were found to be isospectral. This was an unexpected result at first, as the associated potentials are different, even within this regime. Following [3], we managed to prove analytically this isospectrality. For Proca field perturbations, our numerical results suggest that the isospectrality is maintained for vector-type modes and electromagnetically polarized scalar-type modes. An analytical proof of this is however still missing.
- In the small black hole regime, the frequencies approach those of pure AdS. In particular, electromagnetically and non-electromagnetically polarized modes approach, respectively, the AdS modes with total angular momentum  $l - 1$  and  $l + 1$ .
- The numerical methods implemented only allowed to find modes up to the fourth overtone. However, in large Schwarzschild-AdS black holes, the behaviour of the spectrum in the asymptotically high overtone regime, studied in [20, 21, 62], is already captured by the lowest overtones, due to their linear scaling with the radius of the horizon. In particular, our numerical results for the  $k = 0, 1, 2, 3, 4$  modes of Maxwell field perturbations in large Schwarzschild-AdS black holes support the monodromy calculations of [21], although studies employing Leaver’s method of continued fractions [26] still need to be performed in order to confirm its analytical predictions. Moreover, the

small sample of overtones did not allow to accurately infer on the effect of the Proca field's mass on the spectrum in this limit, which gives another reason of why methods more capable to compute higher overtones should be implemented. It should be noted, however, that neither the mass of the field nor the perturbation-type should affect the asymptotic spectrum gap.

- In the eikonal limit, modes may become particularly long-lived. In the large black hole regime, our numerical results for Proca field perturbations agreed with the scalar field analytical predictions of [63] and therefore showed support for the universal  $l$ -dependence of the quasinormal modes, suggested in [64]. For small black holes, we found that the imaginary part of the modes decreases (in magnitude) exponentially with  $l$ , supporting [63–65].

Finally, we studied if Proca and Maxwell field quasinormal modes in small Schwarzschild-AdS black holes could be analytically described by matching the asymptotic solutions at the horizon and at infinity in an overlap region, which is formed in the long-wavelength approximation. It turned out that this method is quite restrictive, as the solutions only have the same functional form in the overlap region if both  $d$  is even and  $2l/(d-3)$  is non-integer: otherwise, non-common logarithmic dependences appear in the solutions that do not allow such matching. We showed that quasinormal mode frequencies in small Schwarzschild-AdS black holes exhibit an additional imaginary correction term in comparison to normal modes in AdS spacetime, i.e.  $\omega = \omega_{\text{AdS}} + i\delta$ , with  $|\delta| \ll |\omega_{\text{AdS}}|$  and  $\delta < 0$ . The  $\delta$  dependence with  $r_h$  was found to be  $\delta \sim (r_h/L)^{2l+d-2}$ , in agreement with [65, 74]. Also, for the allowed cases, analytical and numerical results agreed up to the fourth significant figure, although further numerical support is needed, using, for example, the Breit-Wigner resonance method of [39, 65]. Additionally, we could not use this method to describe the scalar-type sector of higher Proca multipoles, as the two scalar-type degrees of freedom remain non-trivially coupled, even within this approximation.

## 5.2 Future Work

A natural extension of our work involves attempting to analytically decouple the Proca field scalar-type degrees of freedom in Schwarzschild-AdS. One possible solution is to use the FKKS ansatz of [48] for Kerr-NUT-(A)dS geometries, after setting the black hole angular momentum and NUT parameter to zero. [51] did this for 4-dimensional Schwarzschild-AdS and showed that, although the FKKS ansatz decouples the scalar-type sector, it does not capture the vector-type mode. Yet, this is a great breakthrough, as the vector-type mode is decoupled and can be described using the spherical harmonic expansion. Is the FKKS ansatz capable to decouple the scalar-type modes in higher dimensions as well? This is definitely worth pursuing, since such decoupling would not only allow to approach analytically Schwarzschild-AdS stability against higher multipoles of scalar-type Proca perturbations, but also to obtain improved numerical results for the scalar-type quasinormal modes.

Additionally, implementing Leaver's method of continued fractions [26] in our study is of great interest: on the one hand, it would in principle allow to obtain the high overtone limit of the spectrum and compare it with the analytical results of [21]. Besides, this would also numerically establish the effect, if any, of

the field's mass on the asymptotic spectrum. On the other hand, it would be important to confirm the existence of the “special” purely imaginary modes found for scalar-type Maxwell perturbations, which scale with the inverse of the black hole radius. Also, it would be interesting to analytically establish isospectrality between vector-type and electromagnetically polarized scalar-type modes, suggested by our numerical results, as such could hint for a decoupling in the scalar-type sector.

The eikonal limit in asymptotically AdS spacetimes needs further studies as well. Can the “quasinormal mode/circular null geodesics correspondence” be extended to perturbed spacetimes whose potential diverges at infinity? The answer to this question remains elusive and it could provide physical insight on the quasinormal spectrum in this limit, as well as a possible way to decouple the scalar-type degrees of freedom of the Proca field.

Finally, it would also be interesting to verify our analytical expressions for quasinormal modes of small Schwarzschild-AdS black holes with a numerical method better adapted to this regime, such as the Breit-Wigner resonance method discussed in [39, 65]. Furthermore, extending our analytical results to odd dimensional spacetimes is of great interest, in order to have a complete analytical picture of the spectrum in this regime.

# Bibliography

- [1] R. Penrose, “The Structure of Space-Time”, in *Battelle Rencontres 1967 Lectures in Mathematical Physics*, eds B. DeWitt, J. A. Wheeler, 121 (Benjamin, New York, 1968).
- [2] S. W. Hawking and G. F. R. Ellis, *The Large Scale Structure of Space-Time*, (Cambridge University Press, Cambridge, 1973).
- [3] S. Chandrasekhar, *The Mathematical Theory of Black Holes*, (Oxford University Press, New York, 1983).
- [4] LIGO Scientific Collaboration and Virgo Collaboration, “Observation of gravitational waves from a binary black hole merger”, *Phys. Rev. Lett.* **116**, 061102 (2016); arXiv:1602.03837 [gr-qc].
- [5] The Event Horizon Telescope Collaboration, “First M87 Event Horizon Telescope results. I. The shadow of the supermassive black hole”, *Ap. J.* **875**, L1 (2019); arXiv:1906.11238 [astro-ph.GA].
- [6] C. V. Vishveshwara, “Stability of the Schwarzschild metric”, *Phys. Rev. D* **1**, 2870 (1970).
- [7] C. V. Vishveshwara, “Scattering of gravitational radiation by a Schwarzschild black hole”, *Nature* **227**, 936 (1970).
- [8] B. Carter, “Axisymmetric black hole has only two degrees of freedom”, *Phys. Rev. Lett.* **26**, 331 (1971).
- [9] R. A. Matzner, “Scattering of massless scalar waves by a Schwarzschild singularity”, *J. Math Phys.* **9**, 163 (1968).
- [10] T. Regge and J. A. Wheeler, “Stability of a Schwarzschild singularity”, *Phys. Rev.* **108**, 1063 (1957).
- [11] F. J. Zerilli, “Effective potential for even-parity Regge-Wheeler gravitational perturbation equations”, *Phys. Rev. Lett.* **24**, 737 (1970).
- [12] H. Kodama and A. Ishibashi, “A master equation for gravitational perturbations of maximally symmetric black holes in higher dimensions”, *Progress of Theoretical Physics* **110**, 701 (2003); arXiv:hep-th/0305147.
- [13] H. Kodama and A. Ishibashi, “Stability of higher-dimensional Schwarzschild black holes”, *Progress of Theoretical Physics* **110**, 901 (2003); arXiv:hep-th/0305185.

- [14] H. Kodama and A. Ishibashi, “Master equations for perturbations of generalised static black holes with charge in higher dimensions”, *Progress of Theoretical Physics* **111**, 24 (2004); arXiv:hep-th/0308128v4.
- [15] H. Kodama and M. Sasaki, “Cosmological perturbation theory”, *Progress of Theoretical Physics Supplement* **78**, 1 (1984).
- [16] E. Calabi and L. Markus, “Relativistic space forms”, *Annals of Mathematics* **75**, 63 (1962).
- [17] S. J. Avis, C. J. Isham, and D. Storey, “Quantum field theory in anti-de Sitter space-time”, *Phys. Rev. D* **18**, 3565 (1978).
- [18] C. P. Burgess and C. A. Lütken, “Propagators and effective potentials in anti-de Sitter space”, *Physics Letters B* **153**, 137 (1985).
- [19] A. Ishibashi and R. M. Wald, “Dynamics in non-globally-hyperbolic static spacetimes iii: anti-de Sitter spacetime”, *Class. Quant. Grav.* **21**, 2981 (2004); arXiv:hep-th/0402184.
- [20] J. Natario and R. Schiappa, “On the classification of asymptotic quasinormal frequencies for d-dimensional black holes and quantum gravity”, *Adv. Theor. Math. Phys.* **8**, 1001 (2004); arXiv:hep-th/0411267.
- [21] A. López-Ortega, “Electromagnetic quasinormal modes of D-dimensional black holes”, *Gen. Rel. Grav.* **38**, 1747 (2006); arXiv:gr-qc/0605034.
- [22] J. Maldacena, “The large-N limit of superconformal field theories and supergravity”, *International Journal of Theoretical Physics* **38**, 1113 (1999); arXiv:hep-th/9711200.
- [23] P. K. Kovtun, D. T. Son, and A. O. Starinets, “Viscosity in strongly interacting quantum field theories from black hole physics”, *Phys. Rev. Lett.* **94**, 111601 (2005); arXiv:hep-th/0405231.
- [24] S. S. Gubser and I. Mitra, “The evolution of unstable black holes in anti-de Sitter space”, *JHEP* **08**, 018 (2001); arXiv:hep-th/0011127.
- [25] S. Chandrasekhar and S. Detweiler, “The quasi-normal modes of the Schwarzschild black hole”, *Proceedings of the Royal Society of London. Series A, Mathematical and Physical Sciences* **344**, 441 (1975).
- [26] E. W. Leaver, “An analytic representation for the quasi-normal modes of Kerr black holes”, *Proceedings of the Royal Society of London. Series A, Mathematical and Physical Sciences* **402**, 285 (1985).
- [27] H.-P. Nollert, “Quasinormal modes of Schwarzschild black holes: the determination of quasinormal frequencies with very large imaginary parts”, *Phys. Rev. D* **47**, 5253 (1993).
- [28] J. S. F. Chan and R. B. Mann, “Scalar wave falloff in asymptotically anti-de Sitter backgrounds”, *Phys. Rev. D* **55**, 7546 (1997); arXiv:gr-qc/9612026.

- [29] H.-P. Nollert, “Quasinormal modes: the characteristic ‘sound’ of black holes and neutron stars”, *Class. Quantum Grav.* **16**, R159 (1999).
- [30] G. T. Horowitz and V. E. Hubeny, “Quasinormal modes of AdS black holes and the approach to thermal equilibrium”, *Phys. Rev. D* **62**, 024027 (2000); arXiv:hep-th/9909056.
- [31] V. Cardoso and J. P. S. Lemos, “Scalar, electromagnetic and Weyl perturbations of BTZ black holes: quasi normal modes”, *Phys. Rev. D* **63**, 12401 (2001); arXiv:gr-qc/0101052.
- [32] V. Cardoso and J. P. S. Lemos, “Quasi-normal modes of Schwarzschild anti-de Sitter black holes: electromagnetic and gravitational perturbations”, *Phys. Rev. D* **64**, 084017 (2001); arXiv:gr-qc/0105103.
- [33] R. A. Konoplya, “On quasinormal modes of small Schwarzschild-anti-de-Sitter black hole”, *Phys. Rev. D* **66**, 044009 (2002); arXiv:hep-th/0205142.
- [34] V. Cardoso, J. P. S. Lemos, and R. A. Konoplya, “Quasinormal frequencies of Schwarzschild black holes in anti-de Sitter spacetimes: a complete study on the asymptotic behavior”, *Phys. Rev. D* **68**, 044024 (2003); arXiv:gr-qc/0305037.
- [35] A. Zhidenko, “Linear Perturbations of Black Holes: Stability, Quasi-normal Modes and Tails”, PhD thesis, IFUSP, Sao Paulo (2009); arXiv:0903.3555 [gr-qc].
- [36] E. Berti, V. Cardoso, and A. O. Starinets, “Quasinormal modes of black holes and black branes”, *Class. Quantum Grav.* **26**, 163001 (2009); arXiv:0905.2975 [gr-qc].
- [37] R. A. Konoplya and A. Zhidenko, “Quasinormal modes of black holes: from astrophysics to string theory”, *Rev. Mod. Phys.* **83**, 793 (2011); arXiv:1102.4014 [gr-qc].
- [38] A. Flachi and J. P. S. Lemos, “Quasinormal modes of regular black holes”, *Phys. Rev. D* **87**, 024034 (2013); arXiv:1211.6212 [gr-qc].
- [39] P. Pani, “Advanced methods in black-hole perturbation theory”, *International Journal of Modern Physics A* **28**, 1340018 (2013); arXiv:1305.6759 [gr-qc].
- [40] D.V. Gal'tsov, G.V. Pomerantseva, and G.A. Chizhov, “Behavior of massive vector particles in a Schwarzschild field”, *Sov. Phys. J.* **27**, 697 (1984).
- [41] A. Pawl, “Time scale for loss of massive vector hair by a black hole and its consequences for proton decay”, *Phys. Rev. D* **70**, 124005 (2004); arXiv:hep-th/0411175.
- [42] R. A. Konoplya, “Massive vector field perturbations in the Schwarzschild background: stability and quasinormal spectrum”, *Phys. Rev. D* **73**, 024009 (2006); arXiv:gr-qc/0509026.
- [43] R. A. Konoplya, C. Molina, and A. Zhidenko, “Late time tails of the massive vector field in a black hole background”, *Phys. Rev. D* **75**, 084004 (2007); arXiv:gr-qc/0602047.

- [44] J. G. Rosa and S. R. Dolan, “Massive vector fields on the Schwarzschild spacetime: quasinormal modes and bound states”, *Phys. Rev. D* **85**, 044043 (2012); arXiv:1110.4494 [hep-th].
- [45] T. V. Fernandes, D. Hilditch, J. P. S. Lemos, and V. Cardoso, “Normal modes of Proca fields in AdS spacetime”, *Gen. Relativ. Gravit.* **55**, 5 (2023); arXiv:2301.10248 [gr-qc].
- [46] C. Herdeiro, M. O. P. Sampaio, and M. Wang, “Hawking radiation for a Proca field in D-dimensions”, *Phys. Rev. D* **85**, 024005 (2012); arXiv:1110.2485 [gr-qc].
- [47] K. Ueda and A. Ishibashi, “Massive vector field perturbations on extremal and near-extremal static black holes”, *Phys. Rev. D* **97**, 124050 (2018); arXiv:1805.02479 [gr-qc].
- [48] V. P. Frolov, P. Krtouš, D. Kubizňák, and J. E. Santos, “Massive vector fields in rotating black-hole spacetimes: separability and quasinormal modes”, *Phys. Rev. Lett.* **120**, 231103 (2018); arXiv:1804.00030 [hep-th].
- [49] V. Cardoso, Ó. J. C. Dias, G. S. Hartnett, M. Middleton, P. Pani, and J. E. Santos, “Constraining the mass of dark photons and axionlike particles through black-hole superradiance”, *JCAP* **1803**, 043 (2018); arXiv:1801.01420 [gr-qc].
- [50] J. Percival and S. R. Dolan, “Quasinormal modes of massive vector fields on the Kerr spacetime”, *Phys. Rev. D* **102**, 104055 (2020); arXiv:2008.10621 [gr-qc].
- [51] T. V. Fernandes, D. Hilditch, J. P. S. Lemos, and V. Cardoso, “Quasinormal modes of Proca fields in a Schwarzschild-AdS spacetime”, *Phys. Rev. D* **105**, 044017 (2022); arXiv:2112.03282 [gr-qc].
- [52] M. Wang, “Quantum and Classical Aspects of Scalar and Vector Fields Around Black Holes”, PhD thesis, Universidade de Aveiro (2016); arXiv:1606.00811 [gr-qc].
- [53] T. V. Fernandes, “Vector Fields and Black Holes”, MSc thesis, Instituto Superior Técnico (2020).
- [54] M. Wang, C. Herdeiro, and M. O. Sampaio, “Maxwell perturbations on asymptotically anti-de Sitter spacetimes: generic boundary conditions and a new branch of quasinormal modes”, *Phys. Rev. D* **92**, 124006 (2015); arXiv:1510.04713 [gr-qc].
- [55] C. Chen, H. Cho, and A. S. Cornell, “A new (original) set of quasi-normal modes in spherically symmetric AdS black hole spacetimes”, *Chinese Journal of Physics* **67**, 646 (2020); arXiv:2004.05806 [gr-qc].
- [56] T. Delsate, V. Cardoso, and P. Pani, “Anti de Sitter black holes and branes in dynamical Chern-Simons gravity: perturbations, stability and the hydrodynamic modes”, *J. High Energy Phys.* **06**, 055 (2011); arXiv:1103.5756[hep-th].
- [57] A. Rostworowski, “Quasinormal frequencies of D-dimensional Schwarzschild black holes: evaluation via continued fraction method”, *ActaPhys. Polon. B* **38**, 81 (2007); arXiv:gr-qc/0606110.
- [58] R. A. Konoplya and A. Zhidenko, “Stability of higher dimensional Reissner-Nordström-anti-de Sitter black holes”, *Phys. Rev. D* **78**, 104017 (2008); arXiv:0809.2048 [hep-th].

- [59] E. Berti and K.D. Kokkotas, “Quasinormal modes of Reissner-Nordström-anti-de Sitter black holes: scalar, electromagnetic and gravitational perturbations”, *Phys. Rev. D* **67**, 064020 (2003); arXiv:gr-qc/0301052.
- [60] G. Siopsis, “Low frequency quasi-normal modes of AdS black holes”, *JHEP* **05**, 042 (2007); arXiv:hep-th/0702079.
- [61] S. Hod, “Bohr’s correspondence principle and the area spectrum of quantum black holes”, *Phys. Rev. Lett.* **81**, 4293 (1998); arXiv:gr-qc/9812002.
- [62] S. Musiri, S. Ness, and G. Siopsis, “Perturbative calculation of quasi-normal modes of AdS Schwarzschild black holes”, *Phys. Rev. D* **73**, 064001 (2006); arXiv:hep-th/0511113.
- [63] G. Festuccia and H. Liu, “A Bohr-Sommerfeld quantization formula for quasinormal frequencies of AdS black holes”, *Advanced Science Letters* **2**, 221 (2009); arXiv:0811.1033 [gr-qc].
- [64] J. Morgan, V. Cardoso, A. S. Miranda, C. Molina, and V. T. Zanchin, “Quasinormal modes of black holes in anti-de Sitter space: a numerical study of the eikonal limit”, *Phys. Rev. D* **80**, 024024 (2009); arXiv:0906.0064 [hep-th].
- [65] E. Berti, V. Cardoso, and P. Pani, “Breit-Wigner resonances and the quasinormal modes of anti-de Sitter black holes”, *Phys. Rev. D* **79**, 101501 (2009); arXiv:0903.5311 [gr-qc].
- [66] V. Cardoso, A. S. Miranda, E. Berti, H. Witek, and V. T. Zanchin, “Geodesic stability, Lyapunov exponents and quasinormal modes”, *Phys. Rev. D* **79**, 064016 (2009); arXiv:0812.1806 [hep-th].
- [67] R. A. Konoplya, “Further clarification on quasinormal modes/circular null geodesics correspondence”, *Physics Letters B* **838**, 137674 (2023); arXiv:2210.08373 [gr-qc].
- [68] K. Glampedakis and H. O. Silva, “Eikonal quasinormal modes of black holes beyond general relativity”, *Phys. Rev. D* **100**, 044040 (2019); arXiv:1906.05455 [gr-qc].
- [69] H. Furuhashi and Y. Nambu, “Instability of massive scalar fields in Kerr-Newman spacetime”, *Progress of Theoretical Physics* **112**, 983 (2004); arXiv:gr-qc/0402037.
- [70] V. Cardoso and Ó. J. C. Dias, “Small Kerr-anti-de Sitter black holes are unstable”, *Phys. Rev. D* **70**, 084011 (2004); arXiv:hep-th/0405006.
- [71] V. Cardoso, Ó. J. C. Dias, and S. Yoshida, “Classical instability of Kerr-AdS black holes and the issue of final state”, *Phys. Rev. D* **74**, 044008 (2006); arXiv:hep-th/0607162.
- [72] J. G. Rosa, “The extremal black hole bomb”, *JHEP* **06**, 015 (2010); arXiv:0912.1780 [hep-th].
- [73] M. Wang and C. Herdeiro, “Superradiant instabilities in a D-dimensional small Reissner-Nordström-anti-de Sitter black hole”, *Phys. Rev. D* **89**, 084062 (2014); arXiv:1403.5160 [gr-qc].
- [74] M. Wang, C. Herdeiro, and J. Jing, “Dirac perturbations on Schwarzschild-anti-de Sitter spacetimes: generic boundary conditions and new quasinormal modes”, *Phys. Rev. D* **96**, 104035 (2017); arXiv:1710.10461 [gr-qc].

- [75] A. Chodos and E. Myers, “Gravitational contribution to the Casimir energy in Kaluza-Klein theories”, *Annals of Physics* **156**, 412 (1984).
- [76] A. Higuchi, “Symmetric tensor spherical harmonics on the N-sphere and their application to the de Sitter group  $SO(N,1)$ ”, *J. Math. Phys.* **28**, 1553 (1987).
- [77] P. van Nieuwenhuizen, “The compactification of IIB supergravity on  $S_5$  revisited”, in *Strings, Gauge Fields, and the Geometry Behind: The legacy of Maximilian Kreuzer*, 133 (2012); arXiv:1206.2667 [hep-th].
- [78] L. Hui, A. Joyce, R. Penco, L. Santoni, and A. R. Solomon, “Static response and Love numbers of Schwarzschild black holes”, *JCAP* **04**, 052 (2021); arXiv:2010.00593 [hep-th].
- [79] M. Abramowitz and I. A. Stegun, *Handbook of Mathematical Functions with Formulas, Graphs, and Mathematical Tables*, (Dover, New York, 1964).

# Appendix A

## Spherical harmonics on the $n$ -sphere

### A.1 Initial considerations

The decomposition in spherical harmonics explores the rotational invariance of the background and is crucial to study the structure of the perturbations and to isolate the physical degrees of freedom of the fields. Here, we discuss in more detail the properties of these functions. For more details we refer to [14, 75–78]. Spherical harmonics on the  $n$ -sphere can be constructed recursively by dimensional reduction (see e.g.[76]). However, this approach becomes cumbersome when constructing vector spherical harmonics. The approach we adopt here follows [75], where spherical harmonics are constructed by embedding  $\mathcal{S}^n$  in  $(n + 1)$ -Euclidean space,  $\mathbb{R}^{n+1}$ . Within this framework, spherical harmonics on  $\mathcal{S}^n$  are harmonic homogeneous polynomials in  $\mathbb{R}^{n+1}$  restricted to  $\mathcal{S}^n$ .

Let  $\mathcal{H}_l$  be the space of homogeneous polynomials of degree  $l$  in  $\mathbb{R}^{n+1}$ . A polynomial  $h_l : \mathbb{R}^{n+1} \rightarrow \mathbb{C}$  belongs to  $\mathcal{H}_l$  if

$$h_l(\lambda \mathbf{x}) = \lambda^l h_l(\mathbf{x}) \quad , \quad (\text{A.1})$$

for any  $\lambda \in \mathbb{R}, \mathbf{x} \in \mathbb{R}^{n+1}$ . Furthermore, a polynomial is harmonic in  $\mathbb{R}^{n+1}$  if

$$\square_E h = 0 \quad , \quad (\text{A.2})$$

where  $\square_E$  is the laplacian in  $\mathbb{R}^{n+1}$ . The space of homogeneous and harmonic polynomials of degree  $l$  in  $\mathbb{R}^{n+1}$  is denoted  $\mathcal{A}_l$ . Then, spherical harmonics are defined as functions  $Y : \mathcal{S}^n \rightarrow \mathbb{C}$  such that, for some  $h_l \in \mathcal{A}_l$ ,  $Y_l(\boldsymbol{\eta}) = h_l(\boldsymbol{\eta})$  for all  $\boldsymbol{\eta} \in \mathcal{S}^n$ .

### A.2 Scalar spherical harmonics

In spherical coordinates, the  $\mathbb{R}^{n+1}$  line element,  $ds^2 = g_{\mu\nu} dx^\mu dx^\nu$ , is related to the  $\mathcal{S}^n$  line element,  $d\Omega_n^2 = \gamma_{ij} d\theta^i d\theta^j$ , by

$$ds^2 = dr^2 + r^2 d\Omega_n^2 \quad . \quad (\text{A.3})$$

Using Eq. (2.13), the non-vanishing Christoffel symbols associated to  $(\mathbb{R}^{n+1}, g)$  in these coordinates are

$$\Gamma_{ij}^r = -r\gamma_{ij} \quad , \quad \Gamma_{rj}^i = \frac{1}{r}\delta_j^i \quad , \quad \Gamma_{jk}^i = \hat{\Gamma}_{jk}^i, \quad (\text{A.4})$$

and the condition for a homogeneous polynomial of degree  $l$ ,  $h_l$ , to be harmonic in  $\mathbb{R}^{n+1}$  reads

$$\square_E h_l = \frac{1}{r^n} \partial_r (r^n \partial_r h_l) + \frac{1}{r^2} \hat{\square} h_l = 0 \quad , \quad (\text{A.5})$$

where  $\hat{\square} = \gamma^{ij} \hat{\nabla}_i \hat{\nabla}_j$ . Moreover, the homogeneity condition yields, with  $x^\mu = r \hat{x}^\mu$ ,

$$h_l(x^\mu)|_{\mathcal{S}^n} = h_l(r \hat{x}^\mu)|_{\mathcal{S}^n} = r^l h_l(\hat{x}^\mu)|_{\mathcal{S}^n} = r^l \mathbb{S}_l(\theta^i) \quad , \quad (\text{A.6})$$

so that, substituting in Eq. (A.5), one has

$$\hat{\square} \mathbb{S}_l = -l(l+n-1) \mathbb{S}_l \quad , \quad l = 0, 1, 2, \dots \quad (\text{A.7})$$

$\mathbb{S}_{(l)}$  are thus eigenvectors of the operator  $\hat{\square}$ , designated scalar spherical harmonics. These can be further expanded in the basis  $\vec{k}_s$ , containing  $l$  and the  $n-1$  azimuthal quantum numbers,  $l_i$ , corresponding to the eigenvalues of the respective lower-dimensional embedded spheres, and in turn satisfying  $|l_1| \leq l_2 \leq \dots \leq l_{n-1} \leq l$ . We then refer to the *non-degenerate* scalar spherical harmonics as  $\mathbb{S}_{\vec{k}_s}$ , obeying the eigenvalue equation

$$\hat{\square} \mathbb{S}_{\vec{k}_s} = -l(l+n-1) \mathbb{S}_{\vec{k}_s} \quad , \quad l = 0, 1, 2, \dots \quad , \quad (\text{A.8})$$

as well as the orthogonality condition on  $\mathcal{S}^n$

$$\int d\Omega_n \mathbb{S}_{\vec{k}_s} \mathbb{S}_{\vec{k}'_s}^* = \delta_{\vec{k}_s \vec{k}'_s} \quad , \quad (\text{A.9})$$

and forming a complete basis on  $\mathcal{S}^n$ .

### A.3 Vector spherical harmonics

Vector spherical harmonics can be constructed in the same way as scalar spherical harmonics, only this time one considers polynomials on  $\mathbb{R}^{n+1}$  as vector functions  $V_\mu^l : \mathbb{R}^{n+1} \rightarrow \mathbb{C}^{n+1}$ . Using the Helmholtz-Hodge theorem,  $V_\mu^l$  can be written (in analogy to Eq. (2.17)) as

$$V_\mu^l dx^\mu = V_r^l dr + (W_i^l + \hat{\nabla}_i \sigma^l) d\theta^i \quad , \quad \hat{\nabla}^i W_i^l = 0 \quad , \quad (\text{A.10})$$

where  $W_i^l$  is a vector on the  $n$ -sphere and  $V_r^l, \sigma^l$  are scalars. Expanding  $\square_E V_\mu^l$  in spherical coordinates, and assuming that  $h_\mu$  is harmonic, one has

$$\square_E W_i^l = \partial_r^2 W_i^l + \frac{n-2}{r} \partial_r W_i^l - \frac{n-1}{r^2} W_i^l + \frac{1}{r^2} \hat{\square} W_i^l = 0 \quad , \quad (\text{A.11})$$

as well as two coupled equations for the scalars  $h_r$  and  $\sigma$  [75], which yield the eigenvalue equations for scalar harmonics. Here, we are interested in the eigenvalue equation for  $W_i^l$ , that is, for vector harmonics. Since  $V_\mu^l$  is homogeneous of degree  $l$  in  $\mathbb{R}^{n+1}$ , then

$$W_i^l(x^\nu)|_{S^n} \sim r^{l+1} \mathbb{V}_i^l(\theta^j) \quad , \quad (\text{A.12})$$

where the extra  $r$  factor appears due to the Jacobian matrix of the transformation to polar coordinates. Finally, substituting Eq. (A.12) in Eq. (A.11) yields

$$\hat{\square} \mathbb{V}_i^l = -[l(l+n-1) - 1] \mathbb{V}_i^l \quad , \quad l = 1, 2, \dots \quad , \quad (\text{A.13})$$

which is the eigenvalue equation for vector spherical harmonics. Note that now  $l \geq 1$ , as for  $l = 0$  there are no non-trivial  $\mathbb{V}_i^l$  satisfying Eq. (A.11) [75].  $\mathbb{V}_i^l$  are usually called transverse vector spherical harmonics, as they obey the transverse condition  $\hat{\nabla}^i \mathbb{V}_i^l = 0$ . One can also construct longitudinal vector spherical harmonics, which are defined as the gradient of scalar spherical harmonics,  $\hat{\nabla}_i S^l$ , obeying the eigenvalue equation

$$\hat{\square} (\hat{\nabla}_i S^l) = -[l(l+n-1) - (n-1)] \hat{\nabla}_i S^l \quad , \quad l = 1, 2, \dots \quad . \quad (\text{A.14})$$

While the number of independent harmonics  $\hat{\nabla}_i S^l$  is the same as the number of scalar harmonics  $S^l$ , the number of  $\mathbb{V}_i^l$  is different [75], meaning that the basis used to expand  $S^l$  cannot be used to expand  $\mathbb{V}_i^l$ . The basis used to expand  $\mathbb{V}_i^l$  will be denoted  $\vec{k}_v$ , containing  $l$  and the  $n-1$  azimuthal numbers, which now cover a different range than the one covered by  $\vec{k}_s$ . As for scalar harmonics, vector spherical harmonics obey the orthogonality relation

$$\int d\Omega_n \gamma^{ij} \mathbb{V}_{\vec{k}_v i} \mathbb{V}_{\vec{k}'_v j}^* = \delta_{\vec{k}_v \vec{k}'_v} \quad , \quad (\text{A.15})$$

and form a complete basis on  $S^n$ .

## A.4 Properties under rotation and parity transformations

The action of the  $SO(n+1)$  Casimir operator,  $\hat{J}^2$ , on scalar and vector spherical harmonics is [19]

$$\hat{J}^2 S^l = l(l+n-1) S^l \quad , \quad \hat{J}^2 \hat{\nabla}_i S^l = l(l+n-1) \hat{\nabla}_i S^l \quad , \quad \hat{J}^2 \mathbb{V}_i^l = [l(l+n-1) + n-2] \mathbb{V}_i^l \quad . \quad (\text{A.16})$$

For  $l \geq 1$  and  $n > 2$ , the Casimir eigenvalues of both scalar spherical harmonics and longitudinal vector spherical harmonics are the same. One then expects these modes to mix. On the other hand, the Casimir eigenvalues of the transverse vector spherical harmonics are never equal ( $n > 2$ ) to the eigenvalues of the longitudinal vector spherical harmonics, so that these completely decouple. For  $n = 2$ , these are equal and one would expect to have mixed modes. However, in this case, the modes are decoupled due to their different parity eigenvalues. Under parity transformations  $\theta_{i=1} \rightarrow \pi + \theta_{i=1}$  and  $\theta_{i \neq 1} \rightarrow \pi - \theta_{i \neq 1}$ , one has

$$\hat{P}S^l = (-1)^l S^l, \quad \hat{P}\hat{\nabla}_i S^l = (-1)^l \hat{\nabla}_i S^l, \quad \hat{P}\mathbb{V}_i^l = (-1)^{l+1} \mathbb{V}_i^l. \quad (\text{A.17})$$

(Note that a vector,  $A_{\theta_i}$ , on the  $n$ -sphere transforms under parity as:  $A_{\theta_{i=1}} \rightarrow A_{\theta_{i=1}}, A_{\theta_{i \neq 1}} \rightarrow -A_{\theta_{i \neq 1}}$ ). Thus, the scalar-type sector is also referred to as the even- or polar-sector, while the vector-type sector is referred as the odd- or axial-sector.

## Appendix B

# Hypergeometric differential equation

### B.1 Main properties

The equations of motion ruling the dynamics of the perturbation variables are often second-order ordinary differential equations with three regular singular points. It follows then that they can be transformed by an appropriate change of variables into the hypergeometric differential equation, which takes the form

$$z(1-z)\frac{d^2\Psi}{dz^2} + [c - (a+b+1)z]\frac{d\Psi}{dz} - ab\Psi = 0 \quad , \quad (\text{B.1})$$

where  $a, b, c$  are parameters that depend on the background geometry and type of perturbation. The regular singular points of the equation are located at  $z = 0, 1, \infty$ . Solutions of Eq. (B.1) are found by using Frobenius method near each of these regular points. In the main text, the solution is expanded near  $z = 0$  and the region of interest is  $0 < z < 1$  (note that it coincides with the radius of convergence of the solution near  $z = 0$ ). The behaviour near  $z = 1$  can be easily obtained by applying the linear transformation relation  $z \rightarrow 1 - z$  (which we describe below) to the solution near  $z = 0$ . The solution of Eq. (B.1) near  $z = 0$  can be written in terms of the hypergeometric functions  $F_1[a, b, c; z]$ , for non-integer  $c$ , as [79]

$$\Psi(z) = AF_1[a, b, c; z] + Bz^{1-c}F_1[a - c + 1, b - c + 1, 2 - c; z] \quad , \quad (\text{B.2})$$

where  $A, B$  are constants of integration. On the other hand, if  $c$  is integer and  $c > 1$  one has [79]

$$\begin{aligned} \Psi(z) = & AF_1[a, b, c; z] + \\ & + B \left[ F_1[a, b, c; z] \log(z) + \right. \\ & + \sum_{i=1}^{\infty} \frac{(a)_i (b)_i}{(c)_i i!} z^i (\psi(a+i) - \psi(a) + \psi(b+i) - \psi(b) - \psi(c+i) + \psi(c) - \psi(i+1) + \psi(1)) - \\ & \left. - \sum_{i=1}^{c-1} \frac{(i-1)!(1-c)_i}{(1-a)_i (1-b)_i} z^{-i} \right] \quad , \end{aligned} \quad (\text{B.3})$$

where  $(x)_i$  and  $\psi(z)$  are, respectively, the Pochhammer symbol and the digamma function, defined as

$$(x)_i \equiv \frac{\Gamma(x+i)}{\Gamma(x)} \quad , \quad \psi(z) = \frac{\Gamma'(z)}{\Gamma(z)} \quad . \quad (\text{B.4})$$

Similar relations can be found for integer  $c < 1$  [79]. To study how the solutions behave near  $z = 1$ , it is useful to introduce the transformation  $z \rightarrow 1 - z$  of the hypergeometric function. For non-integer  $c - a - b$ , one has [79]

$$F_1[a, b, c; z] = \frac{\Gamma(c)\Gamma(c-a-b)}{\Gamma(c-a)\Gamma(c-b)} F_1[a, b, 1+a+b-c; 1-z] + (1-z)^{c-a-b} \frac{\Gamma(c)\Gamma(a+b-c)}{\Gamma(a)\Gamma(b)} F_1[c-a, c-b, 1+c-a-b; 1-z] \quad , \quad (\text{B.5})$$

whereas if  $c - a - b = -m$  with  $m = 1, 2, \dots$

$$F_1[a, b, a+b-m; z] = \frac{\Gamma[m]\Gamma[a+b-m]}{\Gamma[a]\Gamma[b]} (1-z)^{-m} \sum_{i=0}^{m-1} \frac{(a-m)_i (b-m)_i}{i!(1-m)_i} (1-z)^i - \frac{(-1)^m \Gamma[a+b-m]}{\Gamma[a-m]\Gamma[b-m]} \sum_{i=0}^{\infty} \frac{(a)_i (b)_i}{i!(i+m)!} (1-z)^i (\log(1-z) - \psi(i+1) - \psi(i+m+1) + \psi(a+i) + \psi(b+i)) \quad . \quad (\text{B.6})$$

For  $c - a - b = \tilde{m}$  with  $\tilde{m} = 0, 1, 2, \dots$  one can find similar transformation rules [79], although we usually choose the parameters so that, without loss of generality,  $c - a - b < 0$ .

## B.2 Normal modes in pure AdS

### B.2.1 Proca field and vector-type Maxwell field perturbations

Equation (3.13) in the main text is of the type

$$\partial_{r_*}^2 q_{(i)} + \left( \omega_{(i)}^2 - \frac{k_1^{(i)}}{\sin^2\left(\frac{r_*}{L}\right)} - \frac{k_2}{\cos^2\left(\frac{r_*}{L}\right)} \right) q_{(i)} = 0 \quad , \quad (\text{B.7})$$

where  $k_1^{(i)} = [4j_{(i)}(j_{(i)} + n - 1) + (n - 2)n] / 4L^2$  and  $k_2 = [(n - 2)n + 4\mu^2 L^2] / 4L^2$ , with  $j_{(i)}$  taking the values  $l - 1, l, l + 1$ , for  $l \geq 1$ . By making the change

$$q_{(i)}(z) = z^{\alpha_{(i)}} (1-z)^{\beta} \Psi_{(i)}(z) \quad , \quad (\text{B.8})$$

with  $z = \sin^2\left(\frac{r_*}{L}\right)$ , one can transform Eq. (B.7) into the hypergeometric differential equation Eq. (B.1) with  $a_{(i)} = \alpha_{(i)} + \beta + \frac{\omega_{(i)} L}{2}$ ,  $b_{(i)} = \alpha_{(i)} + \beta - \frac{\omega_{(i)} L}{2}$ ,  $c_{(i)} = 2\alpha_{(i)} + \frac{1}{2}$  and

$$\alpha_{(i)} = \frac{1}{4} \left[ 1 + \sqrt{1 + 4L^2 k_1^{(i)}} \right] = \frac{2j_{(i)} + n}{4} \quad , \quad \beta = \frac{1}{4} \left[ 1 + \sqrt{1 + 4L^2 k_2} \right] = \frac{1}{4} \left( 1 + \sqrt{(n-1)^2 + 4\mu^2 L^2} \right) \quad . \quad (\text{B.9})$$

Following the analysis of Section B.1, the solutions of Eq. (B.1) for even  $n$  ( $c_{(i)}$  is non-integer) are given by

$$\Psi_{(i)}^{(\text{even})}(z) = A_{(i)} F_1 [a_{(i)}, b_{(i)}, c_{(i)}; z] + B_{(i)} z^{1/2-2\alpha_{(i)}} F_1 [a_{(i)} - c_{(i)} + 1, b_{(i)} - c_{(i)} + 1, 2 - c_{(i)}; z] \quad , \quad (\text{B.10})$$

where  $A_{(i)}$  and  $B_{(i)}$  are constants of integration. Then

$$q_{(i)}^{(\text{even})}(z) = A_{(i)} z^{\alpha_{(i)}} (1-z)^\beta F_1 [a_{(i)}, b_{(i)}, c_{(i)}; z] + B_{(i)} z^{1/2-\alpha_{(i)}} (1-z)^\beta F_1 [a_{(i)} - c_{(i)} + 1, b_{(i)} - c_{(i)} + 1, 2 - c_{(i)}; z] \quad . \quad (\text{B.11})$$

On the other hand, for odd  $n$ ,  $c_{(i)}$  is a positive integer and it follows from Section B.1 that the solution for  $q_{(i)}(z)$  is given by Eq. (B.3), multiplied by  $z^{\alpha_{(i)}}(1-z)^\beta$ .

To obtain the normal modes, one needs to impose boundary conditions to the solutions. As stated in the main text, at  $r = 0$  ( $z = 0$ ) one imposes regularity, so that the solution does not diverge there. For even spacetimes, it is immediate to see from Eq. (B.11) that for  $\alpha_{(i)} > 1/2$  one needs to set  $B_{(i)} = 0$  ( $\lim_{z \rightarrow 0} F_1 [a, b, c; z] = 1$ ). When  $\alpha_{(i)} = 1/2$ , which only happens for the  $(-)$  scalar-type polarization in the  $l = 1, n = 2$  case, the exponent in  $z$  vanishes and the solution seems to be finite (and constant) near  $z = 0$ . However, this is just an artifact of having removed the origin when separating the field in spherical harmonics [19]. To see this clearly, one writes the components of the four-dimensional Proca field  $A_r, A_\theta$  and  $A_\varphi$  in terms of  $q_{(+)}, q_{(-)}$  and  $q_\phi$ , yielding

$$\begin{aligned} A_r &= \frac{1}{rf} \sum_{lm} \left( q_{(+)}^{(l,m)} + q_{(-)}^{(l,m)} \right) \mathbb{S}^{(l,m)} \quad , \\ A_\theta &= \sum_{l'm'} q_{(\phi)}^{(l',m')} V_\theta^{(l',m')} + \sum_{lm} \left( \frac{q_{(-)}^{(l,m)}}{l} - \frac{q_{(+)}^{(l,m)}}{l+n-1} \right) \partial_\theta \mathbb{S}^{(l,m)} \quad (\text{B.12}) \\ A_\varphi &= \sum_{l'm'} q_{(\phi)}^{(l',m')} V_\varphi^{(l',m')} + \sum_{lm} \left( \frac{q_{(-)}^{(l,m)}}{l} - \frac{q_{(+)}^{(l,m)}}{l+n-1} \right) \partial_\varphi \mathbb{S}^{(l,m)} \quad . \end{aligned}$$

Since, near the origin,  $q_{(\phi)}^{(l,m)} = q_{(+)}^{(l,m)} = 0$  for all  $l, m$  and  $q_{(-)}^{(l,m)} = K^{(l,m)}$  if  $l = 1$ ,  $q_{(-)}^{(l,m)} = 0$  otherwise, where  $K^{(1,1)}, K^{(1,0)}$  and  $K^{(1,-1)}$  are constants, Eq. (B.12) becomes, near the origin ( $f(r) \simeq 1$ )

$$\begin{aligned} A_r &\simeq \frac{1}{r} \left( K^{(1,1)} \mathbb{S}^{(1,1)} + K^{(1,0)} \mathbb{S}^{(1,0)} + K^{(1,-1)} \mathbb{S}^{(1,-1)} \right) \quad , \\ A_\theta &\simeq K^{(1,1)} \partial_\theta \mathbb{S}^{(1,1)} + K^{(1,0)} \partial_\theta \mathbb{S}^{(1,0)} + K^{(1,-1)} \partial_\theta \mathbb{S}^{(1,-1)} \quad , \\ A_\varphi &\simeq K^{(1,1)} \partial_\varphi \mathbb{S}^{(1,1)} + K^{(1,0)} \partial_\varphi \mathbb{S}^{(1,0)} + K^{(1,-1)} \partial_\varphi \mathbb{S}^{(1,-1)} \quad . \end{aligned} \quad (\text{B.13})$$

The components of a vector field transform as  $A_{\mu'} = \frac{\partial x^\mu}{\partial x^{\mu'}} A_\mu$  to give  $A_{x,y,z} \sim \frac{1}{\sqrt{x^2+y^2+z^2}}$ , in cartesian coordinates. Since the Proca field equations Eq. (2.8) can be written near the origin in cartesian coordinates as

$$\partial^\nu \partial_\nu A_\alpha - \mu^2 A_\alpha = 0 \quad , \quad (\text{B.14})$$

where  $\alpha = \{t, x, y, z\}$ , one has

$$(\partial_x^2 + \partial_y^2 + \partial_z^2) A_{x,y,z} \sim \delta(x)\delta(y)\delta(z) \quad . \quad (\text{B.15})$$

Due to this additional delta term,  $q_{(-)}^{(l,m)} = K^{(l,m)}$ , with  $K^{(l,m)} \neq 0$ , cannot be a solution near the origin and one needs to set  $B_{(-)} = 0$ . This proves that *all* the modes need to have  $B_{(i)} = 0$  to be regular near the origin.

On the other hand, for odd dimensional spacetimes, all the terms of Eq. (B.3) except the last one vanish in the limit  $z \rightarrow 0$ . Regarding the last term, it is guaranteed that it diverges, as the leading-order term is  $q_{(i)}^{(\text{odd})} \sim z^{1/2-\alpha(i)}$  and  $\alpha(i) > 1/2$ . Thus, one also needs to set  $B_{(i)} = 0$  in this case. To summarize: so far, we have shown that the solutions of Eq. (B.7) that are regular at the origin are given by

$$q_{(i)} = A_{(i)} z^{\alpha(i)} (1-z)^\beta F_1[a_{(i)}, b_{(i)}, c_{(i)}; z] \quad . \quad (\text{B.16})$$

As explained in the main text, the remaining boundary condition we impose is a Dirichlet boundary condition at spatial infinity ( $z = 1$ ). To do that, we use the transformation property  $z \rightarrow 1-z$  of the hypergeometric function, given in Eqs. (B.5) and (B.6). We firstly focus on non-integer  $c_{(i)} - a_{(i)} - b_{(i)} = 1/2 - 2\beta$ , where one uses Eq. (B.5) in Eq. (B.16) to analyze the behaviour at infinity. Since  $\beta > 1/2$ , the first term vanishes, as the gamma functions in the numerator are finite ( $c_{(i)} - a_{(i)} - b_{(i)}$  is non-integer and  $c_{(i)} > 0$ ). The remaining term must be 0 to satisfy the reflective boundary condition. This term is proportional to  $z^{1/2-\beta}$  and consequently explodes unless  $a_{(i)}$  or  $b_{(i)}$  are non-positive integers. The additional requirement that  $\omega > 0$  yields the result for the frequencies of the normal modes

$$\omega_{(i)} L = 2k + j_{(i)} + \frac{d-1}{2} + \frac{1}{2} \sqrt{(d-3)^2 + 4\mu^2 L^2} \quad , \quad k = 0, 1, 2, \dots \quad , \quad (\text{B.17})$$

whereas the normal mode eigenfunctions are given by

$$q_{(i)}(r) = A_{(i)} \left(\frac{r}{L}\right)^{\frac{2j_{(i)}+d-2}{2}} \left(1 + \frac{r^2}{L^2}\right)^{k - \frac{\omega_{(i)} L}{2}} F_1\left[-k + \omega_{(i)} L, -k, j_{(i)} + \frac{d-1}{2}; \frac{r^2/L^2}{1+r^2/L^2}\right] \quad . \quad (\text{B.18})$$

Similarly, when  $1/2 - 2\beta = -m$ , with  $m = 1, 2, \dots$ , the transformation law  $z \rightarrow 1-z$  to be used is Eq. (B.6). While the second term of the solution always vanishes when  $z \rightarrow 1$  (the leading-order term is  $\sim (1-z)^\beta \log(1-z)$  and note again that the gamma function in the numerator does not diverge), for the first term to vanish one again needs to impose  $a = -k$  or  $b = -k$ , where  $k$  is a non-positive integer, as there is always the term  $(1-z)^{1/2-\beta}$  in the sum. Thus, one also arrives at Eqs. (B.17) and (B.18).

## B.2.2 Scalar-type Maxwell field perturbations

For the scalar-type Maxwell perturbations,  $q_{(\text{EM})}$  also obeys Eq. (B.7), except now  $k_1$  and  $k_2$  are given after Eq. (3.18), so that  $\alpha = \frac{2l+n}{4}$  and  $\beta = \frac{1}{4}(1+|n-3|)$ . The solution to  $q_{(\text{EM})}$  is also given by Eq. (B.16) after imposing the regularity condition at the origin. However, the expression for  $\beta$  brings interesting consequences that do not appear in the massive case, and one needs to be careful when

obtaining the normal modes. For  $n > 3$  one has  $\beta = \frac{n-2}{4} \geq 1/2$ , so that Eq. (B.7) only obeys the reflective boundary condition at infinity if

$$\omega_{(\text{EM})}L = 2k + l + d - 3 \quad , \quad d > 5 \quad , \quad k = 0, 1, 2, \dots \quad . \quad (\text{B.19})$$

For  $d = 4$  one has

$$\omega_{(\text{EM})}L = 2k + l + 2 \quad , \quad d = 4 \quad , \quad k = 0, 1, 2, \dots \quad . \quad (\text{B.20})$$

For  $d = 5$ ,  $\beta < 1/2$  and the second term in Eq. (B.7) vanishes at infinity without imposing any restriction in the frequencies. Thus, for  $d = 5$ , the spectrum is continuous,  $\omega \in \mathbb{R}^+$ .



## Appendix C

# Chandrasekhar's approach to isospectrality

In this appendix, we investigate why scalar-type and vector-type Maxwell field modes are isospectral in higher-dimensional large Schwarzschild-AdS black holes, following the work developed by Chandrasekhar [3] (see also [32, 36]). For  $r_h/L \gg 1$ , Eq. (4.6) yields, with potentials Eqs. (4.2) and (4.5) (we assume  $l \ll r_h/L$ )

$$\partial_{r_*}^2 u^{(V)} + \left( \omega^2 - V_{(\text{EM})}^{(V)} \right) u^{(V)} = 0 \quad , \quad (\text{C.1})$$

$$\partial_{r_*}^2 u^{(S)} + \left( \omega^2 - V_{(\text{EM})}^{(S)} \right) u^{(S)} = 0 \quad , \quad (\text{C.2})$$

with

$$V_{(\text{EM})}^{(V)} = f \frac{(d-4) \left( d \left( \frac{r_h}{r} \right)^{d-1} + d - 2 \right)}{4L^2} \quad , \quad (\text{C.3})$$

$$V_{(\text{EM})}^{(S)} = f \frac{(d-4) \left( (8-3d) \left( \frac{r_h}{r} \right)^{d-1} + d - 6 \right)}{4L^2} \quad , \quad (\text{C.4})$$

and  $f = \frac{r^2}{L^2} - \left( \frac{r_h}{r} \right)^{d-3}$ . From a preliminary assessment of the equations, nothing would lead us to conclude that these yield isospectral modes. The potentials can be written as [3]

$$V_{(\text{EM})}^{(V)} = W^2 - \frac{dW}{dr_*} + \beta \quad (\text{C.5})$$

$$V_{(\text{EM})}^{(S)} = W^2 + \frac{dW}{dr_*} + \beta \quad , \quad (\text{C.6})$$

with  $W = -\frac{d-4}{2L^2} \left( 1 - \left( \frac{r_h}{r} \right)^{d-1} \right) r$  and  $\beta = 0$ . Potentials satisfying Eqs. (C.5) and (C.6) are known as superpartner potentials. It follows that the corresponding Schrödinger-like equations Eqs. (C.1) and (C.2)

can be written as

$$u^{(V)} = \frac{1}{\sqrt{\beta - \omega^2}} \left( -Wu^{(S)} + \frac{du^{(S)}}{dr_*} \right) , \quad (\text{C.7})$$

$$u^{(S)} = \frac{1}{\sqrt{\beta - \omega^2}} \left( Wu^{(V)} + \frac{du^{(V)}}{dr_*} \right) . \quad (\text{C.8})$$

Quasinormal modes obey the purely ingoing wave at the horizon and the Dirchlet condition at spatial infinity, so that, assuming  $\omega$  to be a quasinormal mode for  $u^{(V)}$ , i.e.

$$u^{(V)} = \mathcal{A}^{(V)} e^{-i\omega r_*} , \quad r \rightarrow r_h , \quad (\text{C.9})$$

$$u^{(V)} = 0 , \quad r \rightarrow \infty , \quad (\text{C.10})$$

Equation (C.8) yields, after substituting  $W$  and  $\beta$ ,

$$u^{(S)} = -\mathcal{A}^{(V)} e^{-i\omega r_*} , \quad r \rightarrow r_h , \quad (\text{C.11})$$

$$u^{(S)} = \frac{1}{\sqrt{-\omega^2}} \left( Wu^{(V)} + f \frac{du^{(V)}}{dr} \right) \Big|_{r=\infty} , \quad r \rightarrow \infty . \quad (\text{C.12})$$

The behaviour of  $u^{(V)}$  near spatial infinity is given by Eq. (4.14), so that  $\left( Wu^{(V)} + f \frac{du^{(V)}}{dr} \right) \Big|_{r=\infty} \sim \frac{d-3}{L^2} r^{2-d/2} \Big|_{r=\infty}$ , which vanishes for  $d \geq 5$ . Thus, if  $\omega$  is a quasinormal mode for  $u^{(V)}$ , it is also a quasinormal mode for  $u^{(S)}$ , and the isospectrality between scalar-type and vector-type modes is proven. Note that there seem to be no dynamical ‘‘algebraically special modes’’, for which  $\omega^2 = \beta = 0$ .